January 2010

NMR Search for Mobile, Aluminum-bearing Species during Reactions of Sodium Alanate

Timothy Ivancic
Washington University in St. Louis

WASHINGTON UNIVERSITY IN ST. LOUIS

Department of Physics

Dissertation Examination Committee:
Mark Conradi, Chair
William Buhro
Sophia Hayes
Martin Israel
Daniel Leopold
James Miller

NMR SEARCH FOR MOBILE, ALUMINUM-BEARING SPECIES DURING REACTIONS OF SODIUM ALANATE

by

Timothy Mark Ivancic

A dissertation presented to the
Graduate School of Arts and Sciences
of Washington University in
partial fulfillment of the
requirements for the degree
of Doctor of Philosophy

August 2010

Saint Louis, Missouri

Acknowledgements:

I would like to thank Mark for the success of my degree. His advice and instruction was fundamental to my learning and understanding of NMR. His teaching always goes beyond the text books and into the lab and workbench. This thesis could not have been written without him.

I also would like to thank Son-Jong Hwang from Caltech for providing MAS spectra and analysis which greatly supplemented this work. Additionally, I would like to thank Bob Bowman from RCB Hydrides, who was a key collaboration and whose long-time experience and expertise in hydrides I could not have done without. In addition, I would like to thank Craig Jensen and Derek Birkmire from the University of Hawaii for their work in synthesizing and doping the majority of the material used in this study. I would also like to thank Terry Udovic from NIST for providing XRD data. Furthermore, the help and advice of Todd Hardt, Denny Huelsman, and Tony Biondo in the machine shop was greatly appreciated, and I was always able to walk away having learned something new. I am also appreciative of the financial support of the DOE for this work (grant DE-FG02-ER46256).

I thank Allison, next to whom I did some of my best thinking and writing. Her patience during the last few months was greatly appreciated, and her support was always uplifting.

Finally, I would like to thank my parents, Mark and Kathy Ivancic. My appreciation of their dedication to my education from the earliest possible time and financial sacrifice to keep me in school cannot properly be expressed, so I dedicate this thesis to them.

TABLE OF CONTENTS:

LIST OF TABLES:

LIST OF FIGURES:

LIST OF ABBREVIATIONS:

CP – Cross-Polarization
CPMAS – Cross-Polarization Magic Angle Spinning
CSA – Chemical Shift Anisotropy
DVM – Digital Voltmeter
DOE – Department Of Energy
EFG – Electric Field Gradient
ID – Inner Diameter
INS – Inelastic Neutron Scattering
LN_2 – Liquid Nitrogen
FID – Free-Induction Decay
FWHM – Full Width at Half Maximum
MAS – Magic Angle Spinning
mol% - Mole Percent
NMR – Nuclear Magnetic Resonance
OD – Outer Diameter
PEM – "Polymer Electrolyte Membrane" or "Proton Exchange Membrane"
PID – Proportional-Integral-Derivative
PRT – Platinum Resistance Thermometer
r.f. – Radio Frequency
R.T. – Room Temperature
SAH – Sodium Aluminum Hydride
S/N – Signal-to-Noise ratio
SS – Stainless Steel
T_1 – Longitudinal relaxation time (spin-lattice relaxation time)
T_2 – Transverse relaxation time (spin-spin relaxation time)
VT-MAS – Variable Temperature Magic Angle Spinning
wt% - Weight Percent
XRD – X-ray Diffraction

CHAPTER 1:

INTRODUCTION

1.1 H_2 Fuel Economy

The Department of Energy has envisioned a hydrogen fuel economy and has joined an international effort to encourage and support research into making the appropriate technologies. References [1]-[5] contain nice reviews of hydrogen storage and the hydrogen fuel economy, and the material in this section can be found in more detail in these publications. H_2 would act as an energy carrier for use in mobile applications. The attractions to H_2 as a fuel are clean combustion (H_2O being the only by-product), higher efficiency vehicles (by using fuel cells in combination with electric motors), and decreased national dependence on foreign energy sources. A conceptual flow chart of a hydrogen fuel infrastructure is depicted in Figure 1.1.

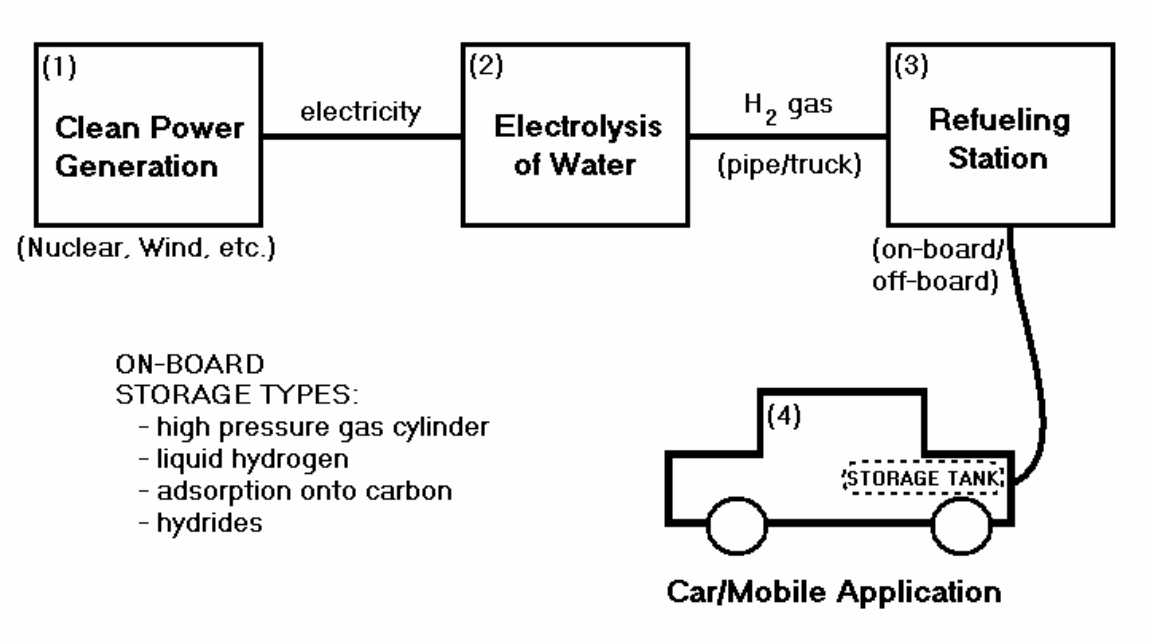

Figure 1.1: Conceptual diagram of H_2 fuel infrastructure.

Electricity would be produced by (clean) energy sources like nuclear power, wind power, solar power, etc. **(1)**. The electricity could then be used to electrolyze water and generate H_2 gas **(2)**. The H_2 could then be piped or trucked to fuel stations where cars, which are powered by fuel cells, could be re-fueled, **(3)** and **(4)**. Or the electricity could be sent directly to the fuel station and electrolysis performed at the fuel station. Another option is production of H_2 gas at the power plant by high-temperature processes such as thermolysis (direct splitting of H_2O, 2230 ^oC) or thermochemical cycles (metal oxide redox reactions, 850^{o}C to 2100^{o}C)[6], which would utilize heat from nuclear reactors or direct solar heating. Then the H_2 would be sent from the power plant to the refueling stations.

For "on board" fuel storage, the cars contain storage tanks that remain on the car and are refueled in place. For "off-board" fuel storage, the empty hydrogen storage tank would be removed from the car and exchanged for a regenerated hydrogen storage tank. These storage tanks could be regenerated at a specialized facility.

The means of storing the hydrogen gas on-board is a difficult problem. The storage medium must be able to satisfy a number of requirements such as affordability, safety, reliability, and fast release/charge kinetics.

There are a few basic options for use as a hydrogen storage medium. The first and obvious option is storage in high pressure gas cylinders. These are available now, but weight is a concern because high pressure gas cylinders are typically made of steel. The pressure cylinders could be made of light weight materials (carbon fiber and composite products), but then cost becomes a problem. Safety is also a concern considering pressures of 5000 to 10000 psi would be required to give the vehicle a reasonable range between refueling.

The second option would be liquid hydrogen storage. However this would require the storage medium to operate at temperatures around 20 K, and continuous loss of fuel due to boil-off would be a problem. Additionally, there is a large energy cost (30-40%) in liquefaction of the hydrogen.

A third option is adsorption onto carbon surfaces. The substrate could be charcoal, graphite, or nanotubes. These usually have very low storage densities at temperatures near 273 K, and the temperatures must be much lower (77 K) to get reasonable storage densities (3 wt%). This again requires some means of keeping the storage tank cool on board the car at some energy cost. Here liquid nitrogen, which is inexpensive, could be used, but this adds weight and volume to the fuel system.

The final option is storage in solid-state hydrides. Adesirable hydride would absorb and release hydrogen gas reversibly. This is a diverse field and there are many different types of hydrides with varied characteristics, from very fast kinetics but terrible

gravimetric storage densities ($LaNi_5H_6$: 1.37 wt%, 2 bar, 298 K), to excellent gravimetric storage densities but high operational temperatures ($LiBH_4$: 13.8 wt%, 1 bar, 623 K). The multiplicity of options and the possibility of tailoring a material for specific characteristics have made hydrides one of the most promising storage mediums. Still, there is no solid-state storage system today that satisfies all the DOE requirements.

One type of hydride that has received a lot of attention because of its relatively high storage capabilities (5 wt% to 15 wt%) and relatively low operational temperatures (350 K to 500 K) is the "complex hydride". This brings us to $NaAlH_4$.

1.2 The $NaAlH_4$ System

Sodium alanate (also called "sodium aluminum hydride" or "SAH") is a complex hydride that decomposes in the well-known step-wise reaction as shown below[7]:

1) $\mathbf{NaAlH_4 \leftrightarrow 1/3\ Na_3AlH_6 + 2/3Al + H_2\ (3.7\ wt\ \%)}$ 1.1

2) $\mathbf{Na_3AlH_6 \leftrightarrow 3NaH + Al + 3/2H_2\ (1.9\ wt\ \%)}$ 1.2

3) $\mathbf{NaH \leftrightarrow Na + 1/2H_2}$ 1.3

The third step is largely ignored because it is not accessible until temperatures in the range of 425°C[8]—which is outside the practical temperature range if we are to think about using this material as a feasible "on board" hydrogen storage material. Thus, the rest of this study is concentrated on the first two steps.

$NaAlH_4$ possesses a tetragonal ($I4_1/a$) structure with lattice parameters a = 5.02 Å and b = 11.3 Å, while Na_3AlH_6 is monoclinic ($P2_1/n$) with a = 5.4 Å, b = 5.5 Å, c = 7.7 Å, and $\beta \approx 90^o$ (89.8°[9], 90.1°[10], [11]). Reaction enthalpies for the first and second steps

are 37 kJ/mol H_2 and 47 kJ/mol H_2 respectively[8], [10], [12], [13]. In both $NaAlH_4$ and Na_3AlH_6 the hydrogen is covalently bonded to the aluminum. In turn, the Al-H units (either AlH_4^{-1} or AlH_6^{-3}) are ionically bonded to the Na^+. This is why the system is called a "complex" hydride; it includes both ionic and covalent bonding.

Steps 1 and 2 were found to be reversible with the addition of a few mol% Ti-dopant[14]. This is especially important for re-hydriding. Shortly thereafter it was found that many transition metals—such as, but not limited to, Fe, V, Cr, Sc, and Hf—could catalyze this reaction[7], [8], [10], [12], [15]. The metal catalysts have been introduced into the alanate in many different ways such as in Ti nano-clusters[16], [17], TiH_2[18], alloys like $TiAl_3$[18], [19], $Ti[OBu]_4$[14] and $Ti[OEt]_2$[7] (where Bu = C_4H_9 and Et = C_2H_5), and as dopant-halide salts like TiF_3, $TiCl_3$ or $TiCl_4$[18]-[17], [20]. The dopants can be introduced in these forms either by ball milling or by solution chemistry.

The catalyst must be introduced at the few mole-percent (2 to 4 mol%) to be effective—as opposed to the ppm level more common in catalysis. The catalyst works to lower the activation energy of the hydriding reactions and make the reaction reversible at temperatures below the melting temperature (see below). After a number of de-/re-hydriding cycles, the material's reversibility decreases—not up-taking nor giving-off as much hydrogen gas[7], [21], [22]. It is thought that the changes upon cycling could be improved.

The initial attraction to $NaAlH_4$ was the comparatively high theoretical hydrogen storage capacity (5.6 wt%) and lower reaction temperatures (100°C to 120°C), at which you can use the waste heat of a PEM (Polymer Electrolyte Membrane) fuel cell. However in reality, after repeated cycling, $NaAlH_4$ typically only provides ~3 wt% of

reversible hydrogen[1]. The DOE had set two targets with an array of characteristics for finding/producing a hydrogen storage material that they estimated could be safely and efficiently used for a hydrogen automotive fuel economy. These goals include gravimetric capacity, volumetric capacity, cost, cycle life, refueling time, and operational pressure and temperature. The first target, which expires this year (2010), sets an experimentally reversible gravimetric capacity of 4.5 wt% H_2 and a volumetric density of 28 g H_2/L and already surpasses the capabilities of the alanate system. The second target expires in 2015 and sets the goal to 5.5 wt% H_2 and 40 g H_2/L[1]. Despite the difficulties, $NaAlH_4$ remains the poster child for an entire family of complex hydrides and has drawn the attention of the hydride community for many years as a case study for understanding these types of hydriding reactions.

Much work has been done in trying to find both the role of the catalyst and the best way to incorporate the catalyst into the alanate with the most effectiveness. It is in large part understood that the Ti remains zero-valent (as in a metallic phase) and lies on the material's surface or in the Al phase after a few cycles, regardless of how the Ti is initially incorporated into the $NaAlH_4$[8], [15], [23]-[25]. However, the focus of this study is not the role of the catalyst.

To de-hydride the $NaAlH_4$, one simply has to heat the powder in a vacuum. Typical temperatures for both de- and re-hydriding lie in the range from room temperature to ~180^{o}C. To reverse the reaction and re-hydride the material requires heating the reaction products in Equation 1.2 in the presence of a H_2 overpressure. Re-hydriding the material in the same temperature range as de-hydriding requires the ability to achieve substantial H_2 over-pressures of 1400 to 1500 psi (100 bar). A few P-T phase

diagrams of the $NaAlH_4$ reaction have been previously published[7], [8], [12] and a version of these is reconstructed below in Figure 1.2.

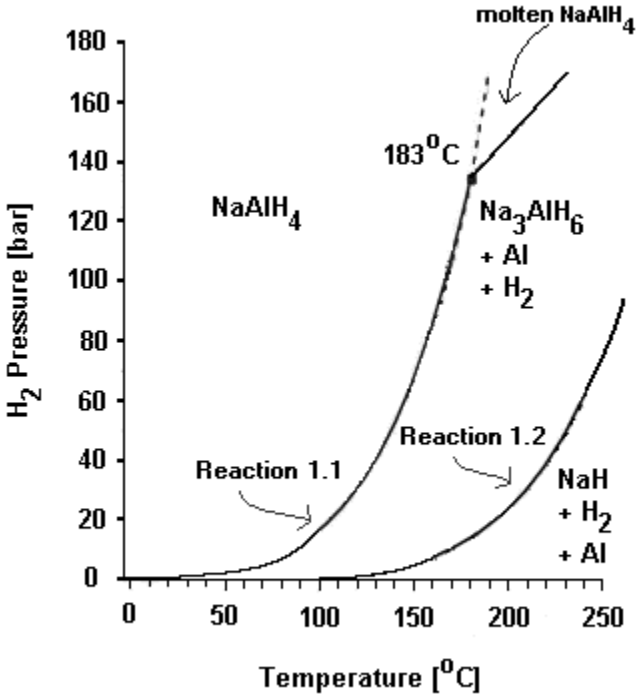

Figure 1.2: Pressure and temperature equilibrium graph of the sodium alanate hydriding reactions[7].

All the samples under investigation were powder samples. When the samples were doped, they were doped with either Ti- or Sc-halides. A more detailed description of the sample material is given in a following chapter (Chapter 2.10).

Consider the first two reaction steps (Equations 1.1 and 1.2), concentrating on the re-hydriding reaction direction. In the presence of H_2 overpressures, the recombination of NaH and bare Al metal forms the Na_3AlH_6 species (also denoted AlH_6^{-3} or simply called the "hexahydride"), and then the continued combination of Al metal and the AlH_6^{-3} species forms $NaAlH_4$ (also denoted AlH_4^{-1} or the "tetrahydride"). That is, one goes from physically separated NaH and Al metal to an intimate (indeed, stoichiometric) compound ($NaAlH_4$). The process requires mobility of Na and/or Al, not just H. This requires large

scale motion on the order of hundreds of nanometers[24]. Hydrogen-deuterium scrambling experiments (on both doped and undoped $NaAlH_4$) have demonstrated that the reaction rate-limiting step is not the hydrogen mobility, but the mass transfer of Al or Na[26]-[28].

Noting the progression of the Na:Al ratio during the reaction illuminates the drastic changes undergone by the hydride system. The Na:Al ratio evolves from 1:1 to 3:1 to 1:0 as one goes $NaAlH_4$ to Na_3AlH_6 to NaH. This requires the existence of mobile Na- or Al-bearing species, which are likely to be crucial chemical intermediates. While this species may provide key understanding of the chemistry, it has yet to be directly detected.

1.3 Study Motivation and Summary

It is the goal of this work to detect the mobile species by building and using a specialized probe to conduct *in situ* NMR measurements during hydriding reactions of sodium alanate. To the author's knowledge, *in situ* NMR of these reactions is original and has not been performed before.

The *in situ* NMR probe (referred to as the "high-pressure probe") can presently go to 350^{o}C, 6000 psi Ar (415 bars) and 3000 psi H_2—limited only by the expensive H_2-compatible pressure transducer. The probe's operation, design, and physical limitations are further described in Chapter 2.1. $NaAlH_4$ (pure or doped with a few mol% Sc or Ti) is reacted in the pressure vessel while doing (typically) ^{27}Al NMR. H_2 pressure is

continuously measured to monitor the reaction progression. At different points in the study ^{23}Na, ^{45}Sc, and ^{1}H NMR was used to supplement the ^{27}Al NMR discoveries.

There were two phases of the research. In the first, *in situ* reactions were conducted. This phase consisted of de-/re-hydriding reactions of the alanate in the normal reaction temperature range of room temperature to 180°C and applying H_2 pressures up to ~1500 psi (the upper pressure limit of the probe at the time of those studies). In those studies a mobile, Al-bearing species was discovered that initially appeared during the sample evolution during de-hydriding. These results and the additional finding that this mobile Al-species could be made to exist at ambient conditions spurred the research into the second phase.

The second phase of research involved high-pressure studies of the alanate system. In this phase high hydrogen pressures—around 3000 psi (207 bar)—were applied within the normal hydriding reaction temperature range for doped samples, or in the case of undoped $NaAlH_4$, up to 215°C to melt the sample. The 3000 psi H_2 over-pressure prevents the $NaAlH_4$ from de-hydriding. The new Al species was successfully generated and caused to persist under ambient conditions and new information surrounding this mobile Al species was discovered. During these studies more information about the mobile Al species was found—such as longevity, relaxation times, temperature effects, and conditions required for its creation. The persistence of this new Al species under ambient conditions allowed for removal of sample material for shipping to our collaborators for magic-angle spinning (MAS) and x-ray diffraction (XRD) analysis. However, a positive identification of the species has not yet been achieved.

CHAPTER 2:

EXPERIMENTAL APPARATUS AND MATERIALS

2.1 High-Pressure Probe

With the main thrust of this project being the ability to take *in situ* spectra during de-/re-hydriding reactions of the alanate, the high-pressure probe is a critical piece of equipment in this work. The typical reaction temperature range spans room temperature to the melting temperature of sodium alanate around 183°C[7]. Being able to go beyond the melting temperature is required in the case of undoped $NaAlH_4$. The probe is capable of reaching 350°C, well above the needed range (the hottest we used for the present work is 215°C).

The pressure needed to be achieved, especially when thinking about driving the material in the re-hydriding reaction direction, requires a minimum of 140 bar for temperatures at or below 180°C[7], [12]. But for studies of the alanate where one wants to halt the decomposition reaction, even at temperatures above the melting temperature, the requisite hydrogen gas pressure must be higher than 140 bar (See Figure 1.2 in the previous chapter for P,T equilibrium diagram). We operated in a pressure regime that is off the chart of the PT diagrams available in the literature, but by extrapolation, 200 bars (2900 psi) is sufficient to prevent de-hydriding of $NaAlH_4$ up to ~280°C.

A schematic of the probe is shown in Figure 2.1 below. A lower pressure conceptual prototype of this probe is described elsewhere[29], but some key changes have

been made to accommodate the higher pressures involved in this study as well as for other practical concerns.

The working idea behind the high-pressure probe is that high hydrogen gas pressures (up to 3000 psi) need to be applied to the alanate samples. But these samples are held in glass containers and glass alone will burst long before 3000 psi could be reached internally. If, however, the glass tube is exposed to an external pressure of argon gas at or above the hydrogen pressures inside the glass, then the sample tube will experience a net compressive force that the glass can easily handle without breaking. The higher exterior Ar pressures will also serve to help hold and seal the sample tube to the H_2 supply assembly.

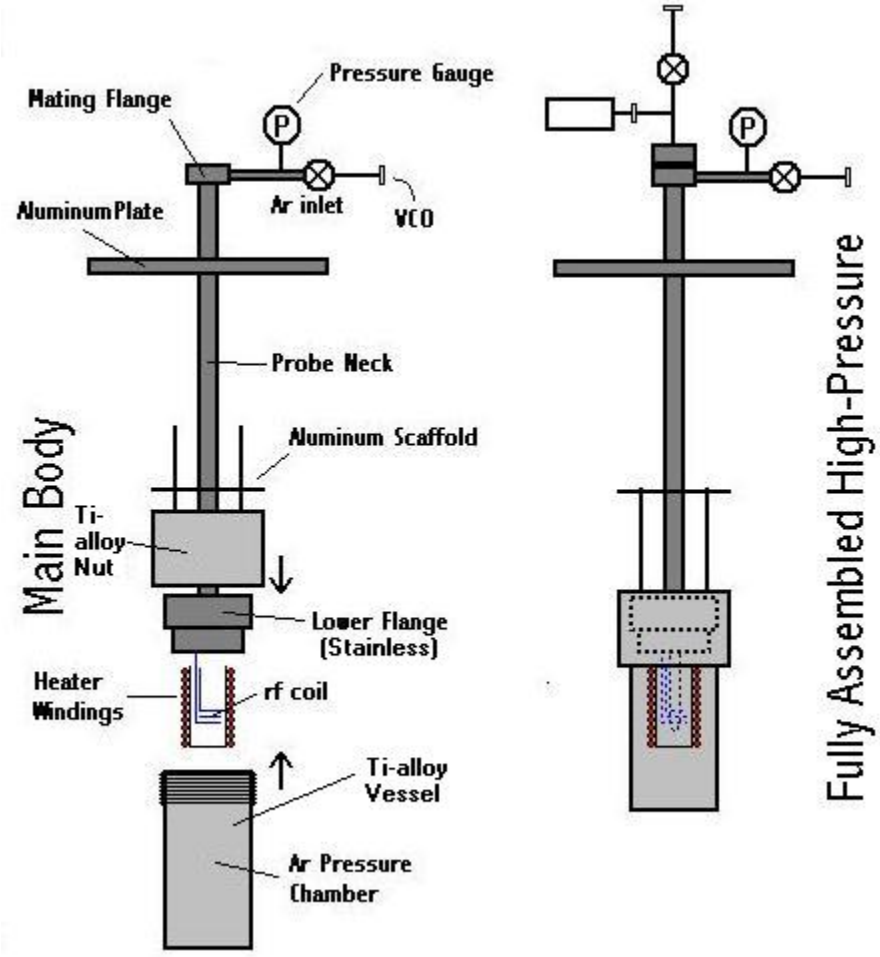

Figure 2.1: High pressure *in situ* probe schematic.

2.1.1 Sample Tubes

The powdered samples are loaded into 0.280" OD, 0.192" ID, 7" long glass sample tubes. Glass was chosen because of its availability, cost effectiveness, and ease to work with. During the course of this study a new sample container was constructed for every sample. Net pressure differences as high as 1800 psia (in the compressive direction) were applied to these tubes without bursting or cracking.

2.1.2 H_2 Supply Assembly

The glass sample tube fits snugly onto a stepped nozzle with two O-rings. A smaller O-ring hermetically seals the inside of the glass tube to the outside of the nozzle when it is compressed as the tube slips over the tip of the nozzle. A second O-ring of a slightly larger diameter acts as a soft seat for the glass tube against the step in the nozzle's diameter (see Figure 2.2). This prevents the glass tube from cracking at the contact between glass and metal that would otherwise result from the large pressure difference, $P_{ext} - P_{int}$. Once affixed to the nozzle tip of the H_2 supply assembly (see Figure 2.3), the glass tube is fed down the probe neck by a long 0.125" OD, 0.0625" ID, tube hard soldered to a 0.5" diameter, flange which mates with a face-sealing O-ring on the probe neck at the top of the probe.

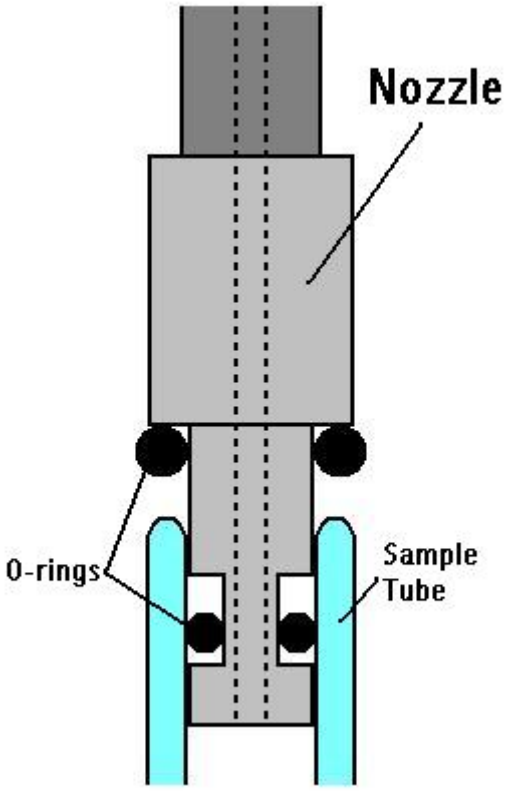

Figure 2.2: Close-up picture of sample tube and nozzle with sealing O-ring (smaller diameter) and O-ring seat (larger diameter) labeled.

The flange is bolted to the top of the probe neck by six ¾" hex-head 10-32 screws. To the flange is attached a stainless steel (SS) integral bonnet needle valve through a swage-T, which allows a pressure transducer to read the pressure over the sample even when the valve is closed. A high-pressure H_2 source and vacuum pump connect by VCO fittings to the valve.

The transducer is attached to the perpendicular arm of the T-connection between the flange and valve by copper gasket VCR. The transducer is a MKS 870 Incoloy® high-accuracy transducer. It has a 0-3000 psia range with a 0-10V full-scale read-out and a scaling accuracy band of 1% of the read-value, allowing the same transducer to be used for both near vacuum and H_2 high-pressure measurements.

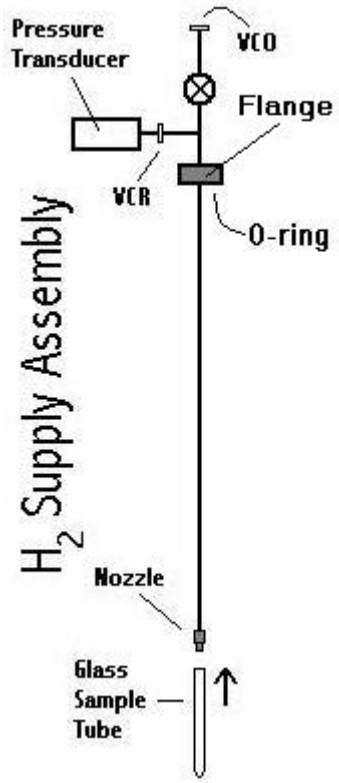

Figure 2.3: H_2 supply assembly schematic.

The entire H_2 supply assembly is constructed of 316 SS for strength. The purpose of this assembly is three-fold. The first is to provide H_2 to the sample. The second is to assure the sample is in the center of the NMR r.f. coil. The H_2 supply assembly is partially fed down the neck of the probe, bringing the attached glass sample tube into the Ar pressure chamber and guiding it into the single loop, Helmholtz style NMR r.f. coil. The third is to provide a convenient way to load air sensitive samples into the probe without having to manipulate the entire probe and disturb the position of the probe in the magnet.

The internal volume of the H_2 supply assembly when the valve is closed was measured to be 11.57 cc. Measurement of the internal volume was done by attaching a pressure cylinder, which has a standardized volume, and pressure gauge to the H_2 supply assembly. Then the assembly was evacuated and the cylinder pressurized with hydrogen. By first measuring the cylinder's pressure, then opening the valve and allowing the gas to fill the entire volume of the cylinder plus the H_2 supply assembly the initial and final pressure were compared and the volume of the assembly was calculated. This process was done several times to improve the accuracy of the measurement.

2.1.3 Main Body

Shifting our attention to the main body of the probe, a 10,000 psi pressure gauge, SS integral bonnet needle valve, and VCO connection are swaged in series and pipe-threaded into the mating flange for the 0.5" flange on the H_2 supply assembly. This is the Ar/vacuum connection and it allows the main probe body to be charged with Ar and valved off. Again, the pressure gauge is located such that with the valve closed, the

pressure of the Ar chamber can still be read (See Figure 2.1 and 2.6). All the components on the Ar inlet are constructed from 316 SS.

The mating flange to which the Ar inlet is attached is welded to a 0.5" OD, 0.375" ID, 316 SS tube. This makes up the probe neck. The probe neck runs through an upper aluminum plate that rests on the top of the superconducting magnet. The upper aluminum plate will be discussed later. After passing though the aluminum plate, the neck ends at a hard solder joint to the lower flange. The bottom flange is 2.625" in diameter and constructed of 316 SS. Through it pass an r.f. and two heater wire high-pressure electrical feed-throughs, along with two metal-sheathed thermocouples. The high-pressure electrical feed-throughs are machined from Torlon® and are one-time use devices. They are described in greater detail elsewhere[30], and so will not be discussed here.

To the bottom of the lower flange are fixed three threaded brass rods which support a thin walled brass tube about which is wound bifilar, resistive thermocouple wire to serve as the heat source inside the Ar chamber. Buried under the heater winding is a type-E thermocouple used to regulate the temperature. The brass tube and heater windings are 1" in diameter and are suspended so that they surround the r.f. NMR coil—where the sample tube is guided into by the H_2 supply assembly.

A second type-E thermocouple is attached to the r.f. coil just exterior to the bottom of the glass sample tube at the level of the sample. The purpose of this second thermocouple is to measure the temperature of the sample.

The Ar pressure chamber consists of a 2.25" OD, 1.75" ID enclosure that is closed on the bottom and the top has exterior 32 threads-per-inch threading. The

threaded end threads into a matching nut that tightens onto the lower flange. Both the nut and enclosure were machined from a single piece of Grade-5 titanium alloy (6Al-4V). This titanium alloy was chosen for its superior strength and magnetic properties when compared to various SS options.

The flange sealed to the inside of the Ar chamber by a plug-sealing O-ring, as shown in Figure 2.4. The plug-seal style was chosen intentionally. The more common face-seal failed repeatedly in high-pressure use. This is because any distortion in the face-to-face meeting of the flange and Ti cylinder caused by the excessive pressure-force pushing them apart and stretching the Ti nut would allow the O-ring to extrude out—even through a gap of a thousandth of an inch or smaller. It should be noted that the probe is designed to withstand pressures of 6000 psi Ar safely. On a 1.75" diameter surface (the underside of the lower flange, which is exposed to the argon gas), this pressure is generating 14,400 lbs of force. With a plug-seal style O-ring groove, the gap that is important is the gap between the inside of the Ar chamber and outer lip of the flange plug. This way even when the face of the flange and Ti cylinder are separated slightly along the axis of the probe due to the stretching of the Ti nut, the precision machined gap (< 0.001") the O-ring presses against is unchanged.

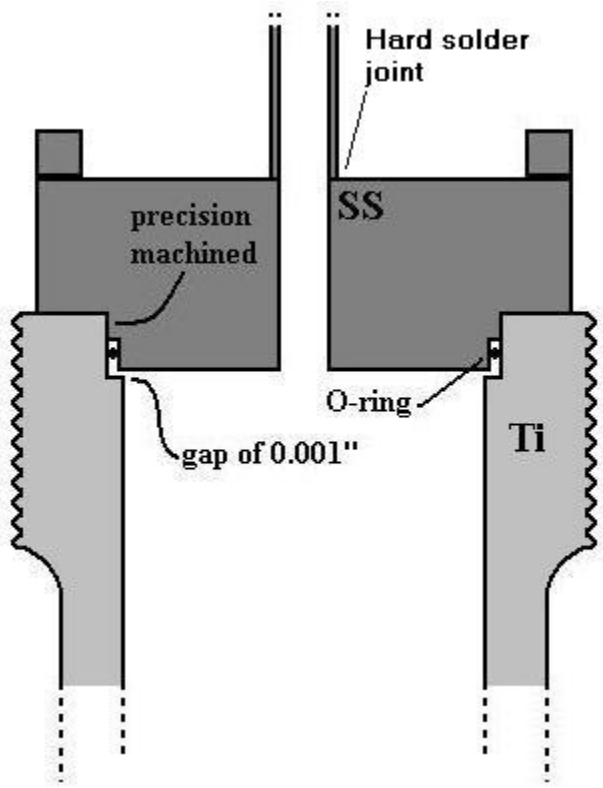

Figure 2.4: Close up of Ar chamber-to-flange plug-seal.

The O-ring type was carefully chosen as well. The plug-seal works with a 90-durometer Viton® O-ring. Typical O-rings made of buna-N have durometers around 70. At the pressures used in this probe 70-durometer O-rings have zero tolerance of any gap, i.e., they will extrude unless there is absolutely no gap[31], as was experienced by the author on many occasions with the face seal design. However, a 90-durometer O-ring at 6000 psi can tolerate up to a 3 thousandths inch gap without extruding[31].

Viton® is a fluoroelastomer and was chosen over buna-N (nitrile) for its durability at higher temperatures. Viton® has an upper limit of 200^{o}C, while buna-N has an upper limit of only 120^{o}C[32]. For testing purposes, a thermocouple was taped on the titanium nut and the probe was heated under normal conditions used during hydriding.

The temperature of the exterior of the nut was measured to reach 130^{o}C (for the highest internal temp of ~180^{o}C).

Due to the 130^{o}C nut temperature, the choice of Viton® as an O-ring material was augmented by the use of water-fed copper cooling coils wrapped around the nut in series with similar cooling coils wrapped around the exterior of the titanium Ar pressure chamber (See Figure 2.6). In addition, a ceramic wool jacket was wrapped around the cooling coils on the Ar pressure chamber to help protect the magnet bore from the higher temperatures.

An aluminum scaffold sits a few inches above the lower flange and nut supported by brass threaded-rods (See photograph below of aluminum scaffold in Figure 2.5, as well as Figure 2.1 for a depiction of the placement of the scaffold on the probe). The high-pressure r.f. feed-through connects the NMR r.f. coil inside the Ar pressure temperature to the rest of the tank circuit housed on the scaffolding. Due to the heat inside the Ar pressure chamber, the tuning capacitors have to remain outside. The scaffolding also acts as a brace, holding a BNC connector, and allowing a coax cable to connect to the tank circuit. Furthermore, the scaffolding provides a sturdy support for a long plastic rod, which connects by means of a mechanical coupler to the tunable capacitor and allows the tank circuit to be tuned from outside the magnet.

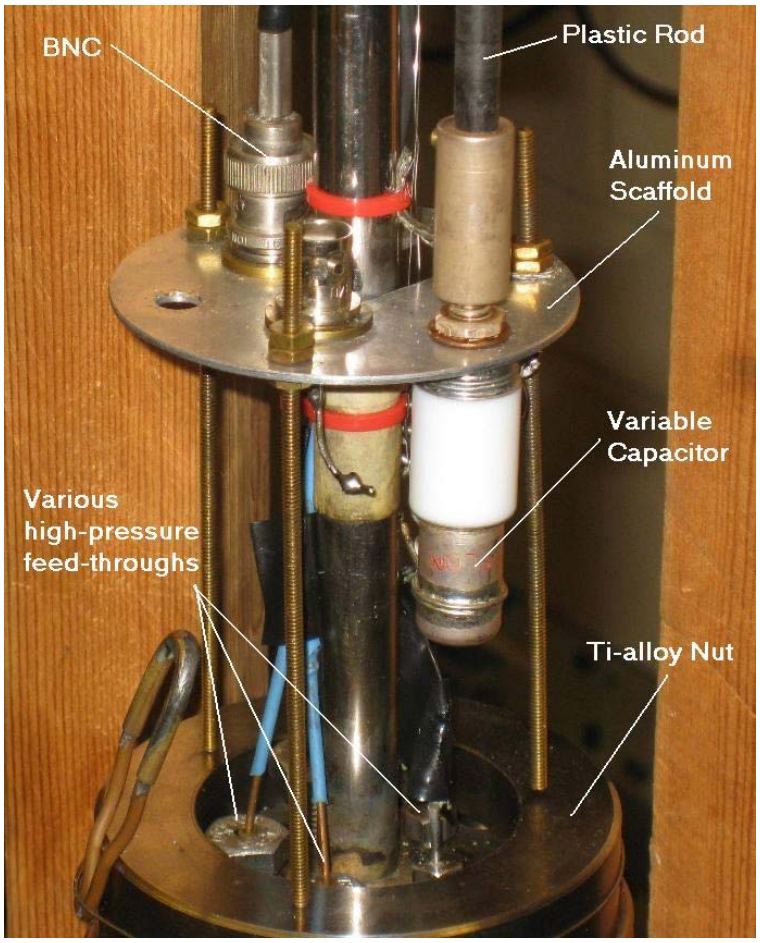

Figure 2.5: Photograph of the aluminum scaffold which supports tank circuit components, the BNC connection, and plastic rod for tuning the resonance frequency of the probe.

The plastic rod, coax cable, temperature regulating thermocouple, sample temperature thermocouple, and heater wire power cables run up the length of the neck (but outside the gas filled tubes) and through the upper aluminum plate mentioned earlier. The upper aluminum plate is designed to bolt to the top of the superconducting magnet. The probe neck can be rotated and moved up and down with respect to the upper aluminum plate, allowing the probe to be adjusted so the sample sits in the "sweet spot" of the magnet where there is maximum field homogeneity.

Noise was a particularly big problem with this probe since the resonant frequency of ^{27}Al is 92.3 MHz in the 8.3 T superconducting magnet. This is the frequency of a

local St. Louis country radio station (92.3 WIL). Because the power wires and thermocouples are in close proximity to the NMR r.f. coil inside the Ar pressure chamber, they are prone to bringing a large amount of r.f. noise from outside the chamber in to the NMR coil. To combat this, multiple ground lugs were screwed into the upper aluminum plate. From the ground lugs to each thermocouple wire and power wire are attached two pairs of ~1000 pF capacitors. From the upper aluminum plate the thermocouple wires were again connected to ground on the magnet's exterior via a pair of ~1000 pF capacitors before plugging into either a digital voltmeter (DVM) or the temperature controller. At a frequency of 100 MHz, a 1000 pF capacitor should have a small reactance around 1.6 Ω.

2.1.4 Electrical Read-outs

Coming from the probe are five electrical elements. Two are the power wires, which provide current to the resistive heater wires around the sample. Two are type-E stainless-sheathed thermocouples: one for regulation of the heater windings and one for measuring the sample temperature. The last is the voltage output of the pressure transducer used to measure the pressure over the sample.

The sample temperature thermocouple runs to a DVM in parallel with a Kipp & Zonen BD-40 pen chart recorder. The pressure transducer also runs to a second DVM in parallel with a second identical chart recorder. The chart recorders track the temperature and pressure of the sample continuously and make reading the instantaneous voltages easy as well as giving the user the ability to quickly assess the trends and changes in

pressure and temperature over the course of the experiments. Moreover, this set-up allows the user to line up or register pressure and temperature events precisely.

The power wires and regulation thermocouple ran to a temperature controller, which is described in more detail later in this chapter (Chapter 2.6). The power wires, before running into the temperature controller, ran through a full-wave bridge rectifier and filter. The current had to be rectified and filtered before running into the probe because the resistive heating wire located in the center of the magnet would otherwise oscillate at 60 Hz and saw themselves apart against the brass tube and rod, even when tied down.

2.2 High-Pressure H_2/Ar Sources

As mentioned above, the probe was designed to safely hold 6000 psi. A schematic layout of the gas connections leading to the probe are shown in Figure 2.6.

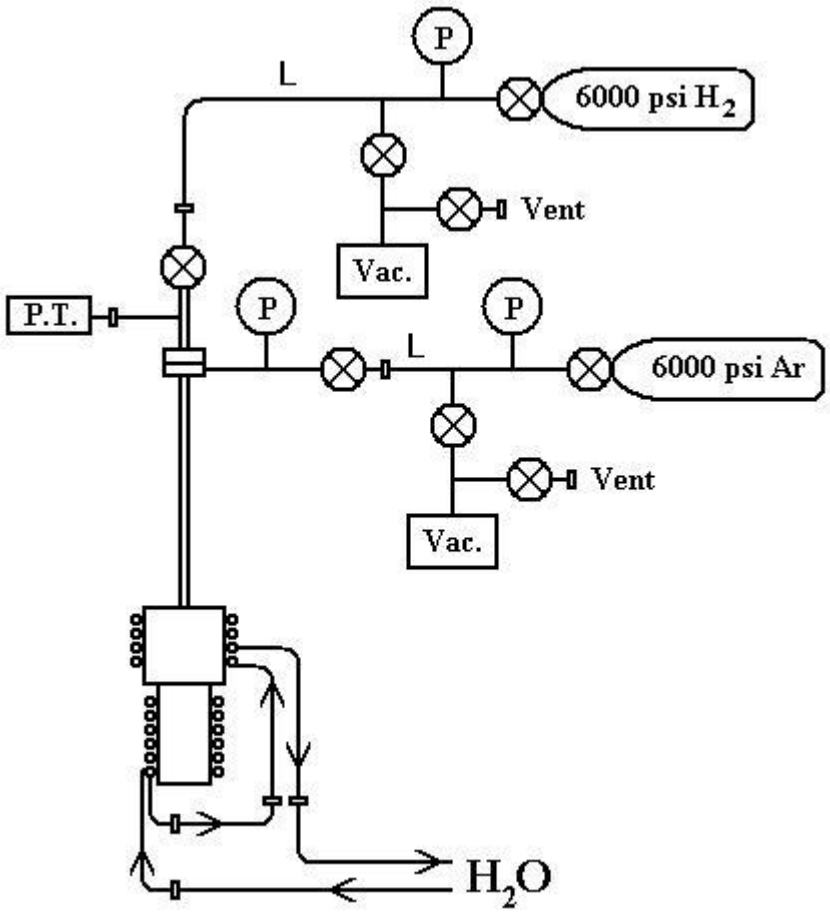

Figure 2.6: Schematic layout of gas hook-ups and water-cooling coils from the High-Pressure probe to the H_2/vacuum supply and Ar/vacuum supply. "L" indicates a long run of small diameter tubing.

High-pressure cylinders were used instead of compressors to pressurize the H_2 and Ar chambers. Both the H_2 and Ar were purchased from Cee-Kay in 6000 psi cylinders. The probe was designed so that if some component failed between the cylinder and the probe, the probe could handle the full 6000 psi tank pressure safely.

Each cylinder is directly connected to a 10,000 psi pressure gauge, and then runs into 1/16" OD, 0.030" ID, SS tubes, which were purchased from High-Pressure Equipment in Erie, PA. Small diameter tubes were chosen for a few reasons. The first is safety. If a connection were to break, the tubes would be less likely to whip around, or if a tube were to burst, the volume is small. The second reason is because the reduced

volume in the lines reduces the amount of gas used—since the probe is to be repeatedly charged and evacuated. The third reason for using the small ID tube is to create a large impedance to the gas flow into the probe for better control. With larger ID tubes, when the gas cylinder's valve is cracked, the line would charge to 6000 psi immediately. In the case of the argon gas, a sintered-metal filter was used in the CGA connection to additionally slow the influx of gas. One can crack the valve and the pressure will rise to 6000 psi in the line in about 5 seconds, giving the user plenty of control.

In the case of the hydrogen gas cylinder the situation is a bit different. Even with the 0.030" ID tube and sintered metal-filter, the hydrogen gas races to 6000 psi immediately. Thus, the sintered-metal filter was replaced with a short copper rod precision machined to entirely plug the CGA fitting. The copper plug rested against a ledge recessed in the mouth of the CGA fitting. However, the copper plug was lightly scored lengthwise—one or two thousandths deep—before being hammered in place (Figure 2.7). This effectively slowed the flow of hydrogen gas into the tubing.

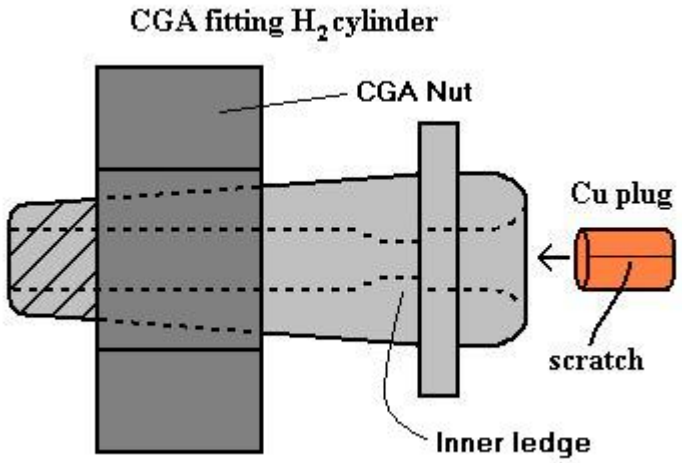

Figure 2.7: Scored, copper plug in hydrogen tank CGA fitting.

The small diameter SS tubes then connect to the either the H_2 supply assembly or Ar inlet via VCO fittings. The pressure line is interrupted by a T-connector that leads to

a valve, a vacuum pump, and a vent (Figure 2.6). Having multiple valved stages and a vacuum/vent connection mid-line between the gas tanks and the probe allows both gas pressures going into probe to be finely adjusted.

2.3 Cold Probe

Some of the work in this project included taking spectra at temperatures lower than room temperature. To achieve this, a probe was constructed which, in combination with the LN_2 boil-off dewar, could reach temperatures of -145^{o}C. Samples for this probe must be loaded in short, 5 mm OD NMR tubes. Most of the time, the samples were flame sealed in Ar atmospheres at 0.8 to 0.9 atm. A schematic of this separate cold probe is shown in Figure 2.8.

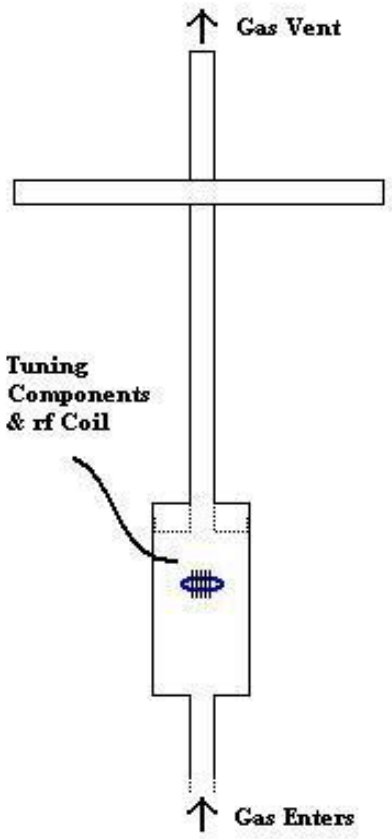

Figure 2.8: Schematic of cold probe.

The probe is of a simple design frequently used in this lab. It consists of a 3/8" OD copper tube running along the axis of the probe. At the top of the probe is an aluminum flange that rests on the top of the magnet and adjusts to holds the probe in the center of the field. A tuning rod, coax, and type-T thermocouple run down through the aluminum flange to a smaller copper flange at the bottom of the copper tube, inside the magnet bore. A hollow, 2" diameter, copper can attaches to the lower copper flange. Inside the can, fixed to the bottom of the lower copper flange are the thermocouple and tank circuit components with a horizontal, six-turn solenoid NMR coil. The NMR coil is wound to accept standard 5 mm OD NMR tubes.

A second 3/8" OD copper tube is soldered to the bottom of the can leading out the bottom of the bore of the magnet. Pipe insulation is wrapped about the exterior of the

entire length of the probe to protect the magnet bore from freezing. When the probe is fully assembled, cold nitrogen gas—supplied by the LN_2 boil-off dewar (Chapter 2.5), and regulated by the temperature controller (Chapter 2.6)—enters the bottom of the probe and vents at the top of the probe, maintaining a cold, dry environment around the sample.

2.4 Box Probe

The ^1H NMR was performed in a third probe. The probe is low-Q and capable of operating in a wide temperature range. This study used the box probe for cold (-110^oC) to room temperature measurements. Built to fit between the poles of an iron-core electromagnet, the probe is constructed of a rectangular, aluminum frame containing the r.f. tuning components. The NMR r.f. coil and a type-T thermocouple are located inside a glass-tube dewar which is open at both ends to allow gas to flow through. In this configuration the r.f. components remain at room temperature while the sample temperature is varied by the cold nitrogen gas.

2.5 LN_2 Boil-off Dewar

When it was desirable to take data at temperatures below room temperature, a LN_2 boil-off dewar was utilized. The boil-off dewar consists of a 25 L dewar with internal resistive heating elements ("boilers") which were submersed in the liquid nitrogen. An interface atop the dewar allowed the two 100 Ω resistors submerged in the LN_2 to be wired in series, parallel, or singly with the additional option of using a diode to

select between full-cycle or half-cycle AC current. By these means, the boil-off rate of the nitrogen could be controlled.

As the internal pressure builds, the gas passes through a copper tube heat exchanger that dips back down into the liquid. Finally, the cold N_2 exits the dewar through an insulated latex hose which is connected to a glass tube. The glass tube houses a long resistive-wire solenoid along the inside and a platinum resistance thermometer (PRT) at the tip of the tube where the cold N_2 finally passes into the NMR probe.

The PRT provides feedback for the temperature controller, which regulates the current for the resistive-wire heater as the cold N_2 passes through the glass tube. This provides stable regulation of the gas temperature as it enters the probe.

The boil-off rates needed for specific temperature ranges varied with the probe in use. For the cold probe, the resistors and diode are wired so that only a single 100 Ω resistor is used with the full AC cycle. This arrangement typically provided 4 hours of stable operation before the dewar needed to be refilled. For the lowest temperature measurement in the cold probe, specifically -145^{o}C, the dewar was set to it's highest boil-off with both 100 Ω resistors in parallel and utilizing full-cycle current. When the LN_2 boil-off dewar is in use on the cold probe in the superconducting magnet, a small resistive heater is attached to the bottom flange of the magnet to protect the O-ring in the magnet from freezing.

The box probe is much smaller and better insulated. The dewar could operate stably for 8 hours without refill when the two 100 Ω resistors wired in series with full-cycle current.

2.6 Temperature Controller

The temperature controller was used for all the probes in this study for both the hot and cold experiments. It is made by Omega and is a Micromega® CN77000 Series Controller. It is equipped with Autotune Proportional-Integral-Derivative (PID) and is capable of reading any type of thermocouple and PRT for use in temperature feedback and monitoring. The was controller operated in an "on-off" mode.

The controller had a $\pm 3^{o}C$ swing range for the hottest temperatures (the most inaccurate) when used to regulate the resistive windings on the high-pressure probe by a type-E thermocouple wound into the heater. The convection of the dense argon gas was responsible for this temperature instability in the high-pressure probe. For regulation of the cold nitrogen gas stream by PRT, the temperature controller stabilized temperatures to $\pm 1^{o}C$ for the cold probe and less than $\pm 1^{o}C$ for the box probe.

2.7 Sample Handling

Sodium alanate is an air and moisture sensitive material. $NaAlH_4$ can oxidize and spoil the sample[33] by forming aluminum oxide and hydroxide layers on the outside of the alanate grains and preventing the reaction of the samples[10]. Moisture is also a problem. The material reacts with water to form sodium hydroxide—a corrosive material—and hydrogen gas. The heat of reaction may be sufficient to ignite the hydrogen gas released[33]. For certain samples, the water content in the air alone could be enough to cause the sample powder to burn, as witnessed before by the author in a

controlled environment. These types of reactions are not unfamiliar in hydrides. Sample handling was an important element to these studies.

In general, because some of the work conducted in this lab is hydride work, the glove-bag system below became a permanent fixture in the group and the techniques described became regular practice for the investigators in the lab.

2.7.1 Glove Bag

The samples are stored and handled in a tape-seal, two-hand glove bag from Sigma-Aldrich. A dry nitrogen gas environment is maintained inside these bags at all times by a constant stream of gas. The gas is bled off from the headspace of a large, exterior LN_2 storage dewar that supplies the entire physics department.

Figure 2.9: Glove bags used for sample manipulation and storage.

As shown above in Figure 2.9, the glove bag system simply consists of two glove bags connected in series. The first bag (”Loading bag”) is where sample loading and manipulation is performed. The second, larger bag (“Storage Bag”) is where the samples and other air sensitive hydride samples were stored. The system was easily maintained, replaceable, inexpensive, and could be adapted to fit into a smaller space when compared with larger glove box systems.

Typically, the N_2 stream is maintained at 2 to 3 SCFH. This provided a positive pressure inside the bags so that if any leak or small holes did develop from use and wear, the N_2 atmosphere would leak out, rather than outside air leak in. Some vigilance was needed to constantly check the bags to see how inflated they were every week. Over time, some of the seals and closures would loosen and need to be replaced. In addition, samples in the storage bag are usually double sealed in jars and bags to prevent the possibility of contaminating all the samples in the case of lost pressure.

2.7.2 Loading Procedures

As well as storing the samples in a dry, oxygen free environment, it is crucial to load these samples into the probe without exposing them. The H_2 supply assembly is completely removable from the probe, making it easy to detach and bring to the glove-bag. The H_2 supply assembly, after being removed from the probe, is purged with dry nitrogen gas, and the nozzle of the H_2 supply assembly is inserted into the glove bag while nitrogen continues to flow through.

The sample is placed in a sealable jar while inside the storage bag (See Figure 2.9). Then the jar is closed in the storage bag, preserving the N_2 atmosphere around the

sample container. Before bringing a sample out of the storage bag into the loading bag, the N_2 flow is increased to about 10 SCFH. The jar holding the sample container is next quickly transferred to the loading bag, along with the glass sample tube and any tool that might be needed to load the sample into the glass tube. The bags are then purged and left for a couple minutes before opening the jar and sample container. This also serves to purge the glass sample tube.

The sample material is loaded into the glass tube and the sample mass can be measured on an electronic scale already in the loading bag. A small piece of glass wool is stuffed into the top of the tube to protect the H_2 supply assembly and vacuum pump from taking in powder from the sample when the tube is evacuated later. The tube is fixed onto the nozzle of the H_2 supply assembly (Figure 2.2), the valve to the H_2 supply assembly shut to stop the N_2 purge, and the H_2 supply assembly, with the filled and attached sample tube, is taken out of the bag and fed into the probe. The hydrogen gas system (See Figure 2.6, Chapter 2.2) is evacuated up to the valve on the H_2 supply assembly, the valve opened slowly to evacuate the sample tube of the nitrogen gas, and the H_2 supply assembly is loosely bolted into place on the main body of the probe.

During the above process, the argon gas system is being evacuated up to the valve of the Ar inlet on the main body of the probe (Figure 2.6, Chapter 2.2). Once the H_2 supply assembly is bolted loosely onto the neck of the probe (See Figure 2.1, Chapter 2.1) the Ar inlet is opened, and the Ar pressure chamber begins to evacuate. As a vacuum is formed in the Ar chamber, the O-ring on the neck of the probe is compressed and the screws on the H_2 supply assembly are progressively tightened, ensuring a good seal. The Ar chamber is left to evacuate for approximately 10 to 15 minutes as the H_2

supply assembly is continuously evacuated. Once the evacuation is complete, the Ar chamber is charged with argon gas and the probe is ready for use.

By this procedure, the sample goes from storage container to probe, ready for study, while being exposed only to N_2 or vacuum.

2.8 Magnets

2.8.1 Superconducting Magnet

The work on ^{27}Al, ^{23}Na and ^{45}Sc were all performed in an 8.3 T, KD 601 dewar, superconducting magnet from Cryomagnet System, Inc in Indianapolis, IN. The magnet has a 3.5" inner-diameter aluminum vertical bore. The Larmor frequencies of the different NMR active nuclei depended very slightly on the probe in use. The unwieldy high-pressure probe has a large SS lower flange (See Figure 2.1, Chapter 2.1), which modifies the local field around the sample and alters the resonant frequency slightly (~1-2 kHz) and reduces the field homogeneity with respect to the cold probe.

The carrier frequency was set to the frequency of $Al(NO_3)_3$ (aq.) (the standard Al reference) for ^{27}Al NMR. In the high-pressure probe this corresponded to 92.286 MHz, and in the cold probe the frequency was 92.285 MHz. For ^{23}Na NMR, NaCl (aq.) is the standard reference and this corresponds to 93.686 MHz in the high-pressure probe and 93.684 MHz in the cold probe. For the few ^{45}Sc spectra taken, $Sc(NO_3)_3$ (aq.) is chosen as a reference. This was performed only in the high-pressure probe and corresponded to 86.035 MHz.

2.8.2 Electromagnet

All the ^{1}H measurements were done at 85.025 MHz (2 T) in a Varian XL-100 iron-core electromagnet with ^{19}F field stabilization[34]. The reference sample used was water. The shift difference of water from the standard ^{1}H reference (TMS) is insignificant given that this is static NMR and the lineshapes are many kHz wide.

2.9 Spectrometer

The spectrometers used for both the electromagnet and the superconducting magnet are almost indistinguishable. They are described in more detail elsewhere[35]. Briefly, they are home-built, pulsed, superheterodyne spectrometers with four transmitter phases and quadrature phase detection. The spectrometers could either be operated independently of the computer or by TTL hardware and Pulse Blaster card. The software used to control the pulse generator was locally written[35].

2.10 Sample Materials

This section discusses some of the specifics of the various sample materials used in this study. All the material used in this study were powder samples. We thank Craig Jensen and Derek Birkmire for their work in the synthesis and doping of the sample materials at the University of Hawaii, Department of Chemistry. Information about sample preparation and doping was related to the author via personal communications.

A couple much older samples that were used came from IFE (Institute for Energy Technology) in Norway, but none of these samples appear in this work.

2.10.1 Doped $NaAlH_4$

The majority of doped samples investigated in this study were Sc-doped. Sc-doping was found to be equivalent to or better than Ti-doping in hydrogenation kinetics and reversibility[36], [37], while not being too heavy to significantly modify the theoretical hydrogen gas storage capability of the material from 5.6 wt% (depending on how much dopant was added).

In the original proposal for this work, Sc was chosen over Ti as a dopant because Sc is more easily studied with NMR due to its naturally abundant NMR active nucleus (100% for ^{45}Sc) and relative sensitivity, as compared to Ti (^{47}Ti and ^{49}Ti have natural abundances of 7.75% and 5.5% respectively, and low NMR frequencies).

In all cases the dopant was of a metal-salt form, but the doping metal and halide varied. The $NaAlH_4$ was either made from a wet chemistry process or was purchased and then purified. Many of these wet and dry methods of making and purifying $NaAlH_4$ are outlined in a highly referenced publication[7].

Dopants were added by ball milling the dopant-metal salt into the pure $NaAlH_4$ at the few mol% level. Typically, doping was done at the 2 or 4 mol% level, but a couple 6 mol% samples were available very early in the *in situ* work. Aluminum metal can be present in the sample material before any hydriding reactions are performed on the material. In some $NaAlH_4$ studies, additional Al powder is added later in the process to improve reversibility[38], [39]. However, this was not done in the synthesis of the samples used in this work. The aluminum that is present in some of the doped samples comes from the original $NaAlH_4$—a type of reaction between the $NaAlH_4$ and the catalyst that

can cause this is shown in Equation 5.2 later (Chapter 5.3.2). Samples used were prepared with $TiCl_4$, $TiCl_3$, $ScCl_3$, ScI_3, ScF_3 or $ScBr_3$. By far, the most frequently used sample type was $NaAlH_4$ doped with 4 mol% $ScCl_3$.

These samples have a grey to black color (depending on the amount of dopant—pure $NaAlH_4$ is white) and are very fine and "sticky". The grain size should be on the order of ~60 nm after milling and larger upon cycling (~60-80 nm). The purity of these samples was sometimes checked with XRD by our collaborator at NIST for some of the earlier synthesized samples. These doped samples would sometimes slightly de-hydride while in storage, but this was never the case with the undoped material.

2.10.2 Undoped $NaAlH_4$

Undoped alanate was acquired either from U. of Hawaii or was purchased from Sigma Aldrich. The material received from U. of Hawaii was synthesized in the same manner as the doped material, only without adding dopant. The material purchased from Aldrich was "technical grade" $NaAlH_4$ powder (90%). A particle size could not be found for this, but it seemed similar to or slightly larger than the samples received from U. of Hawaii. In any event, the powder x-ray diffraction peaks were sharp.

2.10.3 Other Sample Materials

Other types of samples were also acquired and used. A sample of undoped Na_3AlH_6 and a sample of Na_3AlH_6 doped with 3.33 mol% $ScCl_3$ were both received from U. of Hawaii. The undoped and doped Na_3AlH_6 were synthesized and purified so that

only the hexahydride was present in the material. No Al metal powder was added—this would have allowed the sample to form $NaAlH_4$ under pressure and temperature.

Doped and undoped Al metal powder was additionally used. 99.97%, 325 mesh, uncoated aluminum powder was purchased from Alfa-Aesar and used "as bought" for high-pressure hydrogen temperature cycling. The doped Al metal sample came from U. of Hawaii. The doped aluminum powder was synthesized by first mechanically milling aluminum powder with 4 mol% $ScCl_3$ under hydrogen pressure but not elevated temperature, avoiding the creation of AlH_3 in the sample material.

Samples of aluminum halides were additionally used at one point. All of these samples were powders and used "as bought". $AlCl_3$ (99.99%), AlI_3 (99.999%), and AlF_3 (≥99.9%) were purchased from Sigma-Aldrich. $AlBr_3$ (99.997%) was purchased from Alfa-Aesar.

CHAPTER 3:

NMR TECHNIQUES AND BASICS

This chapter contains a brief overview of a few concepts in nuclear magnetic resonance (NMR) and some of the acquisition and analysis techniques that are used in this thesis. The static magnetic field, H_o, is always assumed to be along the z-axis.

3.1 NMR Basics

3.1.1 Introduction

Nuclei possess a property called nuclear spin. The nuclear spin quantum number is denoted, I. The total nuclear spin is the (vector) sum of the individual spins possessed by the nucleons that compose the nucleus. Protons and neutrons are both spin-1/2 and so nuclear spins can possess integer or half-integer spins (I = 0, 1/2, 1, 3/2, etc.). The magnetic moment of the nucleus is proportional to the nuclear angular momentum by a proportionality constant, γ, called the "gyromagnetic ratio". Each type of nucleus has a different γ. In the presence of a magnetic field, H_o, the magnetic moment will precess about the field at a frequency, ω_o. The frequency of precession is called the "Larmor frequency" and is given by the relation,

$$\omega_o = \gamma H_o \qquad 3.1$$

where the Larmor frequency, ω_o, is different for each type of nucleus (because γ is unique to each type of nucleus).

The Hamiltonian for a nuclear spin **I** interacting with an external magnetic field **H** is (traditionally, the external magnetic field, H_o, is oriented along the z-axis.):

$$\mathcal{H} = -\gamma\hbar\mathbf{H}\bullet\mathbf{I} = -\gamma\hbar H_o I_z \qquad 3.2$$

where the I_z states can have the value I, I-1, …, -I.

This is a resonance phenomenon. If, for example, we placed hydrogen (^{1}H), which has $\gamma/2\pi$ = 42.58 MHz/T, into a 10 T field, from Equation 3.1 we get f = 425.8 MHz. Thus, NMR is typically performed in the radio frequency (r.f.) range of the electromagnetic spectrum.

For a macroscopic sample in a magnetic field the spins are distributed among the I_z levels according to the Boltzmann factor, $e^{-E/kT}$, and a net magnetization is established. If we look again at the example of hydrogen atoms, a spin-1/2 nucleus, the ratio of populations between the lower energy state, $N_{\uparrow}$ (where the ↑ represent "spin-up"), and upper energy state, $N_{\downarrow}$, would be:

$$e^{-\Delta E/kT} = e^{-\gamma\hbar H/kT} = \frac{N_{\downarrow}}{N_{\uparrow}} \qquad 3.3$$

which differs only very slightly from one (having a value of about 0.99992) in a 11.7 T field at room temperature.

3.1.2 T_1

Without the presence of a magnetic field, the spins in a sample are evenly distributed between the (2I+1)-degenerate levels. When the sample is placed in the magnetic field, the nuclear spin energy levels are split (Zeeman splitting), and the evenly

distributed spins tend toward the new Boltzmann equilibrium. Energy must be exchanged with the surroundings, or "lattice", in order for the individual nuclear moments to relax to a lower energy level. Depending on the system, energy exchange with the lattice can happen by many different pathways like molecular interactions, or dipolar and quadrupolar interactions, or interactions with electrons.

The return to the Boltzmann distribution and the establishment of a net magnetization typically follows an exponential time dependence and is characterized by time T_1—called the "spin-lattice" or "longitudinal" relaxation time—as shown below.

$$M_z(t) = M_o(1 - e^{-t/T_1}) \qquad 3.4$$

$M_z(t)$ is the magnetization along the direction of the external magnetic field (z-axis) of the sample as a function of time, where M_o is the equilibrium magnetization.

3.1.3 T_2

As the sample relaxes to the Boltzmann equilibrium, a net magnetization is established. If the magnetization is somehow tipped away from the z-axis it will precess according to the Larmor frequency about the external magnetic field.

When the magnetization is pictured in a frame rotating with the Larmor frequency, the magnetization initially appears along the z-axis. If a small, rotating, r.f. field, H_1, is applied *on resonance* with the Larmor frequency along an axis perpendicular to the static field (say, the x-axis), then in the rotating frame H_1 appears as a constant field along the x′-axis. Now the net magnetization precesses about H_1 at $\omega_1 = \gamma H_1$, and the magnetization is tipped away from the static field toward the y-axis. (The magnetization is said to nutate about the r.f. field H_1.)

H_1 is supplied by placing the sample in a coil inductor (the NMR coil) oriented perpendicularly to, or at least with a component perpendicular to, the static magnetic field, and driving a sinusoidal current through the coil at the Larmor frequency. By controlling the duration of the r.f. H_1 pulse, the angle through which the magnetization nutates with respect to the static field can be controlled. A pulse of sufficient duration to rotate the net magnetization 90^o with respect to the static field is appropriately called a "90^o-pulse" or a "$\pi/2$-pulse". Or if the pulse is left on twice as long, the magnetization will rotate through 180^o, completely inverting the Boltzmann equilibrium magnetization (called a "180^o-pulse" or "π-pulse"). The duration of a 90^o-pulse depends on the power of the r.f. amplifier and configuration of the probe tank circuit (relating to H_1), as well as the nucleus of interest (relating to γ); typically the 90^o pulse time is on the order of microseconds.

After the magnetization is rotated into the xy-plane and H_1 is turned off, the magnetization continues to precess about the static field at the Larmor frequency, ω_o. The net magnetization is freely precessing in the xy-plane, so it will induce a Larmor frequency r.f. voltage in the NMR coil, which is detected by the spectrometer. This signal detected by the spectrometer is called a free-induction decay (FID) and is in many cases represented by an approximately exponential decay,

$$G(t) \propto e^{-t/T_2} \tag{3.5}$$

which, under Fourier transform, transforms to a Lorentzian function,

$$G(\omega) \propto \frac{1/T_2}{(1/T_2)^2 + \omega^2} \tag{3.6}$$

with full width at half maximum (FWHM) of $1/\pi T_2$ (in Hz). Because the FIDs are often well approximated by exponential decays, the spectra typically take the form of Lorentzian lineshapes, but there are many exceptions.

The characteristic dephasing time in the xy-plane, T_2 (or "spin-spin" or "transverse" relaxation time), varies depending on the local environment of the spins. The local magnetic field, H_{loc}, across a sample is typically not uniform, and causes slight variations in the precession frequencies within the sample, leading to dephasing. Some examples of H_{loc} modifications are by an inhomogeneous static magnetic field, or from inhomogeneous field due to magnetic susceptibilities in and around the sample, or from dipolar interactions of spins with other spins.

In the case of slowly moving or stationary atoms, an atom spends essentially all its time in one local environment and "sees" only one value of H_{loc} and precesses at that ω_{loc}. The result of all the different spin magnetizations, each with its own ω_{loc}, is faster dephasing in the xy-plane (a shorter T_2), and thus a broader spectral peak. Spins which undergo rapid motion will sample many different H_{loc}s and precess at an average ω_{loc}, which is close to ω_o. Many spins in this case are precessing at the same average ω_{loc}, so they have a longer coherence time in the xy-plane (longer T_2), and produce a narrower spectral peak. This effect is called "motional narrowing". Of course, the averaging effect is dependent on the motion being on a time scale that is faster than the NMR timescale, $\sim 1/\Delta\omega_{loc}$. If the motions are slower than the NMR time-scale, it is called the "rigid lattice regime".

Another effect that modifies the local field at the nucleus comes from the orbital effects of nearby electrons. Static magnetic field induces currents in the electron cloud. This produces a shielding effect on the nucleus that scales with the magnitude and direction of the static field with respect to the electron cloud. This is called "chemical shift". The effect depends on the position of a nucleus within a molecule (so the chemical shift is different for the three kinds of H in ethanol, OH, CH_2, CH_3). Additionally, the shift of a spin resonance depends on the orientation of a molecule in the static field, known as chemical shift anisotropy or "CSA". Since the shifts scale (in frequency units) with the magnitude of the static field, the shifts are stated in ppm; i.e. the difference in frequency from a chosen standard reference chemical divided by the Larmor frequency of that reference. When the shifts are stated this way, then they will remain the same value for all field strengths.

3.2 Data Acquisition and Analysis Techniques

3.2.1 Left-shift

In the alanate system there are many different chemical species that can arise during the hydriding reaction (not all relating directly to the release or absorption of hydrogen), and it is important to be able to distinguish the different species. Because the method used is static NMR, there are a couple of analysis techniques that are applied to separate out the differing reaction components and products.

After the magnetization is tipped into the xy-plane—at which time the decaying FID signal in the NMR coil can be acquired—the multiple decaying components lead to a

superposition of the different components. At the beginning of the multi-component FID, all components are present at their maximum amplitude. As we look further and further out along the time axis, the components with shorter T_2s decay to zero faster and only the components with longer T_2s remain.

One technique used in this thesis is left-shifting the FIDs to filter out broader components and search only for narrow components. As discussed in the previous section, shorter T_2s correspond to broader lineshapes. By taking an FID and shifting the data to the left beyond where the faster T_2 components have already decayed to zero, the resulting modified FID will contain only slower decaying T_2 components, i.e. narrower (often from more mobile species) spectral peaks.

An example from ^{1}H NMR is shown below in Figure 3.1. The FID after a 90^o pulse is shown, **(a)**, with its corresponding spectrum from Fourier transform, **(b)**. The FID shown in **(a)** is from a sample with three species present, two of which are $NaAlH_4$ and Na_3AlH_6. For demonstration purposes an FID from a pure sample of $NaAlH_4$ is shown in **(c)** and an FID from a sample of pure Na_3AlH_6 is shown in **(d)**. As can be seen, both $NaAlH_4$ and Na_3AlH_6 have shorter T_2s (and, correspondingly, each have broader spectral peaks). The FIDs in frames **(c)** and **(d)** have decayed to zero by 70 μs (a red line is drawn on the FIDs to denote t = 70 μs, which will be t' = 0 *after* the left-shift). If the FID in **(a)** is left-shifted by 70 μs, as shown in **(e)**, then the resulting spectrum, **(f)** will contain only the sharp peak.

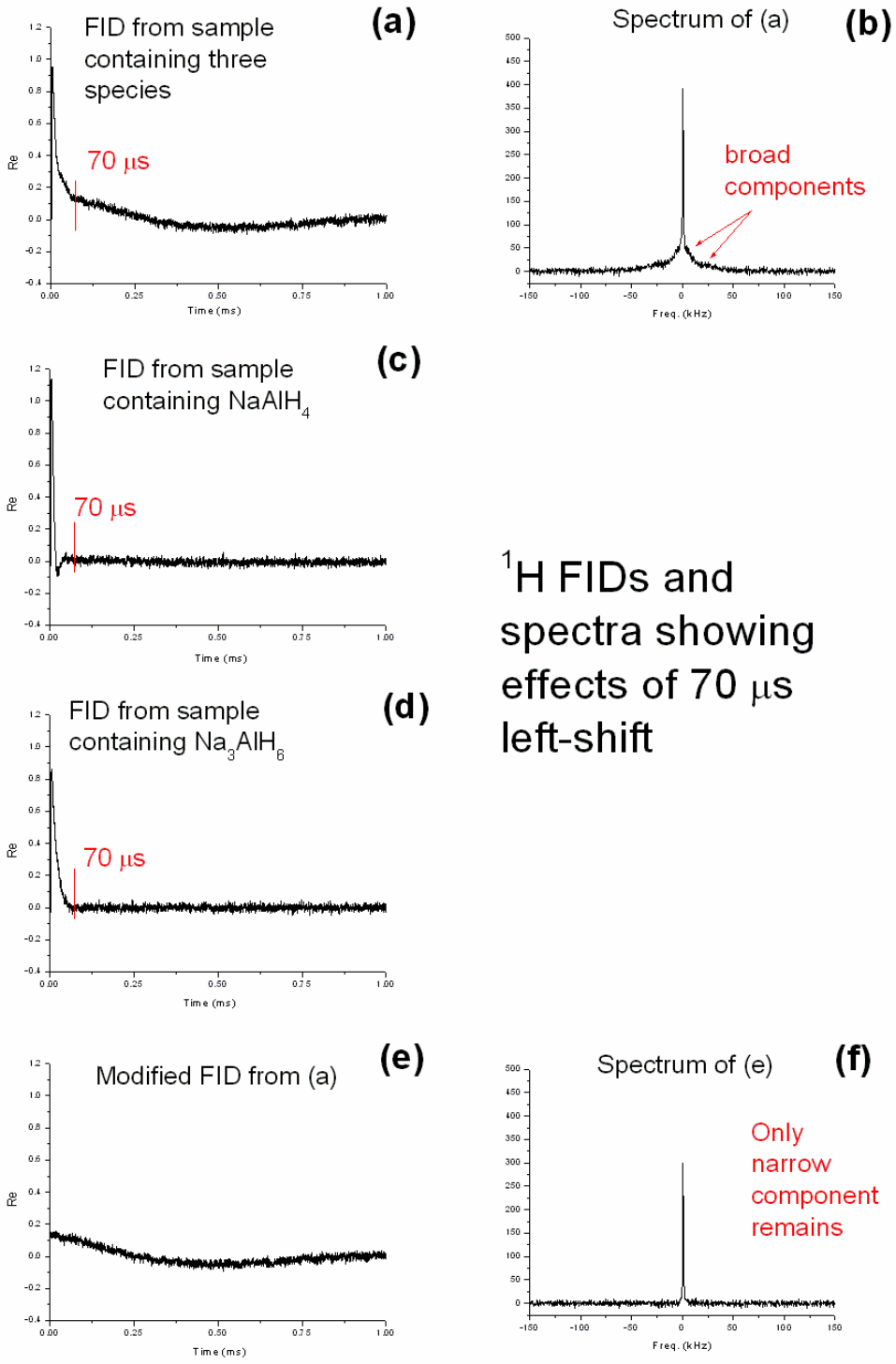

Figure 3.1: ^{1}H FIDs and spectra from a sample that contains three different chemical components. This demonstrates the effects of left-shifting FIDs to filter for highly mobile species in multi-component systems. **(a)** shows FID of sample that contains 3 components: 1) highly mobile species (long T_2), 2) Na_3AlH_6 (shorter T_2), and 3) $NaAlH_4$ (shortest T_2). **(b)** shows resulting spectrum from FID in (a). **(c)** FID of pure $NaAlH_4$. **(d)** FID of pure Na_3AlH_6. **(e)** The resulting FID after (a) is left-shifted 70 μs. **(f)** The spectrum corresponding to (e), now only showing the narrow component.

An example of a spectrum resulting partially from the application of the left-shift technique to a ^{27}Al FID will be shown later in Figure 5.10, Chapter 5.2.4.

It needs be mentioned that this technique should be used with caution because there are negative consequences to using left-shifted FIDs to produce spectra. FIDs are not all perfect exponential decays, and may have other forms. In these cases the lineshape in frequency space might be distorted. If, for example, an FID has a more Gaussian shape—which is flat at the beginning of the decay—a left-shift will cut out the flat portion. When this modified FID is Fourier transformed, the spectral peak will be distorted from Gaussian, and the width of the spectral peak will not give the true width of the resonance. And there is a phase shift proportional to frequency and delay-time: $\Delta\phi = t_{leftshift}\omega_{offset}$, called the "linear phase correction".

3.2.2 Fast Recycle Delays

A second acquisition technique was sometimes applied to filter for highly mobile species during the alanate hydriding reactions. Most of the data acquired for the spectra in this thesis are generated by single effective 90^{o}-pulse FIDs (the meaning of "effective" 90^{o}-pulse will be explained further in the following section). A pulse, acquire, wait, scheme was employed where the wait time between pulses, referred to as the "recycle delay", was used in a way to minimize the signal from species which have longer T_1s. A species undergoing rapid motion is generally expected to have a faster T_1, and being able to distinguish this from other species *in situ* is important to finding such a species that might be buried in a background of other signals. The application of faster recycle delays was used much more frequently at the beginning of the study. Once such a species was

found, it became more advantageous to allow the entire spectrum to relax (to get the true relative spectral intensities), and the technique was used less.

A 90^{o}-pulse destroys any magnetization along the z-axis. Let's say a 90^{o}-pulse is applied every $t = \tau$. This means that after each pulse, the magnetization along z is allowed to build back toward equilibrium for a duration of τ before the magnetization along z is destroyed again. From Equation 3.4 we know how much the magnetization rebuilds along z:

$$\frac{M(\tau)}{M_o} = (1 - e^{-\tau/T_1}) \qquad 3.7$$

This is the recovery percentage as a function of the ratio τ/T_1. If we have a small τ/T_1, $M(\tau)/M_o \approx (1 - (1 + -\tau/T_1) = \tau/T_1$. For $\tau \sim 10^{-1}$ s, and for a given species $T_1 \sim 10^0$ s or 10^1 s (typical for this study), then $M(\tau)/M_o \approx 1\%$ to 10%. The species is not fully recovered and only a small portion of the true (fully relaxed) signal is seen. But for τ/T_1 large, say τ equals several T_1 or more, a given species will fully relax during τ, then $M(\tau)/M_o \approx 1$ and all the signal is seen. In other words, when the recycle delay is much shorter than T_1 for a given species, the signal from that species is suppressed; but for short T_1 species there is no effect upon the signal.

3.2.3 Central Transition Excitation

A nucleus with $I > ½$ has an electric quadrupole moment. This comes from an asymmetry in the distribution of electric charge in the nucleus. The quadrupole moment becomes important in the presence of an electric field gradient (EFG). The nuclear

electric quadrupole moment of the nucleus will interact with the surrounding electric field potential and modify the Zeeman levels. We note the EFG is zero in cubic symmetry. The quadrupolar interaction is treated as a perturbation to the Zeeman interaction. From Abragam[40], below are given the results—to first-order and with a uniaxial EFG tensor—of the energy levels where $E_m^{(p)}$ is the energy contribution to the m'th level to perturbation order p (so $E_m \approx E_m^{(0)} + E_m^{(1)}$):

$$E_m^{(0)} = -\gamma\hbar H m = -h\nu_L m \qquad 3.8$$

$$E_m^{(1)} = \tfrac{1}{4}h\nu_Q(3\mu^2 - 1)(m^2 - a/3) \qquad 3.9$$

For simplicity Abragam defines the following as,

$$\nu_Q = \frac{3C_Q}{2I\,(2I-1)},\quad a = I\,(I+1),\quad \mu = \cos\theta,\quad \nu_L = \frac{\gamma H}{2\pi} \qquad 3.10$$

$E_m^{(0)}$ shows the Zeeman splitting. For the case of ^{27}Al (spin-5/2), there are energy levels for m = -5/2, -3/2, -1/2, +1/2, +3/2, and +5/2. We recognize ν_L as the Larmor frequency in Hz (from Equation 3.1), and note that the 2I transitions of $\Delta m = \pm 1$ are degenerate in frequency to zero'th order. All transitions resonate at the Larmor frequency and contribute to a central peak at ν_L,

$$\nu_L = \frac{E_{m-1}^{(0)} - E_m^{(0)}}{h} \qquad 3.11$$

The quadrupole interaction enters in the first order perturbation, $E_m^{(1)}$. C_Q is called the "quadrupole coupling constant" and is in units of Hz. C_Q depends on the

electric environment at the nucleus as well as the quadrupolar moment of the nucleus of interest, and is typically found experimentally. θ is the angle between the unique principal axis of the EFG tensor and the static magnetic field. The quadrupolar interaction splits the degeneracy of the 2I $\Delta m = \pm 1$ transitions, and we now have a different resonance frequency, $\nu_m = \nu_L + \nu_m^{(1)}$, for each pair of neighboring energy levels where,

$$\nu_m^{(1)} = \frac{E_{m-1}^{(1)} - E_m^{(1)}}{h} = \nu_Q (½ - m) \frac{3\mu^2 - 1}{2} \qquad 3.12$$

We see that to first order the quadrupolar interaction shifts the Zeeman levels by m^2 (Equation 3.9) so that the ±m energy levels shift the same amount and in the same direction, and that the $m = \pm 1/2$ central transition frequency (for half-integer spins) does not change (Equation 3.12).

For the case of what is called the "selective excitation", which is to say $\nu_Q >> \nu_1$, the quadrupole interaction also increases the nutation rate about the r.f. field—which depends on I and m—by a factor of A as compared to a nucleus where the quadrupolar interaction is zero or averaged away; where A is the shift operator matrix element which describes the operation of a rotating magnetic field, H_1, on the populations and coherences of the m-levels[41]-[43],

$$A = [I (I + 1) - m (m + 1)]^{½} \qquad 3.13$$

(where m refers to the upper state, which is lower value of m). E.g., for the central transition, $m = -1/2 \leftrightarrow +1/2$, of ^{27}Al (so I = 5/2 and m = -1/2), A = 3. This also leads to unequal peak intensities because the $|\Delta m| = 1$ *satellite* coherences are less efficient than

the *central* coherence at producing an NMR signal (the ratio of the intensities of the lines go as A^2 and the biggest A is for m = -½). Additionally the central transition will be a fraction of the intensity of the unsplit line such as one would observe in a solution, where the time average $\nu_Q = 0$. Again, for ^{27}Al, the ratios of the intensities of the satellites and central transition is 5:8:9:8:5; so the central transition will have a relative intensity of 9/35. However, if only the central transition is excited, then the system can be treated like an effective spin-1/2[44], [45]. This is the case of $\nu_Q >> \nu_1$, or selective excitation pulses. If T_{90} is the pulse length of a 90°-pulse of a quadrupolar nucleus in an environment where the quadrupole interaction vanishes (as in a liquid), then by applying a pulse of $T_{90}^{eff} = T_{90}/A$ to the nucleus in an environment where a large quadrupole splitting is present, one maximally excites the central transition only. This is called an "effective" 90°-pulse (for the effective spin-1/2).

With the exception of ^1H (I = ½), the nuclei looked at in this thesis are quadrupolar. The 90°-pulse times were found on aqueous tune-up samples for each type of nucleus in each probe (Chapter 2.9). Then the 90°-pulse times were divided by A for each type of nucleus to find the effective 90°-pulse time for use in the single-pulse excitation spectra as well as the pulse sequences used for relaxation time studies. For reference the spin, 1/A, and—for $NaAlH_4$—the location of the large cusps in the satellite transitions (given as $\Delta\nu$ from the Zeeman Larmor frequency) are shown in Table 3.1 below.

Nucleus	Spin	1/A (for –1/2↔+1/2)	Δν (from ν_L) for $NaAlH_4$
^{27}Al	5/2	1/3	±5/2↔±3/2: ± 460 kHz Refs. [46] & [47]
			±3/2↔±1/2: ±230 kHz Refs. [46] & [47]
^{23}Na	3/2	1/2	±3/2↔±1/2: ±35 kHz Refs. [46] & [47]
^{45}Sc	7/2	1/4	—

Table 3.1: Spin, 1/A for the central transition, and location of the large cusps in the satellite transitions (given with respect to the Larmor frequency, ν_L, in kHz) for ^{27}Al, ^{23}Na, and ^{45}Sc for $NaAlH_4$.

3.2.4 Magic Angle Spinning and Cross-Polarization

Although the author does not do magic angle spinning (MAS) or cross-polarization (CP) NMR, a brief explanation is included here because there this thesis includes work in MAS and CPMAS done by our collaborator, Son-Jong Hwang at Caltech.

Motion can average out interactions like dipolar coupling and chemical shift anisotropy—interactions which are dependent on orientation. When these interactions are motionally averaged, the lineshape is narrowed. Powders have a distribution of fixed orientations and typically have much broader lineshapes that make identification of closely spaced species difficult. However, this problem can be overcome by using MAS NMR.

Between two dipole moments, the interaction term is of the form,

$$\frac{1}{r^3}\ (3\cos^2\theta - 1) \qquad 3.14$$

where r is the dipole-to-dipole separation and θ is the angle between the static field, H_o, and the vector between the two dipoles. Notice that if $\theta = \theta_M$ (the "magic" angle) so that $3\cos^2\theta_M - 1 = 0$, then this term vanishes. If we could somehow cause all the dipole inter-nuclear vectors to be effectively oriented at θ_M (~54.7°) to the magnetic field, then the dipolar broadening would vanish in the powder sample. This can be cleverly achieved by physically spinning a sample with the axis of rotation oriented at angle θ_M from H_o— provided the rate of rotation is greater than the linewidth (so that only the time averages of the quantities matter). In fact, any interaction that carries the angular dependence term $3\cos^2\theta - 1$ will vanish under MAS. This includes the first order quadrupolar interaction (Equations 3.9 and 3.12). Under fast MAS, the following are averaged to zero: dipole-dipole interactions, CSA, and 1st-order quadrupole (but actually this is often so large that it is hard to spin fast enough).

MAS can be used in conjunction with a technique called cross-polarization (CP). In cross-polarization the polarization of one type of nucleus is transferred to another type of nucleus by taking advantage of the dipolar coupling, which is a "through-space" coupling. The local magnetic field experienced by one spin is modified by the dipolar field produced by a nearby second spin, and vice versa. If the local field due to the dipolar field of the near-by second spin is modulated at the Larmor frequency of the first spin, it can cause transitions. To conserve energy, one pathway this can happen is by

mutual spin flip. I.e. the first spin undergoes $\Delta m = +1$ and the second spin undergoes $\Delta m = -1$.

If we are talking about two different kinds of nuclei (γ_I and γ_S) then the separation of the energy levels of the two different types of nuclei are not equal, so flip-flops can not occur. Somehow, the effective frequencies must be made equal. By Equation 3.1, the two different nuclei precess at two different rates (ω_I and ω_S) for a given applied r.f. field. In a double-resonance probe two different r.f. fields (H_I and H_S) can be applied such that the nutation frequencies ω_I and ω_S are equal: $\omega_I = \omega_S$. This is called the Hartmann-Hahn condition, and is expressed as:

$$\gamma_I H_I = \gamma_S H_S \quad \text{or} \quad \frac{\gamma_I}{\gamma_S} = \frac{H_S}{H_I} \qquad 3.15$$

In a sample, one type of nuclei, say ^1H, is excited by a 90^o r.f. pulse. The r.f. transmitter is left on (such that M_H is now parallel to its H_1 field, called "spin-locking") and the second r.f. transmitter for the second type of nuclei, say ^{27}Al, is simultaneously turned on such that H_1^H and H_2^{Al} satisfy the Hartmann-Hahn condition. This allows the system to couple, transferring spin magnetization parallel to the effective field in the rotating frame back and forth between ^1H and ^{27}Al. The time the two transmitters are left on is called the "contact time". During the contact time mutual spin flips transfer polarization from ^1H to ^{27}Al. This is denoted ^{27}Al-$\{^1H\}$ CP. After the transmitters are turned off the ^{27}Al NMR can be observed as an FID.

The dipolar interaction falls off as $1/r^3$ (Equation 3.14) and so only those spins that are in close proximity will readily undergo the mutual spin flip. Species that are not

hydrogenated, like the ^{27}Al spins in Al_2O_3, will not be able to transfer polarization from the ^{1}H to the ^{27}Al, unlike a species such as AlH_4^{-1} where the Al-H bond holds the two spins in close proximity. By this way, observing the ^{27}Al NMR after ^{27}Al-$\{^{1}H\}$ CP can indicate whether or not an ^{27}Al resonance peak is associated with hydrogen.

3.3 Relaxation Measurements

3.3.1 Saturation Recovery

Saturation recovery is a pulsing technique that is used to measure T_1. This is done by first destroying all the magnetization along the z-axis and waiting for some time, τ, and then inspecting the z-magnetization. By plotting the recovering amplitude versus the wait time, τ, and by fitting to an exponential recovery (Equation 3.4) the characteristic time, T_1, can be measured.

As mentioned above in Chapter 3.2.2 (on the usage of fast recycle delays), a perfect 90^o-pulse destroys the magnetization along the z-axis. But if the 90^o-pulse is not perfect, then some component is left. A good measurement of T_1 would require (or at least be easier to analyze) that the initial magnetization along z is zero. To avoid any error in the initialization of $M_z = 0$ due to errors in setting the 90^o-pulse time, a "saturation comb" is used. This is a string of saturating pulses (90^o pulses) separated by some time τ_{sat}, such that $T_2 < \tau_{sat} < T_1$. This gives time for the magnetization in the xy-plane to dephase while not giving enough time for the z-magnetization to recover between 90^o-pulses. 10 to 20 pulses (or more, as needed) can be used in this comb, depending on how close the saturating pulses are to a true 90^o-pulse. The magnetization

is completely destroyed after such a comb. After the saturation comb the magnetization is allowed to recover for a wait time, τ_{wait}, followed by a single 90^o inspection pulse, which tips whatever magnetization has recovered along z into the xy-plane where the FID can be acquired and the amplitude of the signal measured. τ_{wait} is varied and the recovery is plotted and fitted (Equation 3.4) to find T_1.

3.3.2 Inversion Recovery

Inversion recovery is a second method for measuring T_1 and works by first inverting the magnetization and then inspecting the recovery along the z-axis over time. There can be a couple advantages to this in certain situations. First, for saturation recovery to be successful, T_2 and T_1 must be different enough to get the timing of τ_{sat} correct ($T_2 < \tau_{sat} < T_1$). This works for many solids, but if this condition cannot be satisfied because $T_2 \sim T_1$, then inversion recovery will still work. In addition, the dynamic range of inversion recovery is ideally twice as big because the magnetization recovers from $-M_o$ to $+ M_o$; whereas in saturation recovery the magnetization recovers from 0 to $+ M_o$.

The pulse sequence is initiated by the application of a 180^o-pulse, which inverts the magnetization. Like the saturation sequence, after a wait time, τ_{wait}, a 90^o-pulse tips the magnetization along z into the xy-plane where the FID can be acquired and the amplitude measured. The FID amplitude versus τ_{wait} is plotted and fit to the recovery relation:

$$M(\tau_{wait}) = M_o(1 - Be^{-\tau_{wait}/T_1}) \qquad 3.16$$

where B is usually adjustable to account for inversion-pulse imperfection; B = 2 corresponds to an ideal inversion-pulse.

One potential problem with inversion recovery is that between each 180^o-τ-90^o sequence the magnetization must be allowed to fully recovery before the next 180^o-τ-90^o can be applied; as opposed to the saturation recovery sequence, which zeros the magnetization as soon as the FID is captured by the next saturation comb. So there is no sense in allowing M to recover, since M will then be destroyed again, and the experiment can be conducted more quickly (by not waiting for recovery between recycles). Another potential problem is incomplete inversion. In the saturation sequence an imperfect 90^o-pulse can be compensated for by repetition of the 90^o-pulse in the saturation comb, but this cannot be performed in the inversion recovery sequence. Furthermore, the inversion pulse is twice as long as the saturation pulse, and so it excites a frequency width half as big. It is best to keep the specific species under investigation exactly on resonance, and perform inversion recovery for each individual species in the spectrum, which additionally increases the experiment time.

3.3.3 90^o-90^o Echo

To measure T_2 (transverse relaxation) one must be able to measure the initial amplitude of the FID accurately. In theory, T_2 could be taken by observing the envelope of the FID. However the initial decay of the FID is obscured in a couple different ways. The FID effectively begins near the middle of the excitation r.f. pulse and the beginning of the FID is obscured by the second half of the r.f. pulse. In addition, after the r.f. pulse there is a period of time in which the energy in the tank circuit is dissipated, called the

"ring-down" time, during which the FID is further obscured. The combination of these effects can mask the first 5 to 10 μs of an FID, depending on the pulse lengths and tank circuit components. For solids, which have large dipolar interactions, T_2 is short and the ring-down time may be a very significant fraction of the total FID decay time, making an accurate measurement impossible.

By applying an echo sequence, the peak of the echo (effectively the new zero of time, regarding the echo as back-to-back FIDs) may be shifted out away from the dead time. One such sequence is performed by a pair of 90^o-pulses separated by a wait time of τ. An echo, which has an envelope shape the same as the FID, will form a time τ after the second 90^o. The first pulse tips the magnetization into the xy-plane, where it begins to dephase over time τ. The second pulse, applied at time τ, acts to refocus the spin evolution in the xy-plane at a time 2τ after the first pulse. When τ is varied, the amplitude of the echo decays by:

$$M(2\tau) = M_o e^{-2\tau/T_2} \qquad 3.17$$

T_2 can be measured by plotting the amplitude of the echo versus 2τ, and fitting to the above equation.

Moreover, the dephasing time may be decreased by local field inhomogeneities from imperfect static field and distortions of the local magnetic field from susceptibility variations around or in the sample. If the local field varies slowly over the sample, then spins in one area of the sample experience a slightly different H_{loc} than spins in a different area. Groups of spins in these differing areas of the local field, called isochromats, precess at slightly different times. But inside each isochromat dephasing from spin-spin couplings happen with the characteristic time, T_2. The superposition of

the different precession frequencies from the different isochromats causes the FID to decay faster than T_2. The echo refocuses the spin evolution of each isochromat, so that the true T_2 can be measured. Many static broadenings (that contribute to the decay of the FID) like inhomogeneous H_o, static susceptibility effects, chemical shift and some quadrupole effects will not cause decay of the echo envelope. But interactions such as like-spin dipole or unlike-spin dipole if the other spin S is modulated by a fast T_1 or S-S flip-flops will cause the echo to decay.

CHAPTER 4:

IN SITU REACTIONS

The first NMR measurements on $NaAlH_4$ in this study were *in situ* reaction measurements using ^{27}Al NMR. In these studies a de-/re-hydriding reaction would be initiated and NMR taken continuously from before the reaction started until after the completion of the reaction. The pressure over the sample—whether initially a vacuum or an externally supplied H_2 atmosphere—was monitored at all times by a high accuracy pressure transducer. Likewise, the temperature of the sample was continuously monitored by a thermocouple placed just outside the sample tube (see Chapter 2.1.3).

The author will mainly refer to pressure in "psi", but for ease of reference 1 bar = 0.986 atm = 14.5 psi. All pressures are absolute (relative to vacuum).

4.1 Preliminary De-/Re-hydriding Findings

Dehydriding reactions were the initial *in situ* measurements. Typically, for dehydriding runs, the sample would initially be evacuated while at room temperature, to remove any N_2, and then heated. Upon heating, the evolving H_2 gas would build up in the now valved-off sample headspace. The hydrogen pressure would increase over time and finally plateau, indicating that the sample reaction had progressed as far as it would. This may correspond to completion of either or both reaction steps, but the reaction may also plateau earlier due to an inactive fraction of the starting material. Figure 4.1 below shows one such dehydriding run performed at 180^{o}C. Data acquisition was initiated

before the heat was turned on and continued through the end of the reaction. The data was collected into "blocks". Each block would represent some length of time in which all the incoming spectra were added, for better S/N.

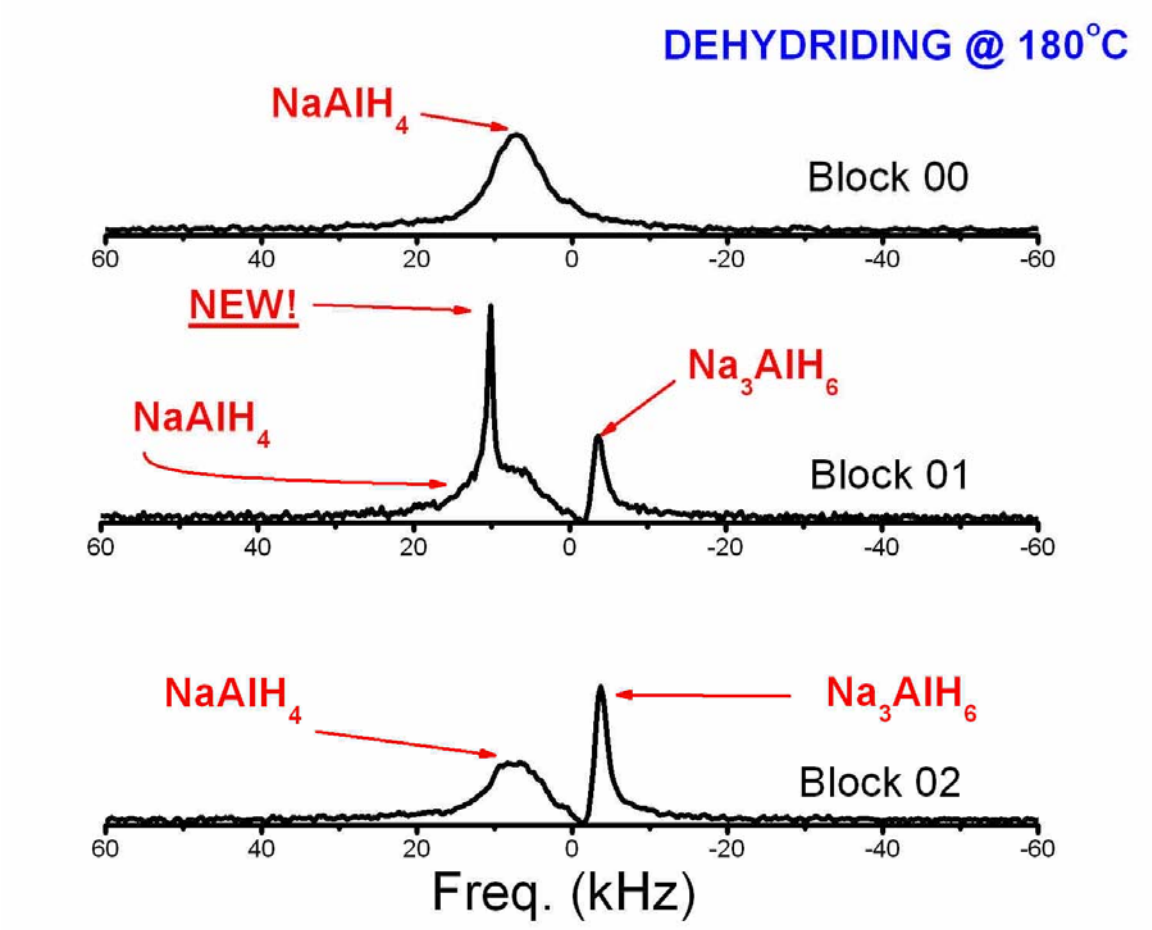

Figure 4.1: First three blocks of de-hydriding spectra taken on a previously unreacted sample. ^{27}Al NMR at 92.276 MHz with $Al(NO_3)_3$ (aq.) reference. Sample was $NaAlH_4$ + 3.18 mol% $ScCl_3$.

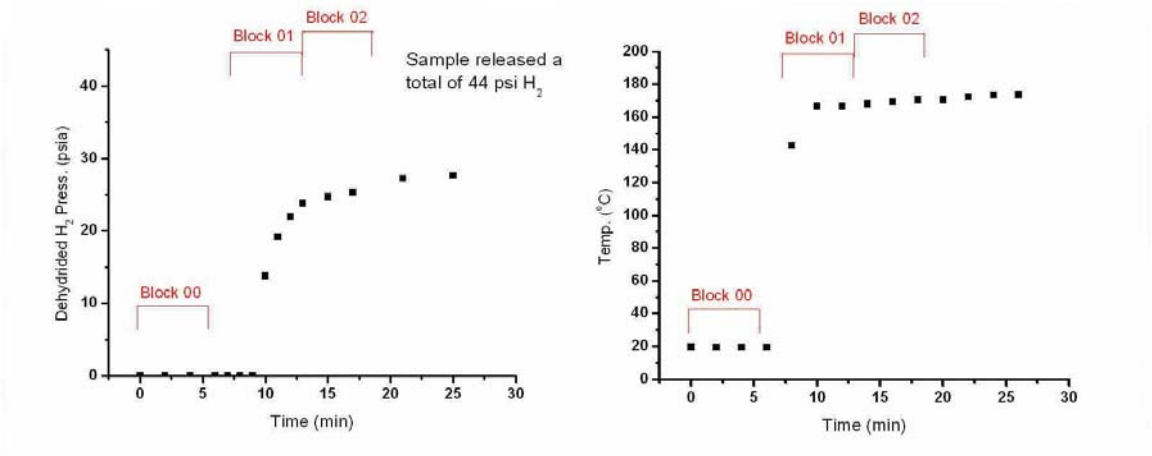

Figure 4.2: Pressure and temperature vs. time for the data shown in Figure 4.1. The labeled brackets indicate the accumulation period in which the individual spectra were added.

For the spectra shown in Figure 4.1, each block represents ~6 min of data accumulation of FIDs following 90^{o} (effective nutation angle) pulses every 0.2 sec. That is, Block 00 is the spectra added from 0 to 6 minutes, Block 01 is 7 to 12 minutes, and Block 02 is 13 to 18 minutes. Figure 4.2 shows the released H_2 gas pressure (from de-hydriding) and temperature vs. time, where the red brackets indicate the periods over which the accumulated spectra were grouped and added. The pause between block 00 and 01 is when the temperature controller was switched on and the automatic data acquisition program initiated.

Block 00 shows a single, broad peak corresponding to $NaAlH_4$. After taking the spectrum in Block 00, the heat is turned on and the automated data acquisition program on the computer initiated. The sample rapidly heats to near 180^{o}C and begins to release hydrogen gas during Block 01 (Figure 4.2). Block 01 still shows the broad $NaAlH_4$ peak, but there are two new peaks: one at -43 ppm (-3.7 kHz), and one at +105 ppm (~10 kHz). The -43 ppm peak corresponds to Na_3AlH_6 (as detected in separate experiments on authentic Na_3AlH_6 material) and is expected from the reaction formulae shown in

Equations 1.1 and 1.2. We can see that this peak grows by Block 02, demonstrating that the sample began to decompose, giving off H_2 gas and producing Na_3AlH_6 (-43 ppm) as well as Al metal (off scale at +150 kHz). Additionally, as might be expected, Block 02 shows a reduction in the $NaAlH_4$ peak intensity as compared to that in Block 00.

The narrowest peak that appears in Block 01 at +105 ppm nearly disappears by Block 02 (where it remains as a very small shoulder on the side of the $NaAlH_4$ peak). The +105 ppm peak is coincident with the fastest evolution of H_2 gas (Figure 4.2) and disappears when the reaction has completed. Moreover, it is very narrow, an indication of fast motion (Chapter 3.1.3), and it is Al-bearing. These initial observations fit the proposed theoretical profile of an intermediate chemical species that may mediate the long-range trafficking of Al atoms necessary for the hydriding reaction to take place, as discussed in Chapter 1.2. It is this peak that is the focus of the present thesis work.

The peak locations of the different species and possible products for sodium alanate are listed in Table 4.1 for future reference. Not all of these species are a direct result of the theoretical hydriding process, but could possibly form given the experimental conditions.

^{27}Al NMR Signal Locations		
Al Species	**Peak Location**	**Literature Reference**
Al metal	150 kHz (1640 ppm)	[38], [20]
$NaAlH_4$	8.6 kHz (95 ppm)	[38], [20]
Na_3AlH_6	-3.7 kHz (-43 ppm)	[38], [20]
Al_3Sc	61 kHz (660 ppm)	[48], [49]
Al_3Ti	31 kHz (335 ppm) (I) 23 kHz (253 ppm (II))	[49]
AlH_3 (three phases: α, β, and γ)	550 Hz (6 ppm) **[α]** 740 Hz (8 ppm) **[β]** 1 kHz (11 ppm) **[γ-(I)]** 3.3 kHz (36 ppm) **[γ-(II)]**	[50]
Al_2O_3 (differing coordination)	740 Hz (8 ppm) **[6-fold]** 3.3 kHz (36 ppm) **[5-fold]** 5.9 kHz (64 ppm) **[4-fold]**	[20], [51]
S105, new species	10 kHz (~105 ppm, static)	(this work)

Table 4.1: A list of the approximate peak locations of various Al species for ^{27}Al NMR with respect to $Al(NO_3)_3$ (aq.).

It is during the rapid H_2 pressure increase that the new ^{27}Al peak has the greatest intensity. The author will refer to this new Al species as the "S105" or nominally as the "+105 ppm peak", since it was initially found around +103 to +105 ppm. The sample continued to evolve hydrogen for some time after Block 01, but very slowly, until finally reaching a plateau in pressure. The samples typically never completely de-hydrided for

these experiments, and would leave behind un-reacted tetrahydride as well as hexahydride. This was very typical for the reactions performed here.

This result was repeated multiple times successfully. In fact, it was observed very early on that the higher the dehydriding temperature, the faster the H_2 would evolve, and the more intense the S105 peak appeared. Usually the samples contained two to three hundred milligrams of material, but never more than 350 mg of material. The gas volume of the sample chamber is 11.57 cc (Chapter 2.1.2). This means that if a reaction had completed the first step (Equation 1.1), and after the probe returned to room temperature, a pressure change of 110 to 170 psia would have been observed, depending on the actual mass of the sample. The experimentally observed reactions would normally produce pressure changes of 40 to 90 psia. So these reactions never saw more than 2 wt% reversible H_2, a far cry from the theoretical 5.6 wt%. With temperatures near 170°-180°C, these de-hydriding reactions would take place in minutes, with only one and *rarely* two of the six-minute blocks showing S105.

After the success of the de-hydriding reactions, re-hydriding reactions were attempted. Data was, again, acquired continuously throughout the reaction in the same manner as in the de-hydriding reactions. Here a previously de-hydrided sample would be pressurized with hydrogen gas at or above the equilibrium reaction pressure (at the time, the probe had an upper limit of ~1500 psi H_2) and then the heat turned on. In these reactions the measured H_2 pressure was observed to drop while the sample took-up hydrogen, re-forming $NaAlH_4$. The pressure would again plateau, indicating that the reaction had ceased. The S105 sharp ^{27}Al NMR signal was seen in these reactions as well, appearing strongest during the fastest H_2 up-take, but never as strong as it did

during de-hydriding. This is likely due to the longer reaction times required for re-hydriding. We note that, at this early stage, we had inadequate "over-pressure" driving the rehydriding reaction for the uppermost temperatures.

These experiments and results were highly repeatable and the same samples could be cycled (de-hydrided then re-hydrided) multiple times, generating the S105 in both reaction directions.

4.2 S105 Discoveries

With the discovery of the new ^{27}Al S105 peak, and having become familiar with the operation of the probe and reaction characteristics, the *in situ* operations could be refined and the techniques updated and improved. By lowering the temperatures and thus slowing the reaction speed, in order to extend the lifetime of the S105 signal (up to a couple hours in some extreme cases, albeit the signal amplitude was reduced), and taking shorter (~2 min) data blocks, the experimental parameters could be varied *in situ* and the conditions for which the +105 ppm signal exists tested.

Some of the parameters tested *in situ* were:

1) Vary temperatures in mid-reaction to anywhere in the range of room temperature to 180^{o}C for both re- and de-hydriding reactions.
2) Apply various H_2 pressures on the sample at various temperatures (0 psia to 1500 psia) during re-hydriding reactions.

3) Allowing the H_2 liberated by the sample in de-hydriding to build-up versus continuously evacuating the sample chamber during the reaction for de-hydriding reactions.
4) Attempting to reverse the reaction direction in mid-reaction. (Begin a de-hydriding experiment and when the sample begins to rapidly deliver H_2 gas, add a large over-pressure of H_2 to halt or reverse the reaction.)

It was found that the +105 ppm signal exists with or without the presence of H_2 in the reaction chamber during sample decomposition. Also, independent of the temperature during de-hydriding, the +105 ppm signal appears when reaction begins and disappears when reaction ends—as measured by the evolution of hydrogen gas. Reactions reversed in the middle of de-hydriding would continue to show S105 through the reversal. Furthermore, the faster the alanate takes-up/gives-off H_2, the stronger the +105 ppm signal appears (generally, the higher the temperature used during the reaction, the faster the reaction would proceed).

Undoped material was also subjected to de/re-hydriding attempts. S105 was never found in these trials. This is not a surprise because the undoped material did not de-hydride (and thus, did not re-hydride) at the temperatures used, which were below the melting point.

Finally, and most importantly, it had been noticed that on just a few samples, but not all, at room temperature and after the application of higher hydrogen gas pressures (~1400 psia) there was a very slight signal at +105 ppm left after the reaction had been completed. (Note: this result was the exception to the majority of samples that were reacted).

Figure 4.3 below shows one such relatively rare example. This spectrum comes from an experiment where de-hydriding was performed at 100^{o}C on a sample of $NaAlH_4$ doped with 4 mol% $TiCl_3$. In mid-decomposition, as the hydrogen gas pressure began to rise, the valve on the H_2 supply assembly was opened, suddenly allowing ~1300 psi of hydrogen gas into the sample chamber. The sample then began to re-hydride. Once the reaction had progressed as completely as it would, the heat was turned off and the sample left to cool to room temperature under H_2 pressure. The spectrum shown (Figure 2.2) was taken once the sample had cooled, but before evacuation of the hydrogen gas from the sample volume. The Al metal, AlH_4^{-1}, and AlH_6^{-3} signals can all be clearly distinguished, demonstrating that the sample had stopped evolving before completely re-hydriding. Furthermore, the signal at +105 ppm can be seen as a shoulder on the AlH_4^{-1} peak, even at room temperature. This evidence then offers the tantalizing prospect that a sample with S105 in it could be recovered at ambient temperature and pressure and sent-out for other studies.

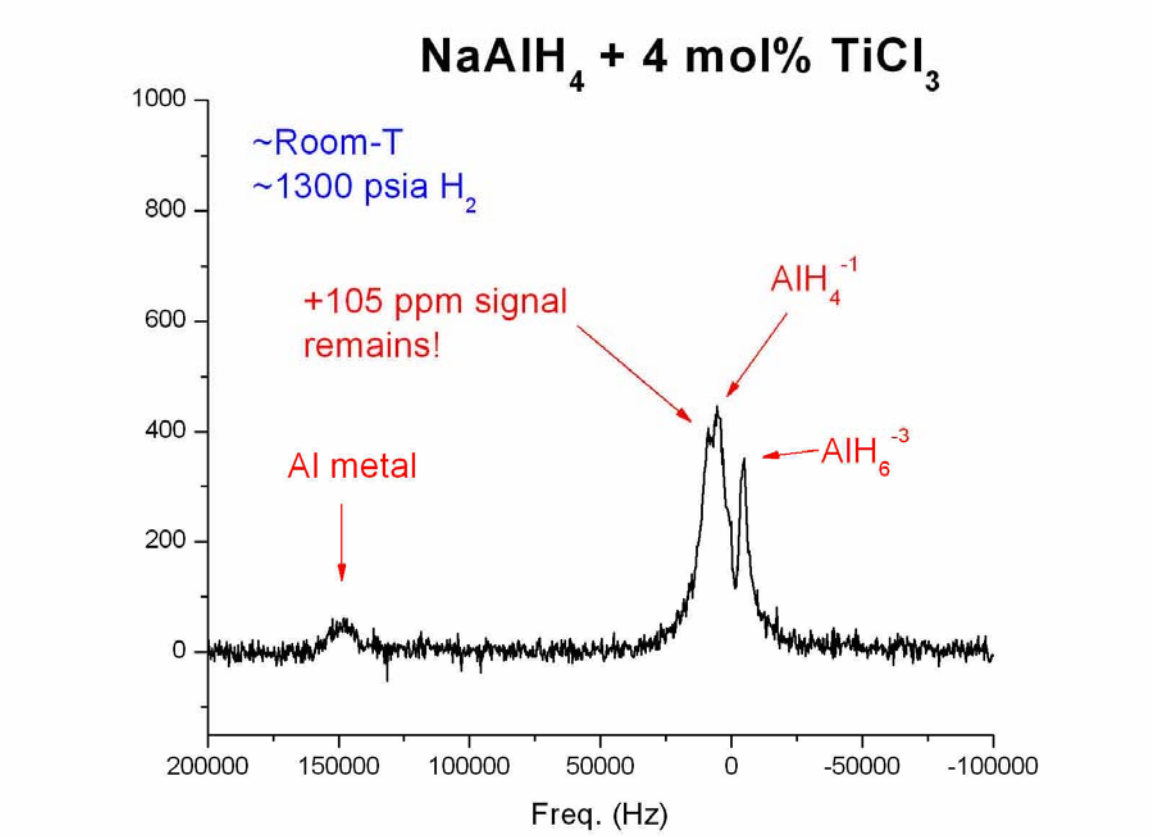

Figure 4.3: ^{27}Al spectrum of $NaAlH_4$ + 4 mol $TiCl_3$, after re-hydriding. The sample has returned to room temperature and 1300 psi H_2 was left over the sample. In these conditions, S105 *still* exists as a small shoulder on the $NaAlH_4$.

4.3 S105 Summary

The exciting new discovery of S105 was worth taking a closer look at since S105 shows a lot of the features expected for a mobile species intimately involved in the chemistry. But, since S105 is transient, it is difficult to make measurements upon. If the signal could be caused to persist for longer periods of time *with greater intensity*, more could be learned about it through NMR.

The new Al species at +105 ppm in ^{27}Al NMR (S105) is seen in both the de-hydriding and re-hydriding directions as well as in both Ti and Sc doped samples but not

in undoped material under normal reaction conditions. The presence of S105 appears to be linked with the evolution of hydrogen gas in these experiments, but can remain (albeit, greatly reduced in intensity) in rare cases once the sample stops taking up H_2 during re-hydriding (interpreted from watching the spectra and the H_2 pressure on the sample). It was possible, then, that greater re-hydriding pressures could intensify the small remnant signal in a few of these samples.

This reasoning spurred the research forward into its second phase. The *in situ* probe was upgraded to its present form (Chapter 2.1) and the high-pressure hydrogen experiments began with the intent of attempting to make the +105 ppm signal persist and enable other measurements to be made on S105 directly.

CHAPTER 5:

HIGH-PRESSURE STUDIES

With the goal now to coax the new +105 ppm peak into longer-lived existence, the initial concept was to first apply hydrogen gas pressures greatly exceeding the 1500 psi required to re-hydride the sample at the higher temperatures used (See Figure 1.2). With high enough pressures the sample could be brought all the way up to its melting temperature (and beyond) and still the reaction would be driven in the $NaAlH_4$ direction (see Equations 1.1 and 1.2 as well as Figure 1.2).

It was indeed found that the S105 signal could be made to persist using high-pressures. After exposure to pressure and heat this signal will stay—even at room temperature and when H_2 overpressure is removed. Moreover, in a surprising result, this +105 ppm peak was eventually created in undoped samples by melting the sample.

The techniques used to create a long-lived, recoverable S105 are described in the following chapter as well as a discussion of the changes that happen to the system after the S105 is created and of newly gained information about S105. The findings are supported by analysis done by our collaborators consisting of MAS from Son-Jong Hwang at Caltech and XRD performed by Terry Udovic at NIST.

5.1 Initial High-Pressure Results

5.1.1 Generation of S105 in Doped Samples

We begin with ^{27}Al NMR and a description of how the peak is generated in doped samples. In general, for doped material, after being loaded into the sample tube and probe in an inert environment, the sample sits in a vacuum at room temperature. The sample is first pressurized with hydrogen gas up to or just below 3000 psi. This was frequently done in 1000 psi stages, at least when the discovery was first made. This was done to make sure that the formation of S105 is not a function of high-pressure hydrogen alone. The pressurization stages are not necessary, and in a few later experiments the sample was charged straight to ~3000 psi from vacuum. The pressurization is performed at room temperature. The 3000 psi H_2 over-pressure assures the reaction is always driven in the direction of $NaAlH_4$ (Equations 1.1 and 1.2). Then the temperature is increased incrementally; typically, 30^{o}C increments were chosen. As with the pressure, the temperature does not need to be increased incrementally, but this is done to observe the state of the system at the various temperatures as the new peak is formed. Once the new +105 ppm peak is formed, the temperature can continue to be increased up to just below the melting temperature of 183^{o}C, but this is not necessary. With S105 now generated in the sample, the heat is turned off and the probe is allowed to cool back to room temperature, maintaining the high-pressure H_2 atmosphere over the sample. Finally the hydrogen gas is evacuated out of the sample chamber, and the process is complete. An example of this is shown in Figure 5.1.

Figure 5.1 shows a series of ^{27}Al spectra taken from a typical PT-cycle. The chart shows this process and is read like a book, left-to-right, then top-to-bottom.

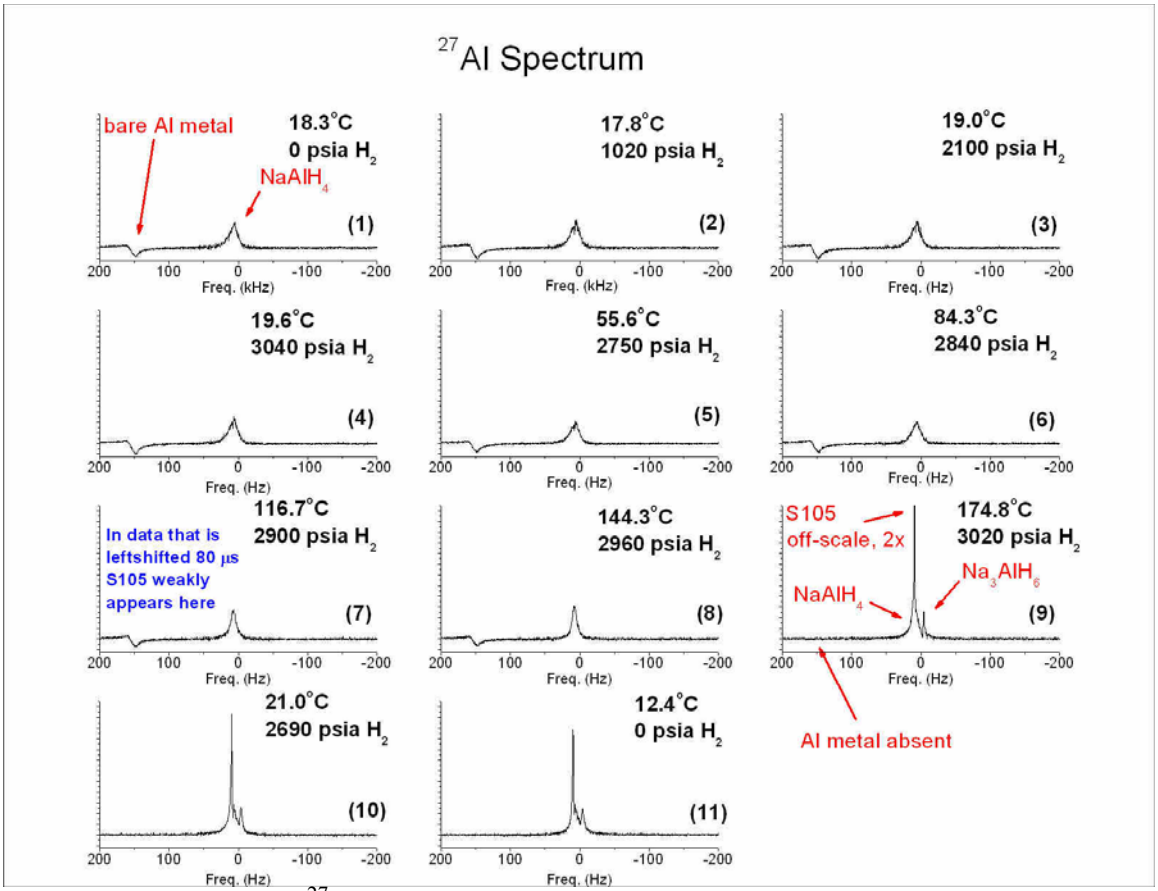

Figure 5.1: Series of ^{27}Al spectra taken during a PT-cycle that generates S105. In this case, the sample was a $ScCl_3$ doped sample. Data taken with a 20 sec recycle delay.

The alanate sample used in the above PT-cycle was doped with 4.04 mol% $ScCl_3$. Each spectrum is made of 100 co-added data acquisitions. The carrier frequency is 92.286 MHz, the frequency of 1M $Al(NO_3)_3$ (aq.), which is the standard reference for ^{27}Al NMR. A single effective 90^o inspection pulse was used with a 20 second recycle delay.

In the upper-left-hand corner, spectrum **(1)**, we see the spectrum of the sample as it was received by Washington University after being prepared at the University of Hawaii. The peak locations to be discussed in the following description are given in Table 4.1. There are only two peaks present at the creation of the material (labeled in red): a peak located at +1640 ppm (~150 kHz) corresponding to the Knight-shifted Al

metal, and the broad $NaAlH_4$ peak centered at +95 ppm (~9 kHz). Due to how the metal catalyst is introduced into the samples in preparation, it is not uncommon for the samples we received to have Al metal present in the sample after it is made. Similar to Equation 5.2 (Chapter 5.3.2)—only with the formation of bare Al and bare Ti instead of an Al-Ti alloy—the ball-milling of the doping metal into the sodium alanate would cause the system to slightly de-hydride, releasing H_2 and leaving behind some bare Al metal [15], [52]. This spectrum, **(1)**, is at room temperature and in a vacuum.

As we continue to move to the right, the H_2 pressure is incrementally increased in ~1000 psi steps up to a total of ~3000 psi by spectrum **(4)**. Moving from spectrum **(4)** to **(5)**, the temperature is increased while the sample remains under high-pressure hydrogen. A small amount of H_2 is intentionally let out of the sample head-space before heating—hence the apparent drop from 3040 psi to 2750. This is done so that the H_2 pressure increase due to thermal gas expansion would not surpass the limit of the pressure transducer (Chapter 2.1.2). As we continue to move right the temperature is increased in 30^oC stages.

The AlH_4^{-1} resonance is seen to narrow as the temperature increases. It is not shown, but if spectrum **(7)** is filtered by left-shifting the time-domain data, S105 can be seen to start forming around 115^oC, in this case. By the time we get to 175^oC in spectrum **(9)**, the spectrum is dominated by the large, new, sharp +105 ppm (~10 kHz) S105 peak. Note that the peak is off-scale, about twice the vertical size of the scale. Interestingly, despite the applied H_2 over-pressure, Na_3AlH_6 appears at -43 ppm (~ -4kHz) in conjunction with S105.

Now that S105 is created, the sample is allowed to cool back down to room temperature (spectrum **(10)**), where the +105 ppm peak remains, but decreases in height and comes into scale. This is due to the temperature effect of broadening upon cooling. After cooling, the hydrogen gas is evacuated in spectrum **(11)**. Another small decrease in height of the S105 peak is observed (See Chapter 5.2.3 for changes in width vs. T and P for S105).

Another very interesting event is observed during the generation of S105, which might have gone unnoticed at first with all the changes around zero-shift. Up at the Al metal resonance (150 kHz or +1640 ppm), the excess bare metal was entirely consumed with the appearance of S105. As S105 begins to be formed at around 115^{o}C (spectrum **(7)**) and between spectra **(7)** and **(8)**, there is a small decrease in the Al metal peak. We note the complete disappearance of the Al metal peak in spectrum **(9)**.

As intriguing as the disappearance of the excess Al metal at the appearance of S105 is, it is not the whole story of S105's link to Al metal. Next we will look at another PT-cycle performed on a sample doped with ScF_3.

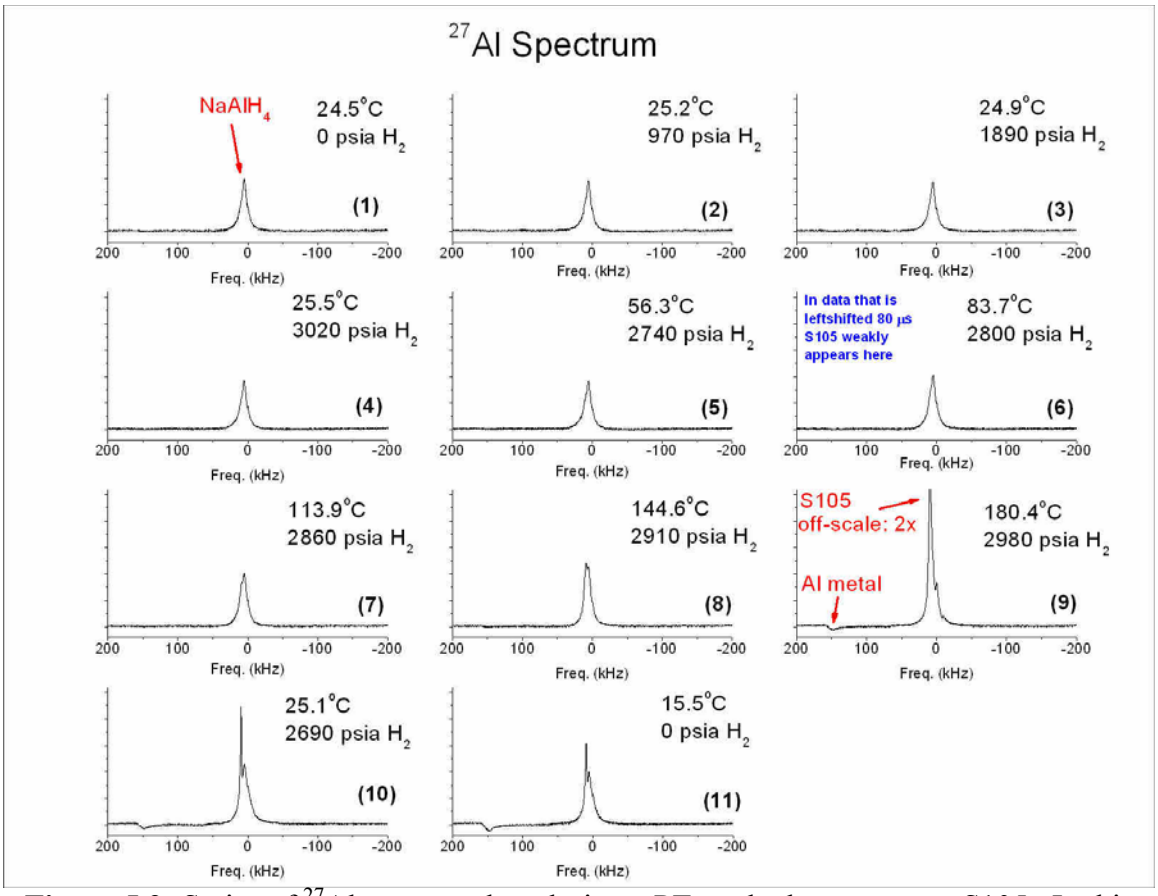

Figure 5.2: Series of ^{27}Al spectra taken during a PT-cycle that generates S105. In this case, the sample was a 2 mol% ScF_3 doped sample and data taken with a recycle delay of 83 ms.

The data in Figure 5.2 was taken under the same conditions as the data in Figure 5.1 with the exception of 83 ms used as the recycle delay (so there will be some suppression of the AlH_6^{-3} signal). Again, we start in the upper-left-hand corner with the sample as received from the University of Hawaii, spectrum **(1)**. Here, there is only one peak in the spectrum: $NaAlH_4$. There is, in this material, no excess Al metal at the start. The PT-cycle is also exactly the same—increasing pressure first in 1000 psi increments, and then heating the sample in 30°C increments. We see S105 begin to appear at 145°C as a small bump on top of the broader AlH_4^{-1} peak (without left-shifting the data). By

180°C S105 is fully-formed, and signatures of the AlH_6^{-3} resonance can be seen slightly, despite the fast recycle delay.

In spectrum **(8)**, a small waiver in the baseline at ~1640 ppm (150 kHz) shows the initial appearance of the +105 ppm peak comes with some Al metal. By spectrum **(9)**, the metal can be seen distinctly in conjunction with the now-large S105 peak (off-scale by 2x). We again see that S105 is linked to Al metal; however in this case, Al metal was *created* at the onset of S105.

In fact, a general rule was observed in sample after sample concerning Al metal in the doped alanate systems. When a sample with an initial presence of Al metal was PT-cycled, the Al metal would be consumed—in part or full—simultaneous with S105's generation; for a sample without an initial presence of Al metal, Al metal would be created together with S105.

The next pertinent question is whether S105 forms from Al metal alone. A sample of Al powder (325 mesh, 0.044 mm opening) was purchased from Alfa Aesar, and taken through the exact PT-course previously described. The Al powder did not react or form S105. A sample of Al powder doped with 4 mol% $ScCl_3$ by ball milling (prepared at U. Hawaii) was also repeatedly PT-cycled without generating S105. Thus, S105 does not arise from the Al metal alone or even from a doped Al metal system. S105 requires the $NaAlH_4$ system to form and it seems that Al metal is involved in some intermediate, or at least sidetrack, reactant or product in the formation of S105.

5.1.2 Generation of S105 in Undoped $NaAlH_4$

The production of S105 in undoped $NaAlH_4$ was one of the more exciting and revealing finds of the study. There are two ways of producing the +105 ppm peak in undoped material with differing effects. The bare alanate samples *must* be melted to form S105. If the material is melted in a high-pressure H_2 atmosphere, then S105 is formed without any aluminum metal being produced. However, if the material is melted in a vacuum, S105 still forms, but aluminum metal is also produced, and a small amount of hydrogen gas is given off. No matter which method is chosen for generating S105, Na_3AlH_6 is always formed.

Let us first look at the case of S105 generation in a high-pressure H_2 environment. Figure 5.3 shows this process with "technical grade" $NaAlH_4$ purchased from Sigma-Aldrich.

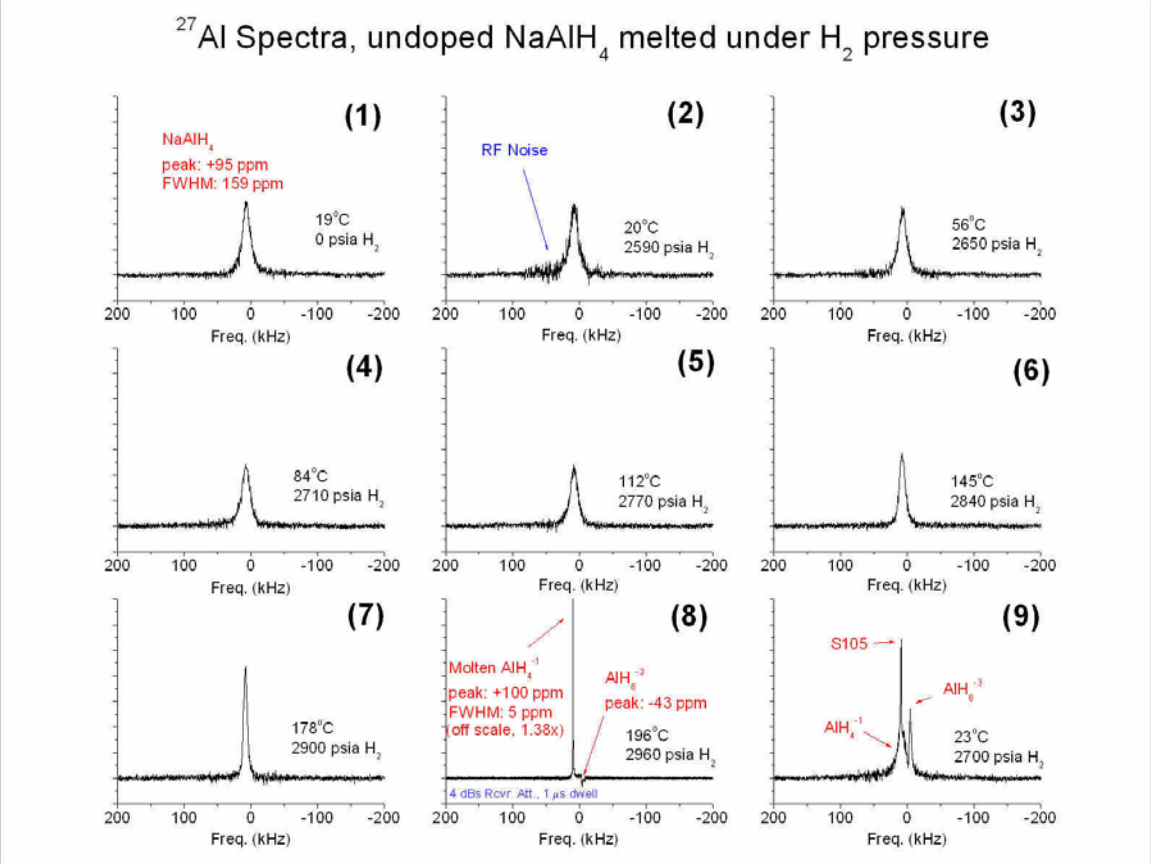

Figure 5.3: Generation of S105 in undoped $NaAlH_4$ by melting under high-pressure H_2. 20 sec recycle delay used.

Starting at spectrum **(1)**, in a vacuum and at room temperature, there is only the single AlH_4^{-1} resonance centered at about +95 ppm (9 kHz) and 160 ppm (14.8 kHz) wide. Moving to the right, ~2600 psi H_2 was let into the sample chamber at room temperature in spectrum **(2)**. There is a large amount of noise in this particular spectrum, and it can be seen in all the following spectra with varying intensity. The r.f. grounding capacitors (Chapter 2.1.4) had broken loose from the ground lugs on the probe and the data was taken before this was noticed. This noise is the local radio station broadcasting in FM at 92.3 MHz.

After the H_2 was let in, the heat was increased incrementally starting in spectrum **(3)**. The AlH_4^{-1} resonance begins to undergo motional narrowing around 145°C (spectrum **(6)**). The spectrum at 196°C (spectrum **(8)**) shows the liquid resonance (recall, the melting temperature for $NaAlH_4$ is 183°C). There are 4 dBs of extra receiver attenuation used in specifically this spectrum and a dwell time (data sampling rate) of 1 μs was used here, rather than the usual 200 ns, to capture the entire (long) FID of the liquid alanate. The liquid peak is centered at +100 ppm (9.2 kHz) and has a FWHM of 5 ppm (460 Hz)—compared to the aqueous $Al(NO_3)_3$ width of 3.6 ppm (330 Hz) due to field inhomogeneity, this is a reasonable liquid linewidth. A small peak from the AlH_6^{-3} is also detected at -43 ppm.

Upon cooling, the solid AlH_4^{-1} lineshape is regained (spectrum **(9)**) with the addition of S105 and a large AlH_6^{-3} peak. When the samples are unloaded after this process, the sample is no longer a powder, but a solid chunk of material that has obviously melted and re-solidified. To transfer the material to other sample containers

for use in the other probes or be shipped to collaborators, the material must be ground out of the sample tube and crushed back into a powder, all performed in the N_2 glove bag.

It was asked at this point if S105 would still form in undoped $NaAlH_4$ even when it is melted without a H_2 over-pressure keeping the material from de-hydriding. New samples of undoped $NaAlH_4$ were loaded and melted in a vacuum. Figure 5.4 shows an abbreviated PT-cycle in an initial vacuum. The sample was first evacuated and heated, but not melted (**(1)** and **(2)**, below). Then it was melted, **(3)**, and cooled to 155°C, **(4)**, and finally allowed to cool all the way back to room temperature, **(5)**.

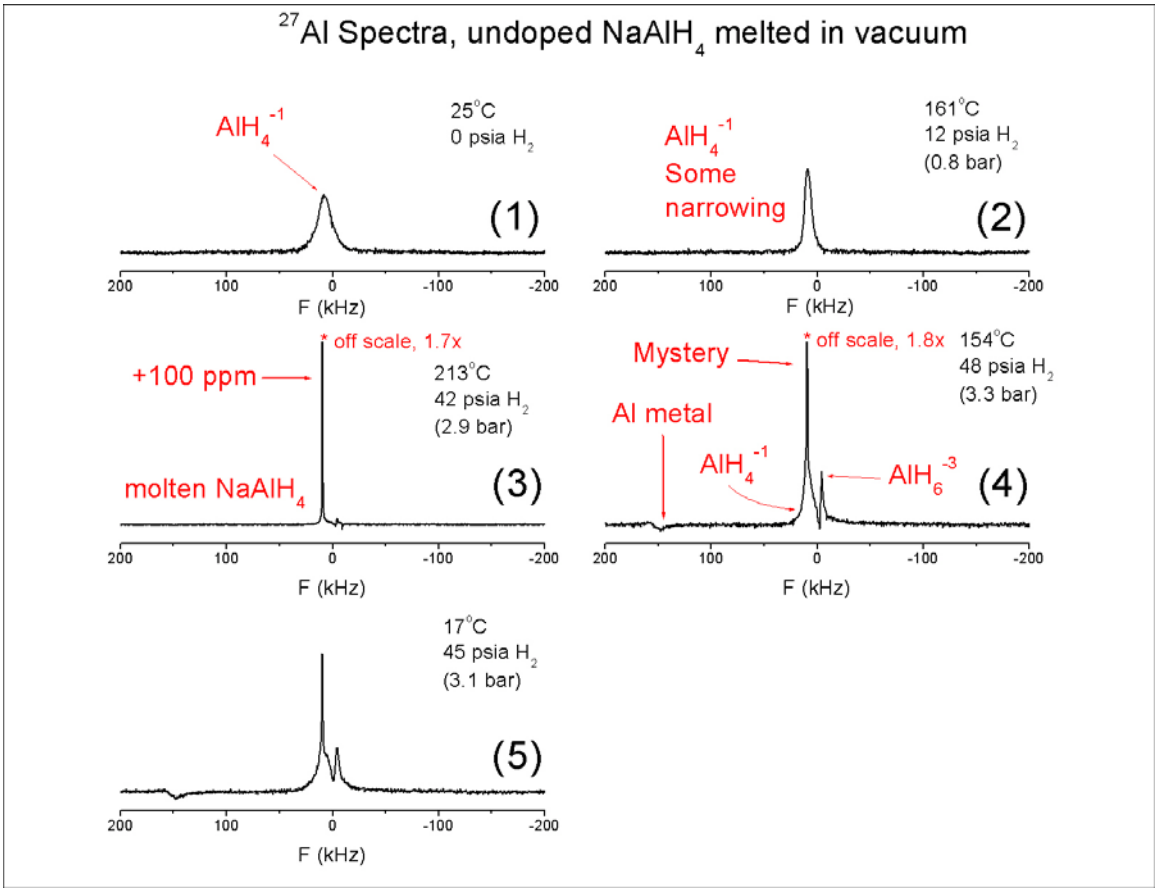

Figure 5.4: Generation of S105 in undoped $NaAlH_4$ in a vacuum. Al metal is evident in **(4)** and a total of 45 psia of H_2 is given off. 20 sec recycle delay used.

The sample was taken to 213°C and the material released 45 psia H_2. In the case of $NaAlH_4$ initially under vacuum and melted, it is plainly obvious that the sample has

partially decomposed as evidenced by the release of 45 psia of gas. The presence of aluminum metal also testifies to the partial decomposition of the system. Based on these observations, it is tempting to argue that the sample evolves AlH_6^{-3} with S105 because the sample has partially de-hydrided following Equation 1.1. This can be tested, as shown in the next section.

5.1.3 Hexahydride Formation

Hexahydride is observed to *always* form in conjunction with S105 in both doped and undoped samples. First let's return to the above case of $NaAlH_4$ being melted in an initial vacuum. If the system is believed to partially undergo the first dehydriding step to evolve some hexahydride, then by Equation 1.1 we should be able to calculate the proportion of reaction products based on the sample's mass and the amount of H_2 released.

The sample shown in Figure 5.4 contained 0.312 g of material, which corresponds to 6 mmol of $NaAlH_4$ formula units, so 6 mmol of Al atoms. If *all* this material were to convert to Na_3AlH_6, then from Equation 1.1, 6 mmol of $NaAlH_4$ will release 6 mmol H_2 molecules. 6 mmol of gas in an 11.57 cc volume corresponds to 12.5 atm (178 psia). So a full conversion of tetrahydride to hexahydride would have produced 178 psia of hydrogen gas. Only 45 psia of H_2 was actually released, which is a conversion of about ¼ of the material. The corresponding reaction equation is:

$$\mathbf{NaAlH_4 \rightarrow 3/4\ NaAlH_4 + 1/12\ Na_3AlH_6 + 1/6\ Al + 1/4\ H_2} \qquad 5.1$$

Thus, the ratios of products expected for a ¼ conversion is 9 : 1 : 2 : 3 for AlH_4^{-1} : AlH_6^{-3} : Al : H_2. We can now check to see if the spectrum shows a 9 : 1 ratio of AlH_4^{-1} : AlH_6^{-3}.

The final spectrum **(5)** at 17°C shown above in Figure 5.4 was fit to a triple Lorentzian (in the same manner described later, Chapter 5.2.2). The ^{27}Al spectral fit gave a 4.56 : 1.09 : 1 ratio for AlH_4^{-1} : AlH_6^{-3} : S105. This means a 4.17 : 1 ratio of AlH_4^{-1} : AlH_6^{-3}. So there is a larger fraction of hexahydride present in the product of the PT-cycle than could have been converted just by sample decomposition (following Equation 5.1, above). This means—at least in part—some other conversion route formed the hexahydride with S105.

Moreover, for the creation of hexahydride in samples with a H_2 over-pressure, Equation 1.1 and Figure 1.2 indicate that the reaction of $NaAlH_4$ to yield hexahydride is blocked under excess H_2 pressure (as used in Figure 5.3). Indeed, in Figure 5.3, no Al metal is generated. So the appearance of hexahydride is surprising, or at least outside the predictions of Equation 1.1.

So can S105 can be generated in bare Na_3AlH_6? The generation of S105 in bare Na_3AlH_6 was attempted. A batch of 3.33 mol% $ScCl_3$ doped hexahydride was also prepared at U. of Hawaii. The material was taken through the same PT-cycle multiple times. No S105 peak was ever formed in either sample. The samples did not appear to react at all.

The fact that they did not re-hydride is not a surprise (not by Equation 1.1, at least). Although the hydrogen gas pressures greatly exceeded the equilibrium pressure, driving the reaction toward tetrahydride formation, there was no excess Al metal in the sample. Thus, the material could not form $NaAlH_4$.

5.1.4 H_2 Evolution in High-Pressure Cases

As discussed above, in the experiments where pure $NaAlH_4$ is allowed to de-hydride into an initial vacuum, H_2 evolution is obvious. But we need to ask, was any H_2 released or absorbed in the high-pressure PT-cycle? This is difficult to answer because we must look for a small change in a large pressure. The pressure transducer has an accuracy of 1% of the reading (not 1% of the full-scale), with some hysteresis and temperature dependences. So it gives excellent vacuum readings, and at the high-pressure limit of ~3000 psi (Chapter 2.1.2) we expect an error in the range of 30 psi—but it is difficult to say *exactly* what the error of the pressure readings are at high-pressure. To address this question, the entire history of data was sorted through, collecting starting and ending pressures and temperatures, where the data is available. In each case, the total pressure difference was measured, ΔP_{tot}. This total pressure difference was adjusted in each case for the slight difference in recorded temperature, ΔT_{rec}, of the sample before and after the PT-cycle ($\Delta P_{adj} = \Delta P_{tot} - \Delta P_{therm}$, where $\Delta P_{therm} = nR\,\Delta T_{rec}/V$). The adjusted pressure difference, ΔP_{adj}, should be the pressure released or absorbed from H_2 evolution.

In samples where S105 is created (both doped and undoped), the ΔP_{adj}'s ranged from positive (apparent sample decomposition) to negative (apparent H_2 absorption). The magnitudes were distributed between zero to ~50 psia. This would appear to tell us that these samples were in fact either taking H_2 up or releasing it, depending on conditions such as the presence or lack of excess Al metal.

However, the same analysis was performed on samples where S105 was not formed and where the sample underwent no reaction of any sort. Samples were used such as Al-halides (which where run very early on to see if S105 could be generated in compounds that might derive from the dopant-salts or the dopant salts themselves), Al

metal samples, Na_3AlH_6 samples, and one ScF_3 doped sample—all of which failed to produce S105. The ΔP_{adj}'s demonstrated the same distribution in the range of about ±50 psia—and thus established the typical error range of the pressure transducer at high-pressure for this type of cycling. Our best estimate then is that the pressure change (after adjustment of temperature) is ±30 psia. For a typical ~300 mg sample, this corresponds to a fraction ±17% of the hydrogen that would be released in the first step reaction (Equation 1.1).

More insight can be found in the specific case of generating S105 under high-pressure hydrogen. Here, although a direct measurement of pressure only establishes an upper bound on the up-take or evolution of H_2, it is reasonable to believe that none has occurred, because there is no Al metal generated.

5.1.5 ^{27}Al "Before" and "After" Comparisons

As we wrap up the section on the initial work in ^{27}Al NMR, there are a few last comparisons to be made concerning the $NaAlH_4$ system before and after the +105 ppm S105 is generated.

There is a significant difference between creating S105 in the doped versus undoped material. The difference is that in doped material the +105 ppm peak can be produced before the sample is melted, whereas the sample must be melted to produce this peak when it is undoped. The catalyst allows the alanate system to undergo changes at lower temperatures, a result in line with the well-known action of the catalyst in lowering the de-hydriding temperatures and making the re-hydriding direction possible.

If we compare the formation temperatures observed for the +105 ppm peak in the doped system, S105 can be seen beginning to form at temperatures as low as 85^{o}C in some doped samples. By the time the sample has reached 175^{o}C, the +105 ppm peak is always fully formed. However, the peak does not consistently begin forming at the same temperature in every doped sample. The final intensity of the S105 peak in the doped material also varies between samples. Sometimes the S105 peak remains a small bump or shoulder on the side of the broad AlH_4^{-1} peak, and in other cases times it dominates the spectrum.

In the case of undoped material, the +105 ppm peak never forms until the sample has melted. The S105 peak is *so* close to that of molten $NaAlH_4$ that the S105 peak is not evident until after solidification. The size of S105 is consistently large in undoped samples. Both the size and formation temperature in the undoped samples are independent of whether or not the sample was heated in a vacuum or high-pressure H_2 environment.

Figure 5.5 shows a collection of spectra where the "after" spectrum (red) is overlaid on the "before" spectrum (black) for a quick comparison of the state of the $NaAlH_4$ system. This also allows the reader to see some of the effects from melting under pressure or vacuum, and effects like the increasing or decreasing presence of the Al metal signal, or the varying intensity of the S105 peak in doped samples. Also note that one of the spectra was taken with an 83 ms recycle delay and the rest with a 20 sec recycle delay.

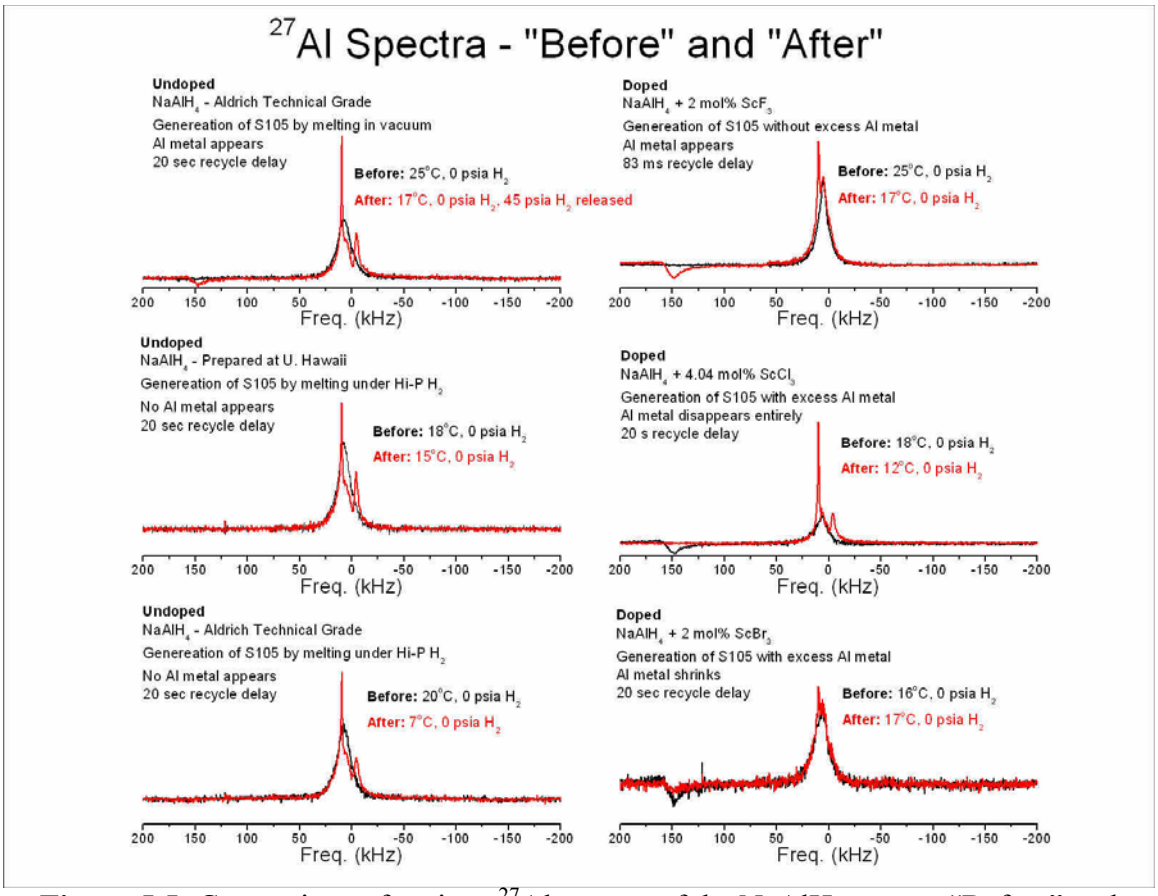

Figure 5.5: Comparison of various ^{27}Al spectra of the $NaAlH_4$ system "Before" and "After" the +105 ppm S105 is created.

As a reminder from Table 4.1, the shifts of each species are: 150 kHz (1640 ppm) for Al metal, 8.6 kHz (95 ppm) for $NaAlH_4$, -3.7 kHz (-43 ppm) for Na_3AlH_6, and 10 kHz (105 ppm) for S105.

5.2 Pressure Studies of S105

5.2.1 Longevity

The issue of longevity of this new +105 ppm Al peak now becomes important for further studies. This peak, after it is created, either in a high-pressure environment or initially in a vacuum, is very long lived. One of the first samples in which S105 was

generated was removed and stored in a sealed container in the N_2 glove bag at room temperature and atmospheric pressure. After 77 days the sample was re-loaded and a ^{27}Al spectrum was taken. The +105 ppm signal remained undiminished in the material. Figure 5.6 below shows a comparison of these two spectra.

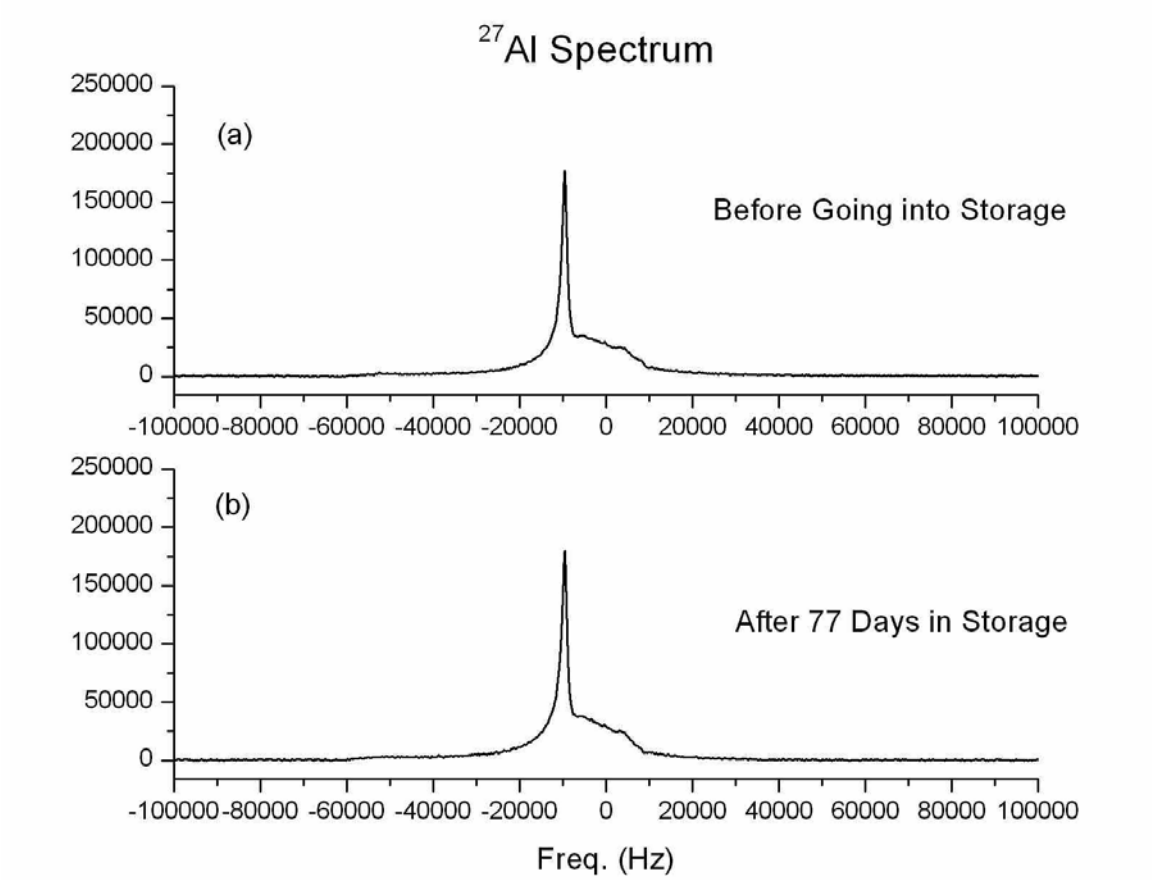

Figure 5.6: Two spectra of a 4.04 mol% $ScCl_3$ doped sample: **(a)** shows the spectrum before going into the N_2 glove bag and **(b)** shows the spectrum after 77 days in the glove bag. The spectra were taken at room temperature in a vacuum. The AlH_6^{-3} signal was being suppressed by the 83 ms recycle delay for data acquisition.

This meant that relaxation measurements and other measurements on the +105 ppm signal could be made directly. In addition, the ability to remove the sample material after S105 is generated and re-load it into other sample containers allowed for the use of the cold probe and box probe for studies of motional narowing. The longevity of the

+105 ppm peak also meant that the samples could be sent to our collaborators for XRD and MAS-NMR analysis to be performed.

5.2.2 Spin Counting and Lorentzian Fit Convolutions

The peak at +105 ppm is tall, and in order to get an idea of how much of the ^{27}Al resides in the S105, the spectra from doped and undoped samples were integrated. In NMR, the amplitude of the signal at each frequency in the spectrum is directly proportional to the number of spins in the sample resonating at that frequency. By selectively integrating the spectrum (taking the area under the curve) one is able to determine the percentage of the sample present as each species.

This is simple enough for spin-1/2 nuclei where the only transition is the ±1/2 transition. ^{27}Al is spin-5/2, and there are 5 transitions, as discussed in Chapter 3.2.3. For all of the species except Al metal, the r.f. pulses excited the central transition only, although if this is not exactly satisfied, there may be some error. The direct proportionality of the spins in the sample to the area in the spectrum breaks down for metals because of eddy current shielding of the r.f. field. The Al metal has all transitions excited together. Additionally, the Al metal is way off resonance. For these reasons, samples showing substantial Al metal were not included for careful spectral integration. With these considerations in mind, the spectra of doped and undoped samples were collected and analyzed to see what could be learned about the size of the mystery resonance in general.

The undoped samples provided better spectra for this type of analysis. First of all, S105 could be generated in the undoped systems without producing Al metal, allowing

for the accounting of all spins before and after S105 is created in the material. Secondly, it was standard practice by the time the research had begun to focus on the undoped system to take *all* data at a slower repetition rate, allowing the entire spectrum to fully relax, and making more spectra available for this type of analysis.

With no Al metal being produced, the total spin count can be directly compared from before and after S105 is generated to assure ourselves that there is no signal missing. There is effectively no difference in area between the two spectra (consistently measured to be less than 1% difference), telling us that all the ^{27}Al is accounted for in these spectra. This result was repeatedly confirmed in the undoped samples where no Al metal was present.

Next the spectra were fit with a triple Lorentzian (See Figure 5.7). The Lorentzian lineshape was chosen for the fitting procedure because that is the shape formed by exponential decay and is very typical in NMR. More to the point, the Lorentzian did a good job fitting the $NaAlH_4$, S105, and Na_3AlH_6 components.

A sample of pure Na_3AlH_6 was first fit to a single Lorentzian, and the width and peak center optimized and recorded. Then a spectrum of the alanate sample before heating—showing only $NaAlH_4$—was fit to a single Lorentzian, and the width and peak center of this fit recorded as well. Then the alanate sample was PT-cycled by melting under excess H_2 pressure; the resulting spectrum at 7^{o}C was fit with a triple Lorentzian by setting the centers and widths of the first two lines from the (already determined) individual Na_3AlH_6 and $NaAlH_4$ fitting parameters, and the letting the parameters of the third line be varied as well as the areas of all three. The fit was good (Figure 5.7), showing that the third peak (S105) was centered at +104 ppm with a FWHM = 13 ppm.

The fit was performed a second time and *all* the width and peak center parameters allowed to float, again producing an accurate fit. This assures us that the total lineshape in static NMR after S105 is generated can be represented well by three peaks. The fits gave a ratio of 8.34 : 1.38 : 1 for AlH_4^{-1} : AlH_6^{-3} : S105, meaning S105 is about 9% of the signal (Figure 5.7). Two other undoped samples in which no Al metal was produced gave AlH_4^{-1} : AlH_6^{-3} : S105 ratios of 6.22 : 1.93 : 1 (11% S105) and 7.20 : 1.59 : 1 (10% S105).

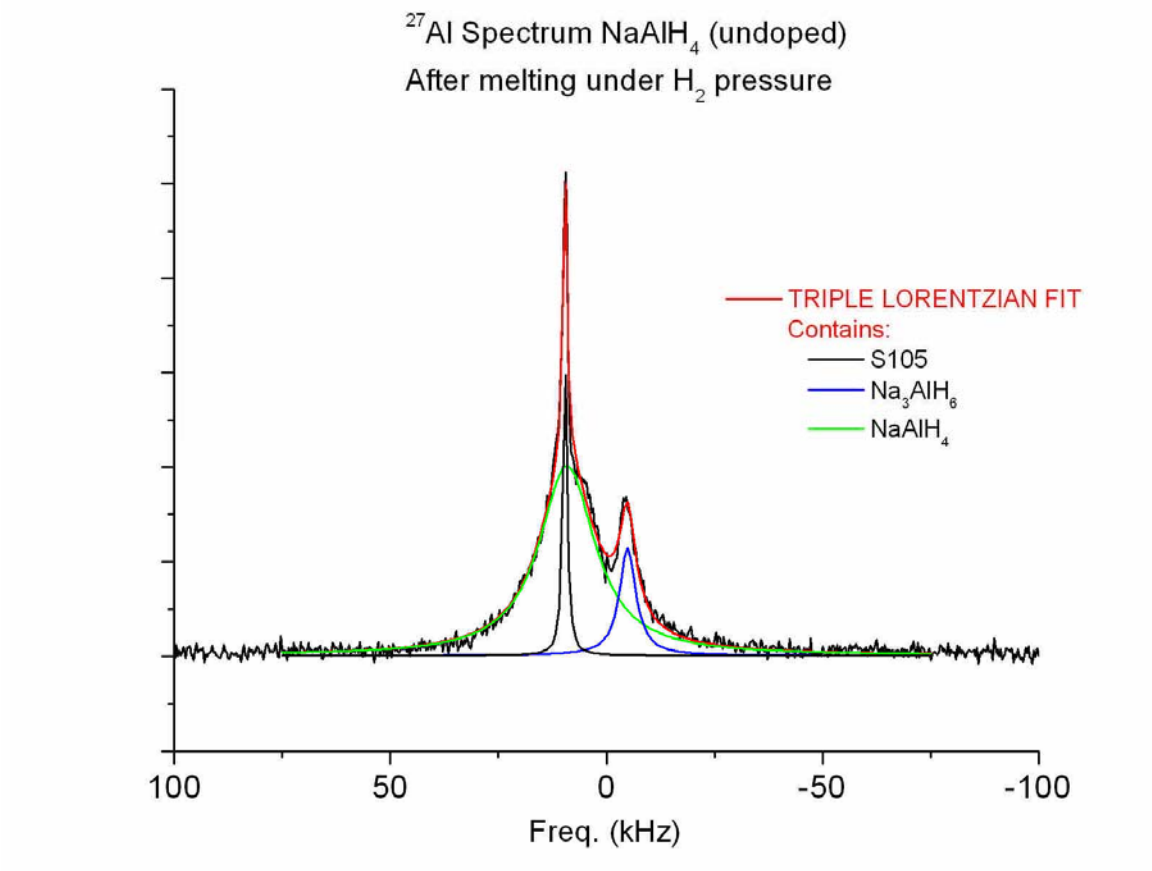

Figure 5.7: Triple Lorentzian fit to a spectrum of undoped alanate where no Al metal shows after S105 is created by melting under H_2 pressure. Spectrum taken at 7°C, 0 psia H_2, 20 sec recycle delay.

5.2.3 FWHM vs. Temperature and Pressure

The FWHM of S105 was measured over the temperature range of 20°C to 180°C on a $ScCl_3$ doped sample. The H_2 pressure on the sample is held near 2900 psia. Figure 5.8 below shows this plot. The FWHM was measured in a similar manner as T_1 and T_2 were (see below) with the exception of not left-shifting the FIDs 80 μs. This means the +105 ppm peak is on top of the broad AlH_4^{-1} peak. The data were not left-shifted because this technique can distort the lineshape of the peak. Here the height of the peak is measured from a baseline established on the broad peak

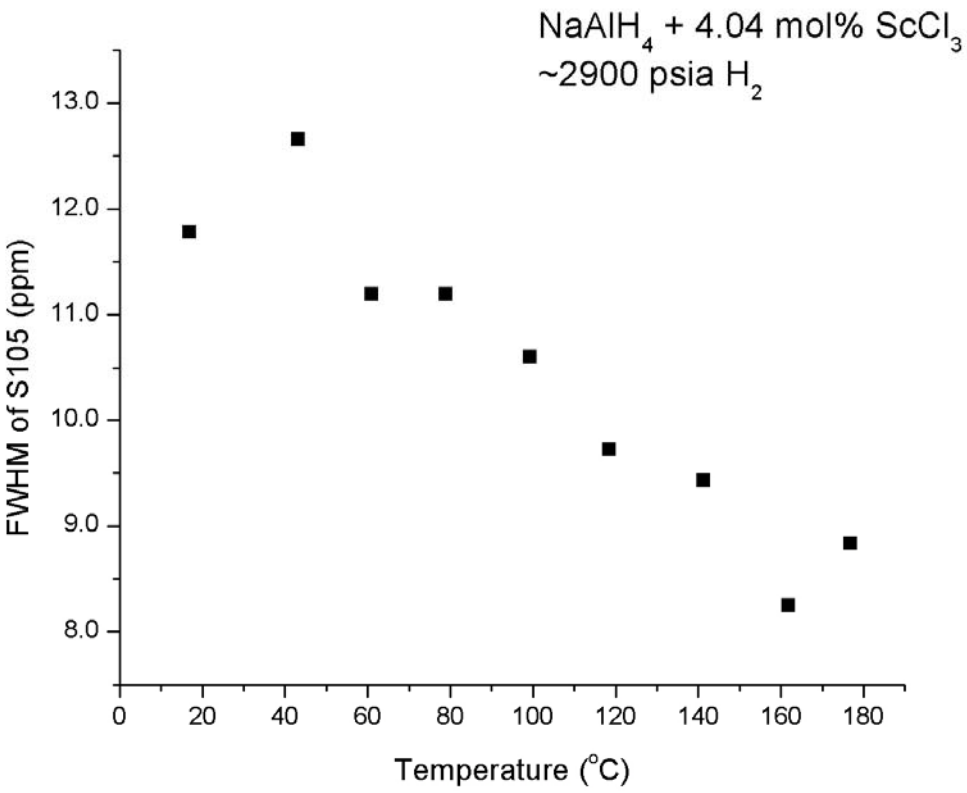

Figure 5.8: FWHM vs temperature. The τ =35 ms data from inversion recovery were used with ~2900 psia H_2 over the sample on resonance with S105.

As the sample heats-up, the +105 ppm peak narrows from about 12.5 ppm to 8.5 ppm (a 30% change). Integration of the peak reveals that the area remains basically unchanged, and accordingly the peak height is seen to rise as the sample temperature

increases. It should be noted that the high-pressure probe, where this measurement was performed, produced a FWHM of 3.6 ppm for a $Al(NO_3)_3$ (aq.) tune-up sample. So some of the linewidth in Figure 5.8 is from field inhomogeneity.

The response of the peak's width to pressure is smaller than its response to temperature. Over the entire range of vacuum to 3000 psia H_2, the FWHM typically changes only 2-3 ppm at room temperature. Nevertheless, when a change in width was observed in response to H_2 pressure, the trend was always the same: the +105 ppm peak would become slightly narrower at higher pressures. This effect was not observed consistently in every sample. In extreme cases, some samples showed no change and some showed a change as much as 4 ppm. The presence or lack of a dopant did not seem to be the determining issue.

5.2.4 T_1 and T_2 vs. Temperature

^{27}Al relaxation times for S105 were also measured in the normal reaction temperature range (room temperature to 180^{o}C) to help characterize S105. In general, the ^{27}Al T_1s of AlH_4^{-1} and AlH_6^{-3} are on the order of 100 milliseconds and 1 second respectively. The plot of T_1 and T_2 of S105 in ^{27}Al NMR is shown below in Figure 5.9.

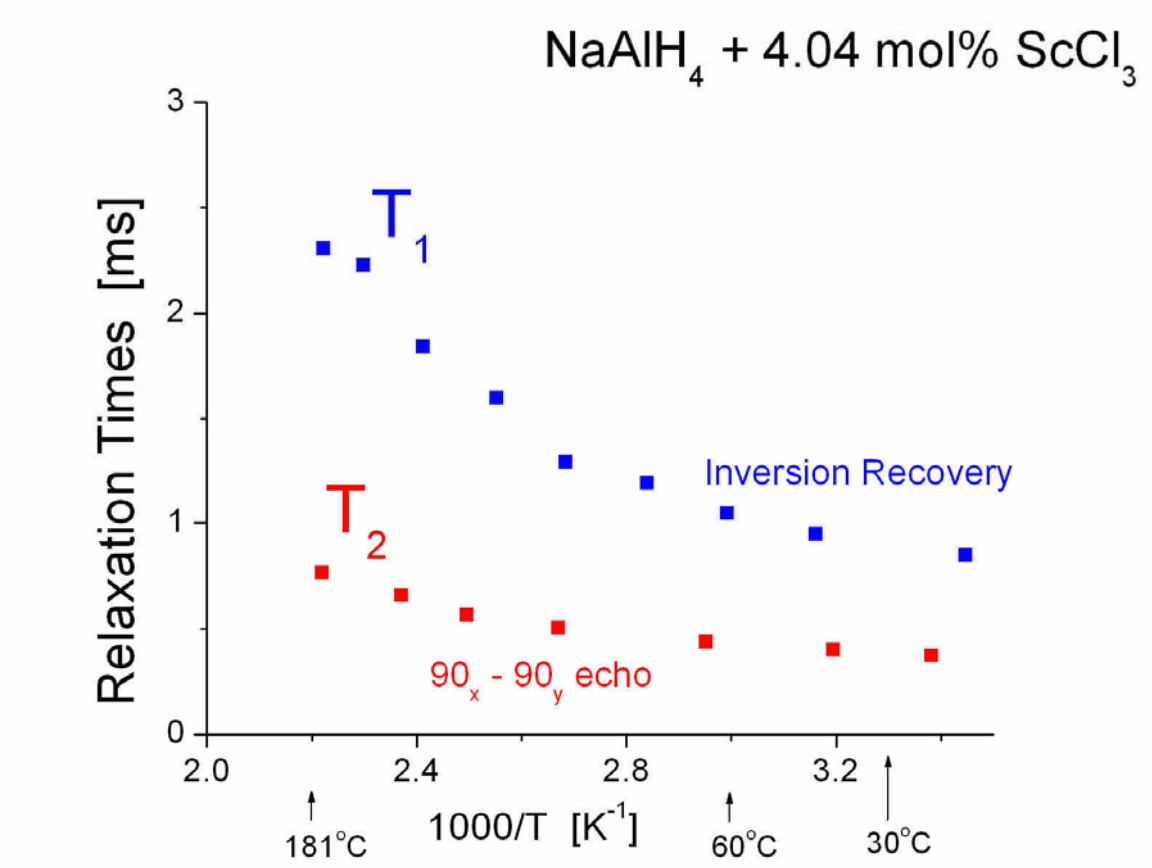

Figure 5.9: T_1 and T_2 of a 4.04 mol% $ScCl_3$ doped sample in 8.3 T field. The x-axis is plotted as 1000 times the inverse temperature in Kelvin. T_1 was measured by inversion recovery sequence and T_2 by a 90^o-90^o echo sequence.

The spin-lattice relaxation time, T_1, was acquired with an inversion recovery sequence (Chapters 3.3.2). T_1 rises from about 845 μs to 2.3 ms as the temperature rises from room temperature to 180°C. T_2, which was measured with a 90^o-90^o echo sequence (Chapters 3.3.3), rises from 370 μs to 765 μs over the same temperature range. The T_1 of S105 is extraordinarily short. This is indicative of a very rapidly fluctuating EFG at the site of the nucleus, which confirms rapid motion of the spins. Nutation measurements showed that S105 has a static quadrupole splitting (not time averaged to zero) larger than the applied r.f. field. (The effective 90^o pulse time was measured to be 10 μs for S105, while the 90^o pulse time was measured to be 30 μs on aqueous $Al(NO_3)_3$; see discussion

in Chapter 3.2.3). Another indicator of rapid motion is the narrowness of the peak. T_2 accounts for 74% of the observed FWHM, as the following calculation demonstrates. The $FWHM^{measured}$ = 12.5 ppm at room temperature. Now we can take the measured room temperature T_2 (370 μs) and use it to calculated a predicted linewidth: $FWHM^{predicted} = 1/\pi T_2^{measured}$ = 860 Hz = 9.3 ppm.

Both relaxation measurements were performed at high H_2 pressures (~2900 psia for T_1 and ~2700 psia for T_2) on the same sample. To isolate the S105 signal from the AlH_4^{-1} and AlH_6^{-3} peaks the recovery analysis was done in the frequency-domain, integrating over only the +105 ppm peak with a baseline established closely on either side of the peak corresponding to S105. This way only the spins associated with S105 were counted. To accentuate the difference between the S105 peak and the broad AlH_4^{-1} resonance, the FID was left-shifted 80 μs in the time-domain before Fourier transforming. Additionally, the data was acquired with a high repetition rate to minimize the AlH_6^{-3} signal (See Chapter 3.2.2). As is seen in Figure 5.10, the S105 peak clearly stands out after the above techniques are applied and the recovery can be accurately measured.

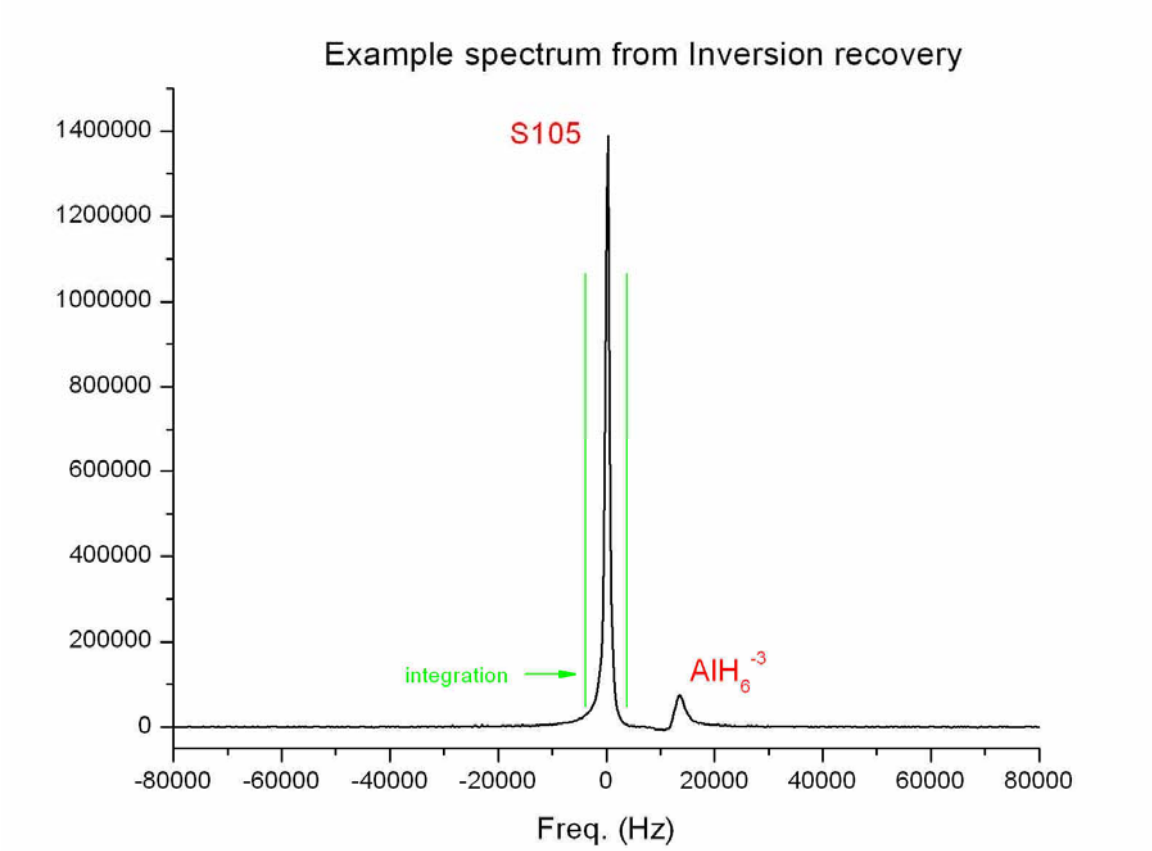

Figure 5.10: Example from inversion recovery data (τ = 35 ms) of a spectrum at 141°C used for relaxation measurements. Green bars show the limits of integration. Data were acquired at 12 s^{-1} repetition rate and left-shifted 80 μs before Fourier transforming. Note that the spectrometer was adjusted so that S105 is exactly on resonance.

5.2.5 Motional Narrowing Confirmed in ^{27}Al

As shown above, the T_1, T_2, and FWHM measurements on S105 suggest a motionally narrowed species. To confirm this, ^{27}Al spectra were taken at colder temperatures.

For ^{27}Al, four different samples were used to examine cold spectra: an undoped $NaAlH_4$ sample, a 3.98 mol% $TiCl_3$ doped sample, a 4.04 mol% $ScCl_3$ doped sample, and a 4 mol% ScI_3 doped sample. Each sample was first loaded into the high-pressure probe and S105 generated in the material by the appropriate PT-cycle. The PT-cycled material

was unloaded from the larger sample tubes, and reloaded into smaller glass sample tubes in the N_2 glove-bag. Finally the smaller sample tubes were flame sealed in an ~0.8 atm (absolute) Ar atmosphere and placed in the cold probe. Figure 5.11 shows the spectra from the undoped $NaAlH_4$ sample.

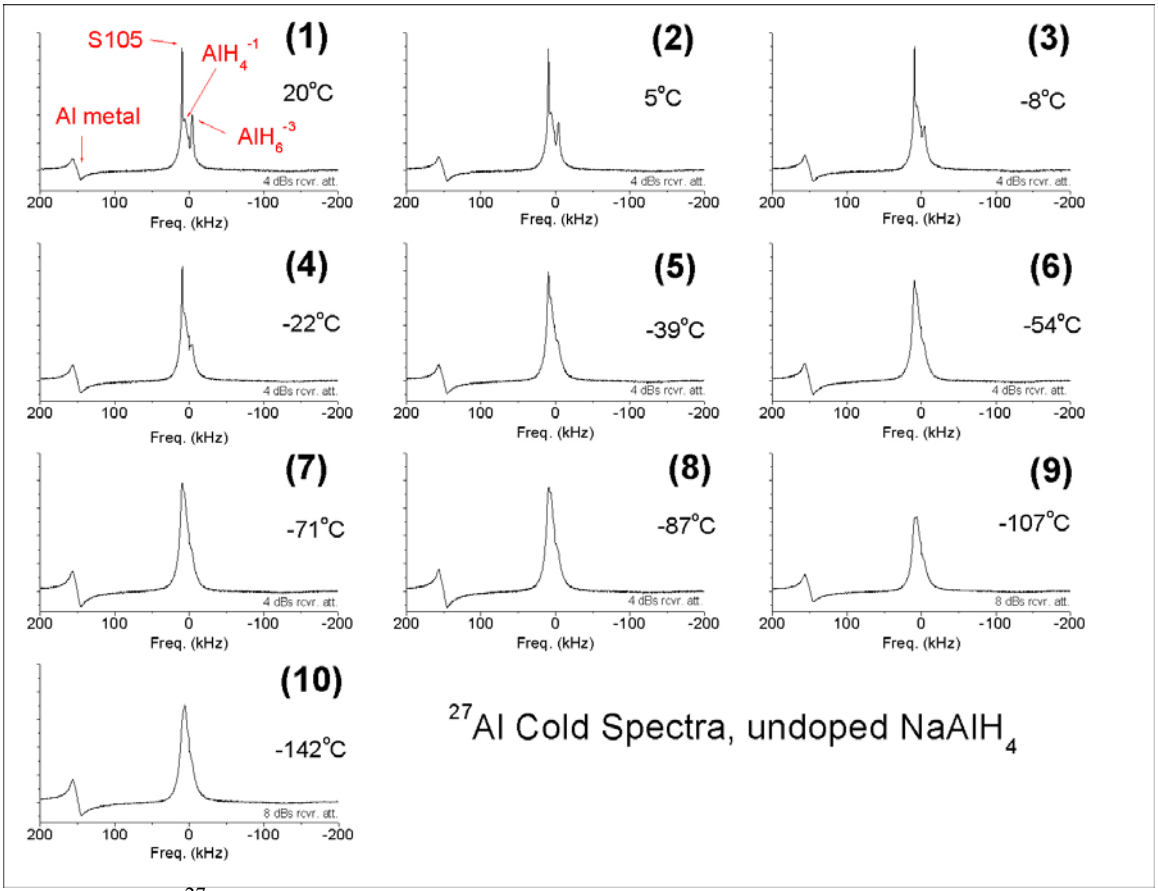

Figure 5.11: ^{27}Al cold spectra of an undoped sample that has been PT-cycled and shows the S105 signal. In this case, AlH_6^{-3} freezes out around -40°C and the S105 around -70°C. Normally 4 dBs of attenuation is applied to the incoming signal, but this was increased to 8 dBs for the last two spectra. 20 sec recycle delay used.

S105 and the AlH_6^{-3} peak can be seen to gradually broaden, finally disappearing into the broader AlH_4^{-1} peak (spectrum **(5)**). The AlH_4^{-1} peak remains unchanged throughout the cold run because it is already at its rigid-lattice linewidth. This is evidenced by the *onset* of line narrowing of the AlH_4^{-1} at temperatures around 145°C, as seen previously in spectra like those in Figures 5.1 and 5.2. The AlH_6^{-3} disappears first,

somewhere between -22°C and -39°C. In this case, the S105 peak continues to broaden and disappears into the broad surrounding signals between -71°C and -87°C (spectra **(7)** and **(8)**). At lower temperatures, further decreases in temperature did not result in additional lineshape changes. This can be confirmed by looking at the spectra after left-shifting 80 μs (not shown), and watching for the signal of S105 to disappear. Upon warming, the sample's lineshape returns to normal.

Above, in the spectra at -107°C and at -142°C (spectra **(9)** and **(10)**), an additional 4 dBs of attenuation was applied to the incoming signal with respect to the other spectra. This had to be done to prevent clipping of the FID. Presumably, this reflects the 1/T (Curie's law) variation of spin magnetization. The probe tuning was also altered due to the freezing of the tuning components. Specifically water, which might have been trapped in the variable capacitor used for tuning the tank circuit, froze because the tuning components are located inside the can of the cold probe (Figure 2.8, Chapter 2.3).

In the other three samples, similar results are observed, as shown in Table 5.1. The temperature of the samples, like in Figure 5.11, was decreased in stages, so the temperature at which the S105 signal disappeared can only be identified approximately. In general, this +105 ppm ^{27}Al species normally undergoes rapid motion, but broadens into the surrounding resonances at a temperature of approximately -60°C.

Sample Doping	**Undoped**	**$TiCl_3$**	**$ScCl_3$**	**ScI_3**
Temperature of S105 disappearance	Between -71°C & -87°C	Between -52°C & -58°C	Between -33°C & -81°C	Between -48°C & -71°C

Table 5.1: Temperatures where S105 disappears into other broad peaks for variously doped samples.

5.2.6 Motional Narrowing Confirmed in ^{1}H

^{1}H spectra were also used to study S105 motional narrowing. In general, the proton T_1's in the alanate system are longer—being measured previously by other groups to be on the order of 100's of seconds to 1000's of seconds for the tetrahydride and shorter T_1's for the hexahydride[47], [53]. The widths have also previously been measured to be 10's of kHz wide for the $NaAlH_4$, with the Na_3AlH_6 and NaH being 1/3 and 2/3 of that respectively[47], [54], [55]. The ^{1}H chemical shift range is small and all the species involved in this system are near zero, so the best way to distinguish these species in static NMR is by relaxation time and width. We were interested simply in identifying something new and fast moving in the ^{1}H NMR.

Two samples were prepared and loaded into sealed NMR tubes for ^{1}H NMR. One was the Aldrich Technical Grade $NaAlH_4$, which was loaded straight from the bottle, as bought, containing only the pure $NaAlH_4$—this is the "Before" sample. The second sample of the Aldrich material was placed in the high-pressure probe and melted in a vacuum. In this second sample ^{27}Al NMR showed the presence of Al metal, $NaAlH_4$, Na_3AlH_6, and S105. The melted sample was crushed back down to a powder and loaded into the box probe—this is the "After" sample. A comparison of the two room temperature spectra is shown in Figure 5.12. The melted sample shows a drastic change. Three different peaks are distinguishable by their width: a low broad peak, a narrow peak, and a sharp peak.

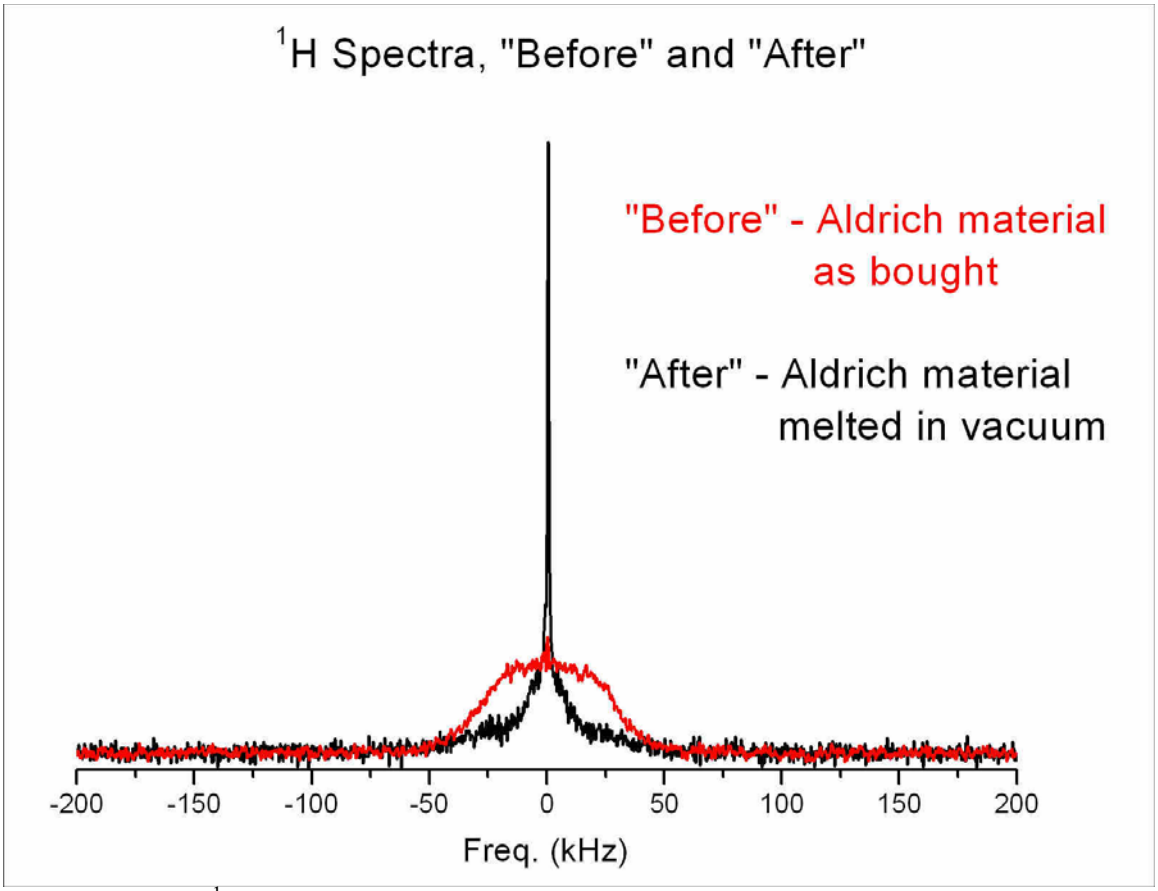

Figure 5.12: ^{1}H spectra of the $NaAlH_4$ system "Before" and "After" S105 is created (verified in ^{27}Al NMR). Material is technical grade $NaAlH_4$ from Aldrich. 10000 sec recycle delay used.

The broad peak in the "After" spectrum is likely the tetrahydride, but it is difficult to measure the width and the S/N is low. The "Before" sample of pure $NaAlH_4$ has a FWHM of 61.1 kHz. T_1 of the "Before" sample was measured by saturation recovery to be 340 seconds. The "before" and "After" samples were two different samples, and so contained different amounts of sample material (since the samples had to be PT-cycled in the high-pressure probe, then re-loaded into the box probe for ^{1}H NMR.). This accounts for the apparent differences in the total area under the curve of the two spectra

The middle, narrower peak has a FWHM of 17 kHz. The spectra of a pure hexahydride (made at U. Hawaii) had a width of 21.3 kHz. The pure hexahydride was

measured to have a T_1 = 580 ms, as measured by saturation recovery. The presence of the hexahydride is expected based on the ^{27}Al NMR of this sample and previous experience, so this middle peak is most likely Na_3AlH_6.

The third, sharp peak is our peak of interest. It has a FWHM of only 740 Hz. T_1 was measured to be 210 ms for the sharp peak. This is the fastest recovery time of all three species, demonstrating more motion than the other two. The peak's sharpness is, again, another indication of rapid motion

^1H spectra of the "After" sample were then taken at colder temperatures. Figure 5.13 shows the spectra throughout the cooling process. The recycle delay for data acquisition was set to 10 seconds. Complete relaxation of the entire spectrum was not necessary for this study because our interest is only the ability to "freeze out" the sharp peak. The sharp peak is seen to steadily decrease down to a small bump on the broader peak at its base. In spectrum **(7)**, taken at -39^{o}C, we see that the peak is still triangular, but in spectrum **(8)**, at -48^{o}C, the peak is rounded and no longer continues to change at lower temperatures. Thus, the initially sharp feature disappears between -39^{o}C and -48^{o}C.

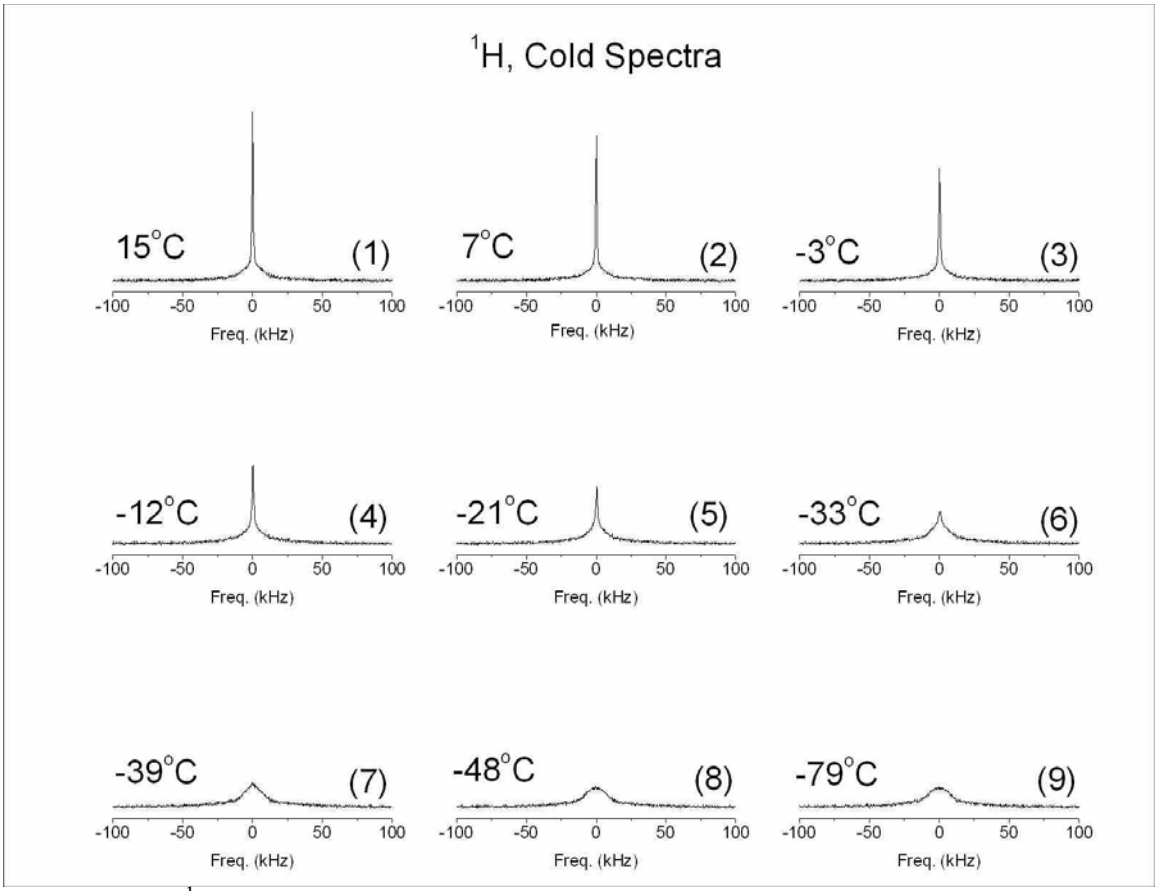

Figure 5.13: ^{1}H spectra at colder temperatures for the "After" Sample. A 10 sec recycle delay was used, so the spectra shown are not fully relaxed. Thus, the broader peak at the base of the sharp peak is Na_3AlH_6.

There is some question as to whether or not the sharp peak is H_2 trapped in voids inside the hydride—as has been identified before in some other hydrides[56]-[58]. However, the freeze-out temperature is *much* too warm for the sharp peak to be associated with hydrogen gas (H_2 solidifies at 14K). For example, NMR of H_2 trapped in solid AlH_3 broadens and disappears as temperature is decreased through approximately 10 K[59]. The ^{1}H sharp peak disappears in Figure 5.13 at a temperature that is close to the temperature that the ^{27}Al S105 freezes out (Figure 5.11). Although this is not a definitive identification in and of itself, when viewed in the context of the narrow FWHM, the short

T_1, and its appearance only in the melted sample that has been confirmed by ^{27}Al NMR to possess S105, we are confident in associating the sharp hydrogen peak with S105 in ^{27}Al.

5.2.7 CPMAS Confirms S105 is Hydrogenated

Some of the material was sent to our collaborator, Sonjong Hwang, at Caltech to have our samples analyzed by magic-angle spinning NMR. For a quick overview of MAS-NMR and the techniques used below, see Chapter 3.2.4.

^{27}Al MAS confirms the existence of S105 (Figure 5.14). It is seen in the PT-cycled material, but not the starting material in both doped and undoped samples. The doped sample also shows a drastically reduced Al metal peak as compared to its starting material, whereas the undoped sample (which was melted under H_2 pressure) shows no metal resonance either before or after melting. Both examples are in agreement with our previous findings regarding the Al metal in these reactions. Both doped and undoped samples show a large amount of AlH_6^{-3} in the PT-cycled material.

To test the idea that S105 is hydrogenated, we asked out collaborator to attempt ^{27}Al-$\{^1H\}$ CPMAS. The results for an undoped $NaAlH_4$ sample are shown below in Figure 5.14. The blue spectrum was taken with MAS at a spinning speed of 15 kHz and the red spectrum was taken with ^{27}Al-$\{^1H\}$ CPMAS. S105 is identified at +100 ppm as a shoulder on the double peak at 95 ppm, which is $NaAlH_4$. The broad peak seen from 85 to 60 ppm in the blue spectrum is an impurity. The peak at 8 ppm is bulk AlH_3. Both the impurity and AlH_3 will be discussed in this next section.

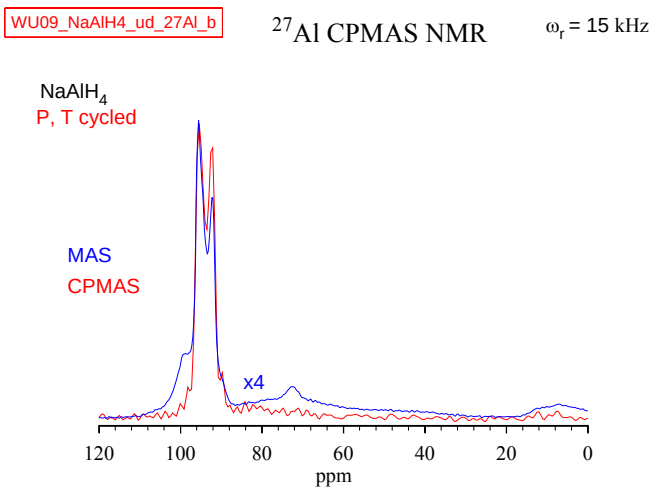

Figure 5.14: CPMAS (red) and MAS (blue) for undoped $NaAlH_4$ melted under H_2 pressure. Spectra taken by Sonjong Hwang at Caltech. AlH_3 appears on right-hand side at ~8 ppm. Some oxide/hydroxide impurity is seen as a broad peak between 85 and 60 ppm. The small bump at ~72 ppm is a spinning sideband from AlH_6^{-3} (off scale at –43 ppm). $NaAlH_4$ is the double peak at 95 ppm. S105 is seen as a shoulder at 100 ppm. A contact time of 0.2 ms was used here with a rotor speed of 15 kHz.

S105 was not initially detected by ^{27}Al-{^{1}H} CP. The contact times were varied from 0.075 ms to 2.0 ms with the same results. This might at first appear to indicate that S105 is not hydrogenated. However, this is not the case. The ^{27}Al-{^{1}H} CP does not work at room temperature because of the *very* rapid motion undergone by S105. Recall that in ^{27}Al NMR the peak can be frozen out around –60°C (Figure 5.11); so at lower temperatures the motion may be slow enough to perform ^{27}Al-{^{1}H} cross-polarization. Figure 5.15 shows a series of spectra from variable temperature (VT) CPMAS performed on a doped sample.

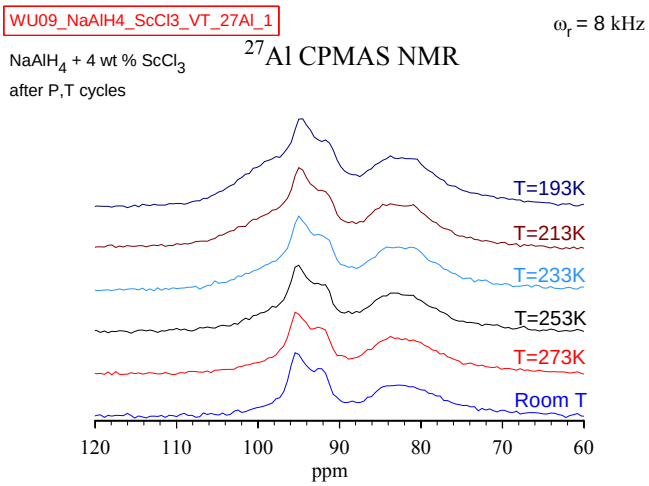

Figure 5.15: VT-CPMAS for a 4 mol% $ScCl_3$ doped sample after PT-cycling to create S105. Spectra taken by Sonjong Hwang at Caltech. S105 (+100 ppm) begins to appear from ^{27}Al-{^{1}H} CP around 213 K, and is obvious by 193 K. A contact time of 200 μs was used.

The VT-CPMAS shows S105 beginning to appear from ^{27}Al-{^{1}H} CP around 213 K (–60^{o}C), or maybe a bit warmer. This is in perfect agreement with the findings of the static ^{27}Al NMR cold spectra of when S105 blended into the surrounding broad signals.

These results tell us that S105 indeed represents a *hydrogenated* Al species that undergoes extremely fast motions at room temperature, such that S105 does not cross-polarize well at room temperature.

5.3 Complementary Findings to the High-Pressure Study

5.3.1 MAS Detection of AlH_3 and an Impurity

There are two peaks that appear in the ^{27}Al MAS which could not be detected in static NMR. The first is a broad peak at ~80 ppm, which appears in the doped and undoped samples both before and after PT-cycling. Our collaborator identifies the ~80 ppm peak with some form of $AlH_x(OH)_{4-x}$ or AlO_4 type species. One other group[60] has reported finding a peak similar to this ^{27}Al peak and has suggested an AlO_4 species. It is hard to imagine *all* our samples oxidized like this, given the care taken in the sample material's treatment, but the only other option is that this possibly happened during shipment of the sample. Information is still being put together on this impurity peak.

A big question is the role, if any, of this other possible oxide/hydroxide in the creation of S105. Further MAS of the undoped Aldrich $NaAlH_4$ and undoped $NaAlH_4$ from U. of Hawaii, which had not been PT-cycled, was done. The U of Hawaii material contained a large amount of oxide/hydroxide. But the Aldrich sample showed little to no oxide/hydroxide. Both the U. of Hawaii material and the Aldrich material *always* generated S105 when PT-cycled.

The ~80 ppm peak appeared in various amounts in a few different samples (doped and undoped) and was very evident in ^{27}Al-$\{^1H\}$ CPMAS (so, a hydrogen bearing species, such as aluminum hydroxide). It was also present both before and after PT-cycling. S105 can be created in samples that do or don't show the oxide/hydroxide, and so it is not likely that the oxide/hydroxide plays a role in generating S105.

The second peak was identified as bulk AlH_3 (See Figure 5.14 for AlH_3). Bulk AlH_3 shifts are shown in Table 4.1. AlH_3 was detected by MAS in both doped and undoped samples. In static NMR, the presence of a small amount of AlH_3 would not be able to be detected because it would be hidden in the large, broad AlH_4^{-1} peak. Thus, in

the analysis done by integration of the spectra (Chapter 5.2.2) any AlH_3 signal would be counted as AlH_4^{-1} (the AlH_6^{-3} shift is too low to overlap, and S105 shift is too high to overlap.) Thus, the measurement of ~10% of the ^{27}Al spins as S105 is not affected.

5.3.2 ^{23}Na NMR

The vast majority of the work done in this project is ^{27}Al, but because the mobile intermediate species could also involve Na, ^{23}Na spectra were taken for comparison in both undoped (Figure 5.16) and doped (not shown) $NaAlH_4$.

There are numerically more peaks to be observed in ^{23}Na NMR than ^{27}Al for the $NaAlH_4$ reactions. Unfortunately, all that could be seen was a single peak (See Figure 5.16). The chemical shifts in ^{23}Na are smaller than ^{27}Al shifts—and with more peaks in a smaller shift range the different species could not be resolved with static NMR. Table 5.2, below, shows peak positions of the ^{23}Na reactants and products involved with de-/re-hydriding, as well as a couple other possible products that may or may not arise given the experimental parameters and treatment of the sample.

^{23}Na NMR Signal Locations		
Na Species	**Peak Location**	**Literature Reference**
NaCl	7 ppm (660 Hz)	[20]
$NaAlH_4$	-9 ppm (-840 Hz)	[38], [20]
Na_3AlH_6	23 ppm (I) (2150 kHz) -10 ppm (II) (-940 Hz)	[38], [20]
NaH	18 ppm (1690 Hz)	[38], [11]
Na metal	1030 ppm (96.5 kHz)	[60]
Na_2O	53 ppm (4970 Hz)	[60]

Table 5.2: ^{23}Na peak locations with respect to NaCl (aq.).

NaCl is included in the above table because it is commonly found in samples doped with metal-chlorides ($TiCl_4$, $TiCl_3$, $ScCl_3$, etc.). When the metal-chloride is either ball-milled or combined in solution together with the $NaAlH_4$, NaCl is typically formed by a reaction like[20]:

$$\mathbf{TiCl_3 + 3NaAlH_4 \rightarrow TiAl_3 + 3NaCl + 6H_2} \qquad 5.2$$

There are other similar chemically favorable routes that can also be taken to form NaCl from the metal-chloride dopant.

A fresh, uncycled sample of undoped alanate (from Aldrich) was loaded into the cold probe and ^{23}Na spectrum taken. This is the "Before" spectrum below in Figure 5.16. Then a sample from the same Aldrich material was melted in the high-pressure probe into a vacuum. This was done while observing ^{27}Al NMR to confirm the creation of the S105. After the S105 peak was created, the sample was loaded into the cold probe and a ^{23}Na spectrum taken. This is the "After" spectrum in Figure 5.16. ^{27}Al NMR spectra were taken before and after taking the ^{23}Na spectra to make sure S105 was still present in the "after" sample.

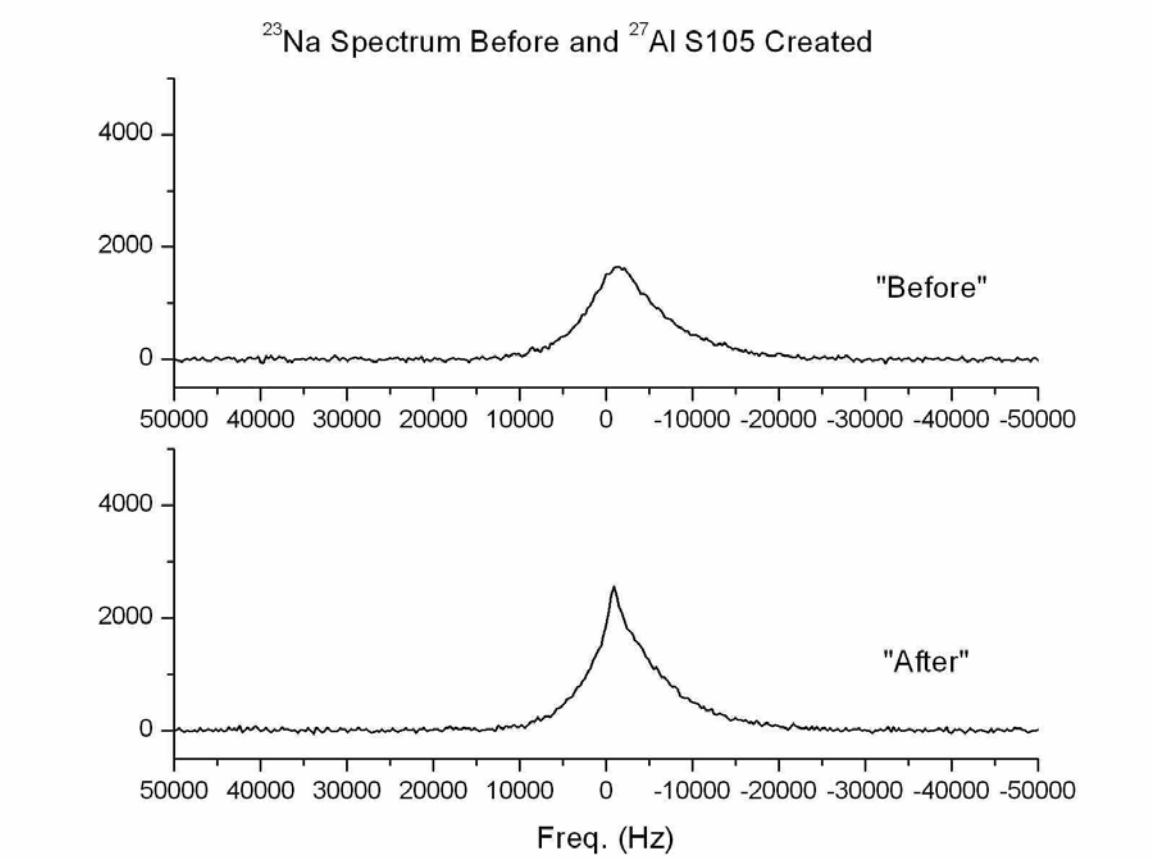

Figure 5.16: ^{23}Na spectrum of undoped $NaAlH_4$ ("Before") compared to spectrum of the same starting sample material which has been melted and cooled initially in a vacuum ("After") to generate S105. 93.684 MHz, 90°-90° echo, τ = 300 μs, 20 sec recycle delay.

The spectra above were taken with a 90°-90° echo (Chapter 3.3.3). The effective 90° pulse length in the cold probe (3 μs) was shorter than the high-pressure probe (10 μs)—when compared at the same transmitter attenuation (18 dBs)—due to the smaller r.f. coil. The transmitter attenuation was then adjusted to make the effective 90°-pulse time 10 μs. (Note: this procedure was replicated for the ^{45}Sc NMR below.)

The noticeable difference in the two ^{23}Na spectra (Figure 5.16) is the sharp feature at the center of the "After" ^{23}Na spectrum. The "Before" spectrum shows a single, asymmetrical peak. The "After" spectrum shows a peak that could be seen as composed

of a slightly broader, unsymmetrical, line and a slightly narrower peak with similar centers.

As in the ^{27}Al NMR, if there is a highly mobile Na species, it will most likely have a narrowed peak in static ^{23}Na spectra. It is difficult to tell whether or not the sharper element of the ^{23}Na is associated only with the presence of Na_3AlH_6 (which is expected from ^{27}Al spectra), or if there is an additional sharp element that may be associated in some way with the highly mobile ^{27}Al S105 species.

^{23}Na MAS of an undoped sample showed AlH_4^{-1} starting material, and the PT-cycled material showed only AlH_4^{-1} plus AlH_6^{-3}. For doped material, the presence of NaCl and AlH_4^{-1} was detected in the starting material, while NaCl, AlH_4^{-1}, and AlH_6^{-3} could be identified in the PT-cycled material. The only difference between the doped and undoped material seen in ^{23}Na NMR is the presence of NaCl, as might be expected by Equation 5.2 (above). No bulk NaH is seen in either sample, so we are likely dealing with only the first reaction step, Equation 1.1. No other Na species seem to be created in the PT-cycle, so S105 seen in ^{27}Al NMR does not incorporate Na.

For these reasons ^{23}Na NMR was not pursued any further.

5.3.3 ^{45}Sc NMR

Just a few spectra were taken of ^{45}Sc NMR in the high-pressure probe. Because most of the samples used were doped with Sc (Chapter 2.10.1)—which is NMR active—there was an opportunity to see if the dopant metal showed up in a mobile phase corresponding to the presence of the ^{27}Al S105 peak.

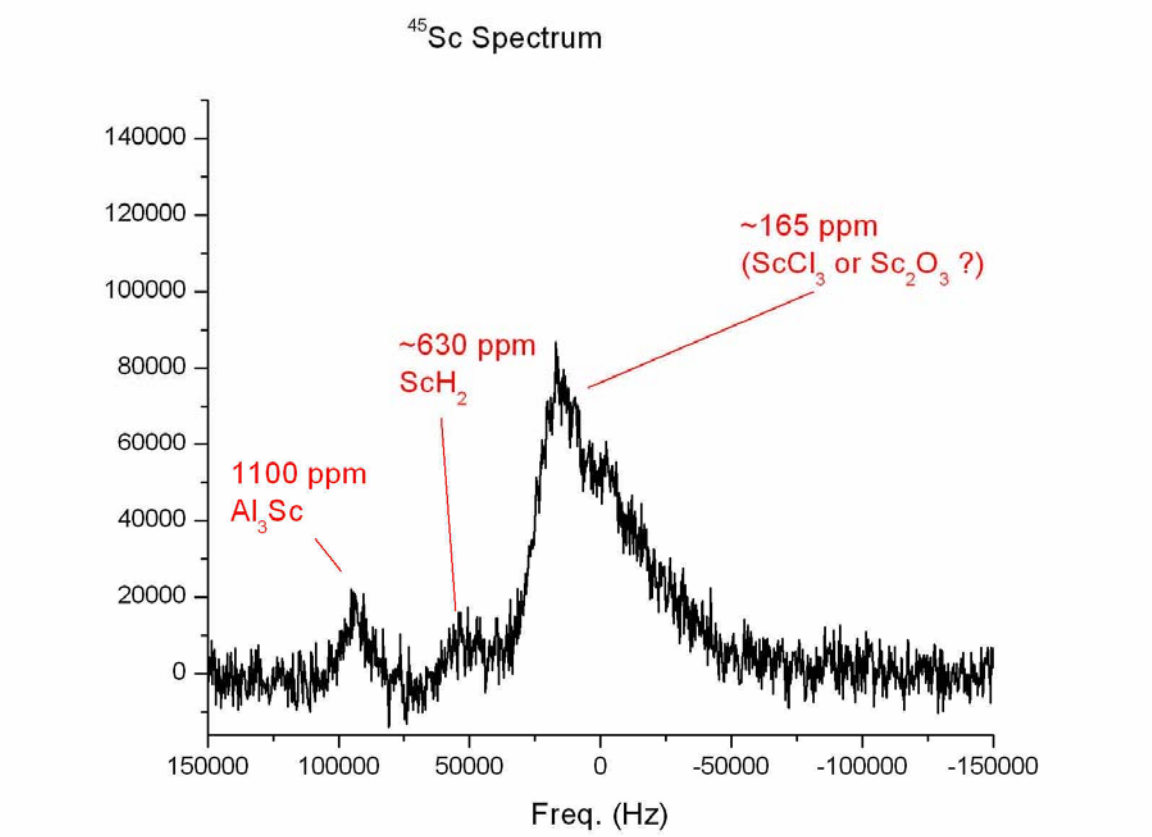

Figure 5.17: ^{45}Sc spectrum (86.035 MHz) of 4.04 mol% $ScCl_3$ doped sample after being PT-cycled to generate the new ^{27}Al species. This spectrum was taken in a vacuum at room temperature with single 10 μs pulses at a recycle delay of 83 ms for 100,000 acquisitions.

Figure 5.17 shows one of the spectra taken on a $NaAlH_4$ sample doped with 4.04 mol% $ScCl_3$. The ^{45}Sc NMR signal is very weak and took an excessively long time to acquire—even at a data acquisition recycle delay of 83 ms. In particular, the above spectrum was taken in vacuum at room temperature after the S105 had been generated in the sample. Again, ^{27}Al NMR was checked before and after the ^{45}Sc NMR was performed to assure that S105 was still present.

Three broad peaks are seen centered at about +1100 ppm (94.6 kHz), +630 ppm (54.2 kHz), and +165 ppm (14.2 kHz). A table of Sc compounds that have been observed before in this system and could possibly be formed is given below in Table 5.3. The peak

at 1100 ppm is Al_3Sc, which is in accordance with what was observed before in ^{27}Al NMR (not shown). The peak at ~630 ppm is most likely ScH_2, while the peak at ~165 ppm is harder to identify and could be either a chloride or oxide of Sc or both.

^{45}Sc NMR Signal Locations		
Sc Species	**Peak Location**	**Literature Reference**
Al_3Sc	1100 ppm (94.6 kHz)	[48], [49], [66]
ScH_2	~600 ppm (~52 kHz)	[67]
$ScCl_3$	225 ppm (19.4 kHz)	[68]
Sc_2O_3	108 ppm (I) (9.3 kHz) 128 ppm (II) (11.0 kHz)	[65]

Table 5.3: ^{45}Sc peak locations with respect to $Sc(NO_3)_3$ (aq.).

Even with the identification of the ~165 ppm peak being uncertain, all three peaks are broad, so the 165 ppm peak is not likely to be associated with the sharp, highly mobile ^{27}Al S105 species.

Because a new sharp peak was not observed and because of the long acquisition times in ^{45}Sc NMR, no further attempts at *in situ* studies were pursued nor were any further investigations beyond the simple spectra, such as shown above.

5.3.4 X-Ray Diffraction

Samples were also sent to our collaborator, Terry Udovic, at NIST for x-ray diffraction (XRD) analysis. Four samples were run at NIST: 1) a sample of undoped, technical grade $NaAlH_4$ powder as purchased from Aldrich which was used to create the other samples sent, 2) a sample of undoped $NaAlH_4$ that was melted under high-pressure H_2, 3) a sample of undoped $NaAlH_4$ that was melted into an initial vacuum, and 4) a

second sample of undoped $NaAlH_4$ also melted into a vacuum. Earlier, a sample of $ScCl_3$ doped $NaAlH_4$ had been sent for XRD analysis, but our collaborator reported that the pattern was dominated by diffraction peaks associated with the catalyst and thus difficult to interpret.

The four XRD patterns are shown below (Figure 5.18) without in-depth interpretation. Our collaborator has not yet been able to provide us with much information beyond these patterns. It can be said that the sample undergoes significant changes, and much of the diffraction pattern simply disappears (note that the vertical scale changes). This most likely indicates a large amount of amorphous or disordered material. The peaks observed in the "As Bought" sample belong to $NaAlH_4$. The $NaAlH_4$ peak at 30^o is still evident after the PT-cycle, but reduced in strength. The other $NaAlH_4$ peaks are greatly reduced. After melting, there is a peak that corresponds to Na_3AlH_6 (identified by comparison to authentic Na_3AlH_6) The relative intensity of the Na_3AlH_6 peak seems to vary from sample to sample.

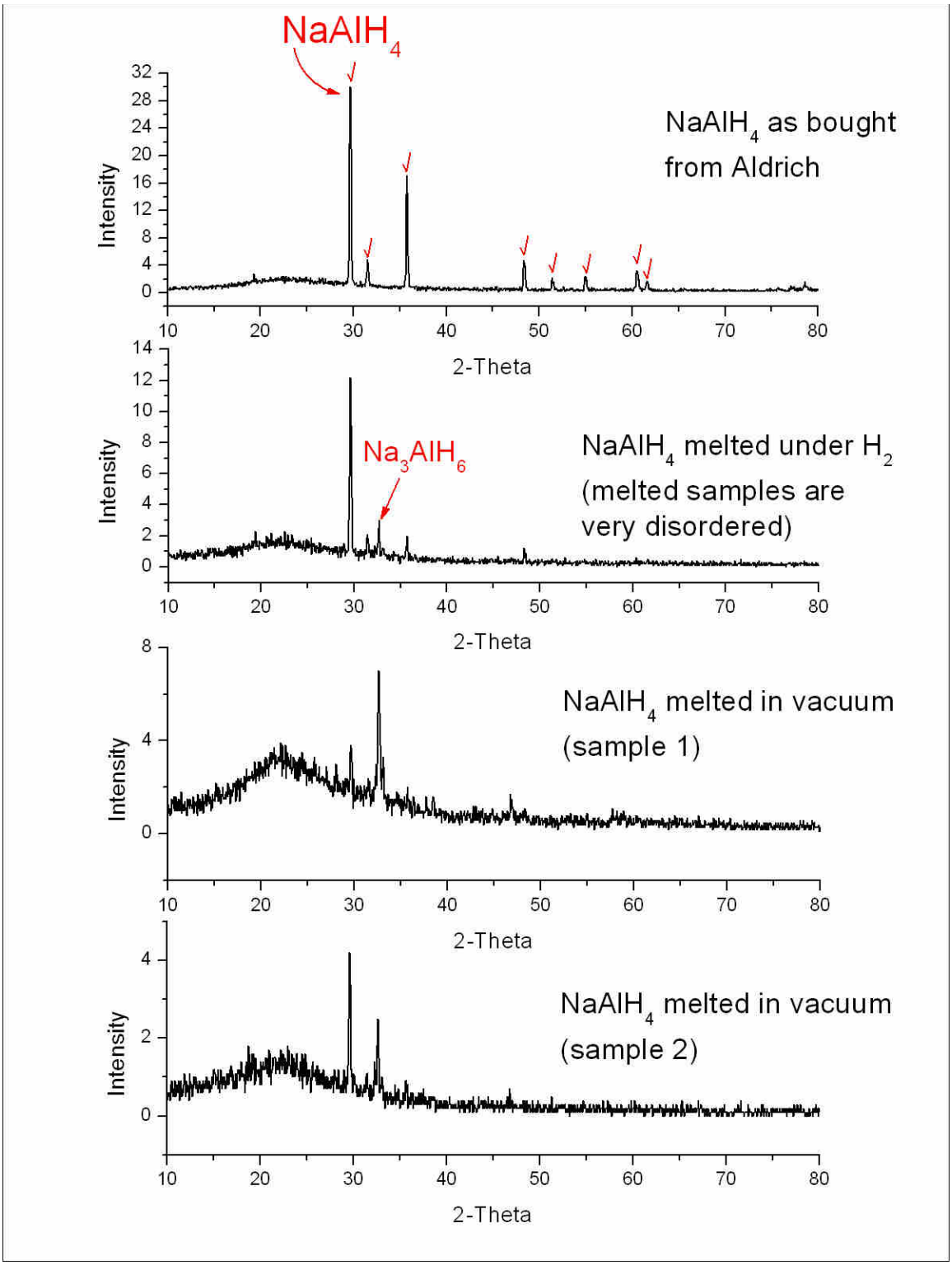

Figure 5.18: XRD patterns of four undoped samples. Red check marks indicate $NaAlH_4$ peaks.

CHAPTER 6:

CONCLUSIONS

This final chapter is to collect and review what is known experimentally through both phases of work. Much has been covered and a summary discussion of the results should help to remind the reader of what was discovered by the NMR methods that have been applied.

Then a discussion is included that relates some findings concerning an increasingly popular hypothesis that the hydriding reactions are mediated by vacancies in the alanate (NaH vacancies or AlH_3 vacancies). The discussion is not conclusive, but seeks only to show how the experimental results of this thesis may or may not fit with some of the ideas that have been proposed about mobile defect complexes in the $NaAlH_4$ system.

Finally the chapter ends with possible directions the research could be continued or ways in which the present findings could be augmented.

6.1 Study Review

Sodium alanate decomposes in a stepwise fashion that requires large-scale transfer of Al or Na atoms. In this reaction, mass transfer of metal atoms through the material is the rate-limiting step, not H_2 exchange. To accomplish this, there must be some highly mobile, intermediate chemical species that contains Al and/or Na atoms. The intermediate species should be detectable by NMR.

We set out to find such a mobile Al- (or Na-) bearing species by utilizing *in situ* NMR in a built-to-purpose probe capable of controlling $NaAlH_4$ hydriding reactions. One such Al species possessing the theoretical characteristics of a mobile, intermediate species was detected and further investigated.

This new Al species, named "S105", was first detected during *in situ* de-hydriding of doped $NaAlH_4$ as a narrow peak in static ^{27}Al NMR, with a chemical shift around +105 ppm with respect to aqueous $Al(NO_3)_3$, just up frequency from $NaAlH_4$ itself. Thus, the chemical shift of S105 suggests an AlH_4^{-1}-like species (AlH_x). S105 appears during both re-hydriding and de-hydriding in both Sc- and Ti-doped samples, but does not appear in undoped samples (not below the melting temperature of the alanate, anyway). We believe this observation is tied to the fact that the undoped samples do not de-/re-hydride below the melting temperature. In both directions of the *in situ* reactions, the ^{27}Al +105 ppm peak appears with the greatest intensity while the reaction is in progress. The peak appears when the material begins taking up or releasing H_2 and disappears—or minimizes in some re-hydriding cases—when the H_2 stops reacting. For re-hydriding, once the sample stops taking up H_2 (interpreted from watching the spectra and the H_2 pressure over the sample) the S105 signal is greatly reduced but can remain (in a few cases) at low intensity. For de-hydriding, the +105 ppm signal exists with or without the presence of H_2 in the reaction chamber during sample decomposition. In both cases, the faster the reaction progresses, the stronger the +105 ppm peak appears. As the reaction slows, the intensity of the mystery signal decreases. For the above reasons, it can be concluded that S105 is linked intimately to the hydriding reactions.

It was discovered thereafter that S105 could be caused to persist in doped samples at ambient temperatures and pressures by the application of H_2 over-pressure (exceeding the equilibrium pressure of $NaAlH_4$ at the highest temperature to be used), and then heating of the sample within the normal reaction temperature range. Once S105 was formed, the sample was returned to ambient pressure and temperature, and S105 remained. The formation temperature of S105 in doped samples varies, as does the intensity of S105's signal.

S105 can also be formed in undoped samples if the sample is melted. The formation becomes apparent as the sample cools from the molten state. This is an important finding. It appears that, the dopant allows for the formation of this new species in doped samples before the $NaAlH_4$ melts, whereas formation in bare samples requires the $NaAlH_4$ to reach the molten state.

There are two different cases for the generation of S105 in undoped material. For undoped $NaAlH_4$ melted into (initially) a vacuum, aluminum metal appears in conjunction with the release of hydrogen gas. However, in undoped samples melted in an excess high-pressure H_2 atmosphere, no aluminum metal is created. Also, it appears no additional H_2 gas is evolved, though the error bars on this last statement are broader than we would like. But we note that, in all of the reactions 1.1 and 1.2, the redox view of the reactions is that Al is reduced (from Al^{+3} to Al^0) and H is oxidized from H^- to H-neutral. Thus, if no Al metal appears, it is most unlikely that H_2 is produced.

The molten-state reaction is different from the solid-state reaction—probably because there is more mobility for every reactant as opposed to just the Al or Na bearing species in the solid-state reaction. The size of the S105 peak in undoped samples is not

much dependent on H_2 pressure or vacuum in the sample chamber and furthermore the intensity of the S105 peak remains more nearly constant across several undoped samples (including ones from the Univ. of Hawaii and Aldrich). The formation of Al metal in the case of melting bare $NaAlH_4$ in a vacuum is likely due in part to partial de-hydriding of the material, as evidenced by the release of some H_2 and the appearance of some Al metal. The de-hydriding takes place because there is no overpressure driving the reaction back toward $NaAlH_4$.

The formation of Na_3AlH_6 (from molten bare $NaAlH_4$ or doped solid $NaAlH_4$)is *always* coincident with the formation of S105, regardless of the presence of a dopant. As mentioned above, during melting of undoped alanate in vacuum the system undergoes partial decomposition into Al metal and H_2, which might be the source of some of the AlH_6^{-3}. However, not enough hydrogen is released to quantitatively explain the production of AlH_6^{-3} through the decomposition pathway in Equation 1.1 alone (Chapter 1.2). More AlH_6^{-3} is created than can be accounted for based on the amount of H_2 released. Crucially, AlH_6^{-3} is also created when the equilibrium pressure is overwhelmingly in favor of AlH_4^{-1} for the case of doped material and for the case of molten undoped material under excess H_2 pressure (where, again, no Al metal is evolved and it appears no H_2 is evolved). Thus, AlH_6^{-3} is created by some other reaction.

There are other interesting formation phenomena associated with S105. S105 requires specifically $NaAlH_4$ in order to form. It does not form from Na_3AlH_6 or Al metal alone. Moreover, S105 is involved chemically with aluminum metal. In those doped samples, for which there is an excess of Al metal in the starting material, the Al metal signal diminishes (or completely disappears) when S105 forms. But when there is

no initial excess Al metal in the doped sample, then when S105 forms, Al metal forms as well. Aluminum metal appears to be an intermediate, or at least sidetrack, reactant or product in the formation of S105.

In general, S105 represents a significant portion of the ^{27}Al content of the sample, occupying around 10% of the ^{27}Al signal in samples without initial or final Al metal. This large signal is long lived. The longest rigorously observed existence at ambient pressures and temperatures was 77 days without the intensity diminishing. But many other samples were stored, manipulated, and shipped at ambient temperatures and pressures for longer periods of time without the S105 signal disappearing.

^{23}Na static NMR shows that a somewhat narrower Na species does appear along with the creation of the ^{27}Al +105 ppm peak. But the static spectra cannot distinguish (because of broad lines and the small range of ^{23}Na shifts) whether the sharper ^{23}Na peak is just Na_3AlH_6 or Na_3AlH_6 plus a second ^{23}Na species with a chemical shift very near to Na_3AlH_6. With the help of ^{23}Na MAS NMR we know that the samples appear to contain only Na_3AlH_6, NaCl, and $NaAlH_4$. So it can be concluded that the S105 observed in ^{27}Al NMR does not incorporate Na. Additionally, it should be noted that no bulk NaH was detected (so we are likely dealing with something like the first reaction step only, Equation 1.1). ^{45}Sc NMR did not show the production of a new, narrow peak in PT-cycled material where S105 was known to be generated. Thus Sc, in all likelihood, is not associated with the sharp, highly mobile ^{27}Al +105 ppm species.

Static ^{1}H NMR does show a narrow peak that is present only when the ^{27}Al +105 ppm peak is present. Thus, the narrow peak in static ^{1}H spectra is likely associated with the +105 ppm peak in ^{27}Al. The ^{1}H shifts are small, so unobservable for these broad lines

in static ^{1}H NMR (recall, f_o^H = 85.025 MHz here and the ^{1}H shift range is only about 10 ppm wide). ^{27}Al-{^{1}H} CPMAS confirms that the S105 is hydrogenated. It also identifies S105 as undergoing fast motion at room temperature because the cross-polarization was not effective until colder temperatures (approximately -80°C), where the motions are slower.

Measured ^{27}Al relaxation times further indicate a high degree of motion. T_1 is very short, ~1 ms at room temperature. We can deduce that tS105 has a large, motionally-modulated EFG. The nutation measurements show that our effective 90°-pulses excite the central transition only (m = +1/2 ↔ -1/2) of S105. Thus S105 has in addition, a large static quadrupole interaction. We note that rapid hopping between sites will not (in general) average away all EFGs in the non-cubic $NaAlH_4$ lattice. T_2 is about half of T_1. The measured T_2 (~0.375 ms) accounts for about 75% of the observed 12.5 ppm linewidth ($1/\pi T_2^{room\text{-}T}$ = 860 Hz = 9.3 ppm) at room temperature. All of this suggests a species with much motion.

Motional narrowing of S105 was directly demonstrated in both ^{27}Al and ^{1}H spectra. The peaks, narrow at room temperature, broaden upon cooling until they are no longer distinguishable from the other, broad signals (-60°C for ^{27}Al and -40°C for ^{1}H). This also completely removes any suspicion of the ^{1}H narrow peak being trapped H_2 gas, which does not solidify until 14 K, and remains motionally narrow down to 10 K in one case that was examined closely[59]. These results, and the ^{27}Al-{^{1}H} CPMAS, indicate S105 has Al and H, so it has the form Al_xH_y.

^{27}Al MAS interestingly detected bulk, crystalline AlH_3 (6 ppm to 36 ppm, depending on the alane phase) in the samples where S105 had been generated. It is

interesting to note that the 4:1 H:Al ratio of the starting material must stay constant in the bare samples melted under H_2 pressure, since these do not liberate Al metal nor appreciable H_2 gas. AlH_6^{-3} is hydrogen rich (H:Al > 4) compared to the starting $NaAlH_4$, and AlH_3 is hydrogen deficient (H:Al < 4). The H:Al ratio of S105, which could provide key information about the make-up of S105, depends on the balance of the AlH_3-to-AlH_6^{-3} ratio. We would need a quantitative measurement of the integral of the AlH_3 peak with respect to the AlH_6^{-3} peak and S105 peak for more certainty. The products remaining ($NaAlH_4$, some Na_3AlH_6, the bulk AlH_3, and S105) must all be measured quantitatively to assess the H:Al ratio of species S105.

Reckoning all these phenomena with each other is imposing. We cannot identify the exact chemical make-up of the S105 species from the data in this thesis alone. But certain characteristics are well established and others can be deduced from what others have published.

6.2 Discussion

The following discussion, as well as the chemical formulae, will proceed from three papers: H. Gunaydin *et al.*[61], V. Ozoliņš *et al.*[69], and some from A. Borgschulte *et al.*[26]. In these papers are found a proposed theory of vacancy mediated hydriding reactions for $NaAlH_4$ that is backed by computational work.

According to this theory, the de-/re-hydriding reactions are mediated by bulk diffusion of neutral vacancies (AlH_3^v and NaH^v, where the superscript "v" denotes "vacancy"). The introduction of a vacancy causes reorganization of the Al-H complexes

in $NaAlH_4$. Such defects may have been detected with anelastic scattering[62], INS[63], and *in situ* XRD[64].

An AlH_3^v is (formally) a Na^+ on a Na^+ site, and an H^- on an AlH_4^- site. This distorts to form $H^- + AlH_4^- = AlH_5^{-2}$ complexes. Clearly, an AlH_3^v means the H:Al ratio increases above 4. Likewise, a NaH^v is (formally) a vacancy on the Na^+ site, and an AlH_3 neutral on an AlH_4^- site. Then one gets $AlH_3 + AlH_4^- = Al_2H_7^-$ complexes. A NaH^v means the H:Al ratio decreases below 4. AlH_3-vacancy mediated reactions are believed to be more likely because the calculated formation and diffusion energies are lowest[61], [69].

Both of these options for neutral vacancies would result in vacancy mediated diffusion. They provide some intriguing connections to what is experimentally observed in this thesis. Immediately we notice that the above reactions do produce AlH_x units with rapid exchange and mass transfer of Al or Na atoms, which should have AlH_4^{-1}-like chemical shifts, in agreement with what is observed. Additionally, both of these options would only form in the $NaAlH_4$ system, and cannot work with only Al metal or pure Na_3AlH_6, as experimentally observed for S105. Moreover, the hydrogen defect complexes would undergo rapid motion as they diffuse about the sample, which would freeze out at colder temperatures, as observed.

But neither option seems to fit perfectly with what is experimentally observed. If NaH vacancies dominate, then it seems likely that Na and H spins will diffuse, but not Al. However, experimentally we see a mobile Al and H species, but not Na. If AlH_3 vacancies are present, this means Al and H will diffuse, but not Na (in agreement with what is experimentally observed). We note that, H. Gunaydin *et al.* and V. Ozoliņš *et al*.

require the release of H_2 and Al metal to form either NaH or AlH_3 vacancies, quite different from our conditions. Generation of the vacancies, if these are present under "hydrogen-blocked" conditions, must be different here than the published scenario. Reconciling the difference in how aluminum metal is involved in the doped and undoped reactions remains difficult to do. A major question is why these vacancies should remain after initially created under high-pressure H_2; perhaps some species have diffused apart from each other.

It is also unlikely that a sufficient number of defects could form to detect the AlH_5^{-2} or $Al_2H_7^{-1}$ complexes directly (recall, S105 is ~10% of the ^{27}Al signal). It is more likely that S105 comes from a region of $NaAlH_4$ that has a lot of defects (say AlH_3 vacancies) so all the Al and H spins in the region are narrowed. This picture automatically leads to a chemical shift that is very close to molten $NaAlH_4$ in static NMR, as experimentally observed (molten $NaAlH_4$ = 100 ppm and S105 = 103 to 105 ppm).

6.3 Looking to the Future

There are some avenues left in which the results of this thesis could be augmented. Early on, the decision was made to forgo directly testing NaH + H_2 reactions. This was based upon the lack of a new Na species found in MAS corresponding to S105 (Figure 5.16, Chapter 5.3.2). In light of the above discussion, it might also be advantageous to go back and hunt more specifically for a mobile Na-

bearing species that may not stick around after the high pressure is evacuated. If none is found, it would rule out the notion of a mobile Na species.

A more detailed XRD analysis would also be useful. The material shows large changes and many peaks in the pattern disappear, so this may not prove to be *much* more helpful, but more certain identification of the peaks that are present could be beneficial.

It would also be beneficial to get the ^{27}Al MAS spectra analyzed to find the proportions of AlH_6^{-3} : S105 : AlH_3. The spectra would need to be run under "quantitative" conditions, i.e., using a data acquisition recycle delay that is much greater than T_1 of every species. This could tell us more accurately the Al/H ratio for S105 and might be able to guide our thoughts about the content of the hydriding reaction. Additionally, sending more samples from other PT-cycled material might be able to answer if AlH_3 is always created. It is not likely that we happened to only send samples with AlH_3 and kept the samples without AlH_3, but MAS of multiple samples cases would solidify this point.

REFERENCES:

1 N.T. Stetson. “Hydrogen Storage Technologies – A Tutorial with Perspectives from the US National Program”. Materials Challenges in Alternative and Renewable Energy sponsored by U.S. Department of Energy. Cocoa Beach, FL. 22 February, 2010. Oral presentation.

2 Züttel, Andreas. *Materials for Hydrogen Storage*. Materials Today: September 2003

3 A. Züttel, Naturwissenschoften 91 (2004) 157-172

4 L. Schlapbach and A. Züttel, Nature 414 (2001) 353-358

5 G.W. Crabtree and M.S. Dresselhaus, MRS Bulletin 33 (2008) 421-428

6 A. Steinfeld, Sol. Energy 78 (2005) 603-615

7 B. Bogdanović, R.A. Brand, A. Marjanović, M. Schwickardi, J. Tölle, J. Alloys Compd. 302 (2000) 36–58

8 C.M. Jensen, K.J. Gross, Appl. Phys. A. 72 (2001) 213-219

9 J. Zhang, M.A. Pilette, F. Cuevas, T. Charpentier, F. Mauri, and M. Latroche, J. Chem. Phys. C 113 (2009) 21242-21252

10 M. Fichtner, Ann. Chim. Sci. Mat. 30 (2005) 5 483-494

11 V.P. Tarasov, and G.A. Kirakosyan, Russ. J. Inorg. Chem. 53 (2008) 13 2048-2081

12 B.M. Lee, J.W Jang, J.H. Shim, Y.W. Cho, B.J. Lee, J. Alloys Compd. 424 (2006) 370-375

13 J Gao, P. Adelhelm, M.H.W. Verkuijlen, C. Rongeat, M. Herrich, P.J.M. van Bentum, O. Gutfleisch, A.P.M. Kentgens, K.P. de Jong, and P.E. de Jongh, J. Phys. Chem. C 114 (2010) 4675-4682

14 B. Bogdanović, M. Schwickardi, J. Alloys Compd. 253-254 (1997) 1-9

15 C. Weidenthaler, A. Pommerin, M. Felderhoff, B. Bogdanović, and F. Schüth, Phys. Chem. Chem. Phys. 5 (2003) 5149-5153

16 M. Fichtner, O. Fuhr, O. Kircher, J. Rothe, Nanotechnology 12 (2003) 778-785

17 B. Bogdanović, M. Felderhoff, S. Kaskel, A. Pommerin, K. Schlichte, F. Schüth, Adv. Mater. 15 (12) (2003) 1012

18 K.J. Gross, E.H. Majzoub, S.W. Spangler, J. Alloys Compd. 356-357 (2003) 423-428

19 M. Resan, M.D. Hampton, J.K. Lomness, D.K. Slattery, Int. J. Hydrogen Energy 30 (2005) 1417-1421

20 E.H. Majzoub, J.L. Herberg, R. Stumpf, S. Spangler, R.S. Maxwell, J. Alloys Compd. 394 (2005) 265-270

21 J. Wang, A.D. Ebner, R. Zidan, and J.A. Ritter, J. Alloys Compd. 391 (2005) 245-255

22 R. Zidan, S. Takara, A.G. Hee, and C.M. Jensen, J. Alloys Compd. 285 (1999) 119-122

23 S. Chaudhuri, J. Graetz, A. Ignatov, J.J. Reilly, and J.T. Muckerman, J. Am. Chem. Soc. 128 (2006) 35 11404-11415

24 B. Bogdanović, U. Eberle, M. Felderhoff, and F. Schüth, Scr. Mater. 56 (2007) 813-816

25 C.M. Anderi, J.C. Walmsley, H.W. Brinks, R. Holmestad, S.S. Srinivasan, C.M. Jensen, and B.C. Hauback, Appl. Phys A 80 (2004) 4 709-715

26 A. Borgschulte, A. Züttel, P. Hug, G. Barkhordarian, N. Eigen, M. Dornheim, R. Bormann, and A.J. Ramirez-Cuesta, Phys. Chem. Chem. Phys. 10 (2008) 4045-4055

27 W. Lohstroh and M. Fichtner, Phys. Rev. B 75 (2007) 184106

28 J.M. Bellosta van Colbe, W. Schmidt, M. Felderhoff, B. Bogdanović, and F. Schüth, Angew. Chem. Int. Ed. 45 (2006)3663-3665

29 D.B. Baker, M.S. Conradi, Rev. Sci. Instrum. 76 (2005) 073906

30 L. Senadheera, Ph. D. Thesis, Washington University (2008), St. Louis, MO

31 Parker Seals. “Parker O-Ring Handbook.” Lexington KY: Parker Seal Group, 1982

32 “O-Ring Material Selection / Comparison Guide”, Marco Rubber & Plastic Products, Inc. Catalogue, 1997. Web. 13 May 2009

33 MSDS for $NaAlH_4$ acquired through Sigmal-Aldrich. Revision date: 29 December, 2008. Print date: 8 March, 2010.

34 R.L. Corey, T.M. Ivancic, D.T. Shane, E.A. Carl, R.C. Bowman, Jr., J.M Bellosta van Colbe, M. Dornheim, R. Bormann, J. Huot, R. Zidan, A.C. Stowe, and M.S. Conradi, J. Phys. Chem. C 112 (2008) 19784-19790

35 C.D. Browning, Ph. D. Thesis, Washington University (2004), St. Louis, MO

36 B. Bogdanović, M. Felderhoff, A. Pommerin, F. Schüth, N. Spielkamp, Adv. Mater. 18 (2006) 1198-1201

37 T. Wang, J. Wang, A.D. Ebner, and J.A. Ritter, J. Alloys Compd. 450 (2008) 239-300

38 B. Bogdanović, M. Felderhoff, M. Germann, M. Härtel, A. Pommerin, F. Schüth, C. Weidenthaler, B. Zibrowius, J. Alloys Compd. 350 (2003) 246-255

39 J. Wang, A.D. Ebner, T. Prozorov, R. Zidan, and J.A. Ritter, J. Alloys Compd. 395 (2005) 252-262

40 Abragam, A. *The Principles of Nuclear Magnetism*. London: Oxford University Press, 1961. Print.

41 Fukushima, Eiichi., Stephan B.W. Roeder. *Experimental Pulse NMR: A Nuts and Bolts Approach*. Westview Press, 1981. Print.

42 Levitt, Malcolm H. *Spin Dynamics: Basics of Nuclear Magnetic Resonance*. Chichester, West Sussex: John Wiley & Sons Ltd, 2008. Print.

43 Slichter, C.P. *Principles of Magnetic Resonance*. Chichester, Berlin: Springer, 1978. Print.

44 A. Wokaun and R.R. Ernst, J. Chem. Phys. 67 (4) (1977) 1752-1758

45 S. Vega, J. Chem. Phys. 68 (7) (1978) 5518-5527

46 V.P. Tarasov and G.A. Kirakosyan, Russ. J. Inorg. Chem. 42 (8) (1997) 1223-1227

47 M.H.W. Verkuijlen, P.J.M. van Bentum, E.R.H. van Eck, W. Lohstroh, M. Fichtner, and A.P.M. Kentgens, J. Phys. Chem. C 113 (2009) 15467-15472

48 S. Celotto and T.J. Bastow, Philos. Mag. A 80 (2000) (5) 111-1125

49 T.J. Bastow, C.T. Farwood, and M.A. Gibson, Phys. Rev. B 58 (1998) (6) 2988-2997

50 S.J. Hwang, R.C. Bowman, Jr., J. Graetz, J.J. Reilly, W. Langley, and C.M. Jensen, J. Alloys Compd. 446-447 (2007) 290-295

51 J.L. Herberg, R.S. Maxwell, and E.H. Majzoub, J. Alloys Compd. 417 (2006) 39-44

52 G. Streukens, B. B. Bogdanović, M. Felderhoff, and F. Schüth, Phys. Chem. Chem. Phys. 8 (2006) 2889-2892

53 W. Langley, M.S. Thesis, University of Hawaii (2010), Honolulu, HI

54 L.E. Valiente-Banuet, G. Majer, and K. Müller, J. Magn. Reson. 200 (2009) 280-284

55 G. Majer, E. Stanik, L.E. Valiente-Banuet, F. Grinberg, O. Kircher, and M. Fichtner, J. Alloys Compd. 404-406 (2005) 738-742

56 R.C. Bowman, Jr. and A. Attalla, Phys. Rev. B 16 (5) (1977) 1828-1846

57 R.C. Bowman, Jr. and A. Attalla, J. Nucl. Mater. 154 (1988) 318-331

58 R.C. Bowman, Jr., Nature 271 (1978) 531-533

59 L. Senadheera, E.M. Carl, T.M. Ivancic, M.S. Conradi, R.C. Bowman, Jr., S.J. Hwang, T.J. Udovic, J. Alloys Compd. 463 (2008) 1-5

60 M.H.W. Verkuijlen, J Gao, P. Adelhelm, P.J.M. van Bentum, P.E. de Jongh, and A.P.M. Kentgens, J. Phys. Chem. C 114 (2010) 4683-4692

61 H. Gunaydin, K.N. Houk, and V. Ozoliņš, Proc. Nat. Acad. Sci. USA 105 (2008) 3673-3677

62 R. Cantelli, O. Palumbo, A. Paolone, C.M. Jensen, M.T. Kuba, and R. Ayabe, J. Alloys Compd. 446-447 (2007) 260-263

63 Q.J. Fu, A.J. Ramirez-Cuesta, and S.C. Tsang, J. Phys. Chem. B 110 (2006) 711-715

64 K.J. Gross, S. Guthrie, A. Takara, G. Thomas, J. Alloys Compd. 297 (200) 270-281

65 D Kim, C.H. Hsieh, and J.F. Stebbins, Chem. Mater. 18 (2006) 3855-3859

66 T.J. Bastow and S. Celotto, Mater. Sci. Eng. C 23 (2003) 757-762

67 Private Communication: 14 March, 2006. ^{45}Sc Spectrum taken by Son-Jong Hwang at Caltech on scandium hydride sample for comparison to a Sc doped NaAlH4 sample prepared by IFE-Norway.

68 C. Kim, S.J. Hwang, R.C. Bowman, Jr., J.W. Reiter, J.A. Zan, J.G. Kulleck, H. Kabbour, E.H. Majzoub, and V. Ozolins, J. Phys. Chem. C 113 (2009) 9956-9968

69 V. Ozoliņš, A.R. Akbarzadeh, H. Gunaydin, K. Michel, C. Wolverton, and E.H. Majzoub, J. Phys. Conf. Ser. 180 (2009) 012076